2006-06

Performance evaluation of different jamming strategies over uncoded noncoherent fast FH/MFSK communication systems

Karkatzounis, Konstantinos

Monterey California. Naval Postgraduate School

NAVAL POSTGRADUATE SCHOOL

MONTEREY, CALIFORNIA

THESIS

PERFORMANCE EVALUATION OF DIFFERENT JAMMING STRATEGIES OVER UNCODED NONCOHERENT FAST FREQUENCY HOPPING MFSK COMMUNICATION SYSTEMS

by

Konstantinos Karkatzounis

September 2004

Thesis Advisor: Tri T. Ha
Second Reader: David C. Jenn

Approved for public release; distribution is unlimited

THIS PAGE INTENTIONALLY LEFT BLANK

REPORT DOCUMENTATION PAGE			Form Approved OMB No. 0704–0188
Public reporting burden for this collection of information is estimated to average 1 hour per response, including the time for reviewing instruction, searching existing data sources, gathering and maintaining the data needed, and completing and reviewing the collection of information. Send comments regarding this burden estimate or any other aspect of this collection of information, including suggestions for reducing this burden, to Washington headquarters Services, Directorate for Information Operations and Reports, 1215 Jefferson Davis Highway, Suite 1204, Arlington, VA 22202–4302, and to the Office of Management and Budget, Paperwork Reduction Project (0704–0188) Washington DC 20503.			
1. AGENCY USE ONLY ***(Leave blank)***	**2. REPORT DATE** September 2004	**3. REPORT TYPE AND DATES COVERED** Master's Thesis	
4. TITLE AND SUBTITLE: Performance Evaluation of Different Jamming Strategies Over Uncoded Noncoherent Fast FH/MFSK Communication Systems			**5. FUNDING NUMBERS**
6. AUTHOR(S) Konstantinos Karkatzounis			
7. PERFORMING ORGANIZATION NAME(S) AND ADDRESS(ES) Naval Postgraduate School Monterey, CA 93943–5000			**8. PERFORMING ORGANIZATION REPORT NUMBER**
9. SPONSORING /MONITORING AGENCY NAME(S) AND ADDRESS(ES) N/A			**10. SPONSORING/MONITORING AGENCY REPORT NUMBER**
11. SUPPLEMENTARY NOTES The views expressed in this thesis are those of the author and do not reflect the official policy or position of the Department of Defense or the U.S. Government.			
12a. DISTRIBUTION / AVAILABILITY STATEMENT Approved for public release; distribution is unlimited			**12b. DISTRIBUTION CODE**

13. ABSTRACT (maximum 200 words)

The fast frequency–hopping technique is considered one of the most effective Electronic Protective Measures (EPM) for military communications systems in order to mitigate the effect of a follower or repeat jammer.

This thesis evaluates the performance of different jamming strategies as barrage noise jamming, partial band jamming and multitone band jamming against an uncoded noncoherent FFH/MFSK system with a conventional receiver.

The theoretical and simulated results showed that the best jamming strategies for the examined modulation orders M=2,4,8 is the optimum case of multitone band jamming.

As a second goal, this thesis also provides a preliminary analysis for an uncoded noncoherent FFH/MFSK system in a Rayleigh fading channel. This analysis includes the theoretical and simulated results for the influence in the performance from a barrage noise jammer along with AWGN.

The results of the theoretical analysis and the simulation modeling for both cases can be used as guidelines to analyze more complicated jamming or combinations of jamming strategies against FFH/MFSK communication system.

14. SUBJECT TERMS FFH/MFSK, Square–Law Linear Combining Receiver, Probability of Bit Error, Follower Jammer, Barrage Noise Jamming, Partial–Band Jamming, Multitone Band Jamming, Gaussian Channel, Rayleigh Channel, Systemview, Simulation Model			**15. NUMBER OF PAGES** 115
			16. PRICE CODE
17. SECURITY CLASSIFICATION OF REPORT Unclassified	**18. SECURITY CLASSIFICATION OF THIS PAGE** Unclassified	**19. SECURITY CLASSIFICATION OF ABSTRACT** Unclassified	**20. LIMITATION OF ABSTRACT** UL

NSN 7540–01–280–5500

Standard Form 298 (Rev. 2–89)
Prescribed by ANSI Std. 239–18

THIS PAGE INTENTIONALLY LEFT BLANK

Approved for public release; distribution is unlimited

PERFORMANCE EVALUATION OF DIFFERENT JAMMING STRATEGIES OVER UNCODED NONCOHERENT FAST FH/MFSK COMMUNICATION SYSTEMS

Konstantinos Karkatzounis
Major, Hellenic Army
B.A., Hellenic Cadet Academy, 1989

Submitted in partial fulfillment of the
requirements for the degree of

MASTER OF SCIENCE IN SYSTEMS ENGINEERING

from the

NAVAL POSTGRADUATE SCHOOL
September 2004

Author: Konstantinos Karkatzounis

Approved by: Tri T Ha
Thesis Advisor

David C. Jenn
Second Reader

Dan C. Boger
Chairman, Department of Information Sciences

THIS PAGE INTENTIONALLY LEFT BLANK

ABSTRACT

The fast frequency–hopping technique is considered one of the most effective Electronic Protective Measures (EPM) for military communications systems in order to mitigate the effect of a follower or repeat jammer.

This thesis evaluates the performance of different jamming strategies as barrage noise jamming, partial band jamming and multitone band jamming against an uncoded noncoherent FFH/MFSK system with a conventional receiver.

The theoretical and simulated results showed that the best jamming strategies for the examined modulation orders M=2,4,8 is the optimum case of multitone band jamming.

As a second goal, this thesis also provides a preliminary analysis for an uncoded noncoherent FFH/MFSK system in a Rayleigh fading channel. This analysis includes the theoretical and simulated results of the system's performance against a barrage noise jammer along with AWGN.

The results of the theoretical analysis and the simulation modeling for both cases can be used as guidelines to analyze more complicated jamming or combinations of jamming strategies against an FFH/MFSK communication system.

THIS PAGE INTENTIONALLY LEFT BLANK

TABLE OF CONTENTS

LIST OF FIGURES

THIS PAGE INTENTIONALLY LEFT BLANK

LIST OF TABLES

THIS PAGE INTENTIONALLY LEFT BLANK

ACKNOWLEDGMENTS

This thesis is dedicated to my loving wife, Efi, who supports me and encourages me in every step of my life and to my loving daughter, Angeliki–Eirini, who gave me a new meaning in my life.

I would like to express my sincere appreciation to my Professor Tri Ha and Professor Clark Robertson. Without their support coupled with clear explanations and supervision, this thesis would not have been possible.

Also, I would like to thank Professor David Jenn for his valuable guidance, support and help as my academic associate during my studies at the Naval Postgraduate School.

Lastly, I must thank the Hellenic Army, for providing an opportunity for me to pursue my postgraduate study here at the Naval Postgraduate School.

THIS PAGE INTENTIONALLY LEFT BLANK

I. INTRODUCTION

It is generally acknowledged that the modern army relies greatly upon command and control as force multipliers. Advance technology greatly enhances a commander's ability to remain abreast of a battlefield situation, affording him a brief opportunity to act or to react in the most effective manner. To be successful, a commander must retain the capability to integrate the actions of his forces and their weapons systems. This coordinated effort produces an economy of force. Reliable communications is a priority for command and control. Just as important, denying the enemy the same needs of communicating, with the help of *electronic countermeasures* (ECM) is essential to success. Communications *jamming and surveillance* are critical to achieve information superiority.

A. PURPOSE OF ECM

Electronic countermeasures (ECM) is the offensive or attack component of Electronic Warfare (EW). ECM is defined as that division of EW involving actions taken to prevent or to reduce an enemy's effective use of the electromagnetic spectrum, through the use of electromagnetic energy. There are three sub–divisions of ECM: Electronic Jamming, Electronic Deception, and Electronic Neutralization.

Electronic jamming is the deliberate radiation, re–radiation or reflection of EM energy that impair the effectiveness of an enemy's electronic devices, equipment or systems.

Command, Control & Communications (C^3) and also *Electronic countermeasures* (ECM) demand strategic planning, high technology and operational experience.

Although C^3 systems with fixed frequencies are vulnerable to unsophisticated ECM, spread spectrum (SS) technology severely challenges the enemy's ECM capabilities by reducing the ability of the enemy to intercept and to jam the C^3 systems that involve SS technology.

B. SCOPE OF THESIS

Electronic Protective Measures (EPM) protect the electronic communication systems from an adversary's EW actions or from friendly mutual interference. EPM is defined as that division of EW involving actions taken to ensure friendly effective use of the electromagnetic spectrum despite the enemy's use of electromagnetic energy.

Fixed–frequency communication channels are vulnerable to electronic countermeasures since an adversary has sufficient time to identify the operating frequency. To decrease this vulnerability, several modes of EPM have been developed. These modes spread the transmitted signal over a large bandwidth in order to reduce the probability of detection and jamming. The two principal forms of EPM are frequency–hopping spread spectrum (FHSS or FH) and Direct Sequence Spread Spectrum (DSSS or DS). Each of these EPM techniques possess advantages and disadvantages for various operational situations. Military applications usually involve the FH technique because it is considered cheaper and easier to implement than the DS technique.

The most effective ECM technique for a slow frequency–hopping technique is considered the follower or repeat jammer. A popular EPM technique that is used in order to mitigate the effect of the repeat jammer is a fast frequency–hopped M–ary frequency–shift keying (FFH/MFSK) modulation technique.

The objective of this thesis was to evaluate the performance of different jamming strategies against an uncoded noncoherent fast frequency–hopped M–ary frequency–shift keying (FFH/MFSK) communication system under an additive white zero–mean Gaussian noise (AWGN) environment. This thesis also evaluates the performance of the FFH/MFSK system in a fading environment along with the influence of AWGN and Barrage Noise Jamming (BNJ).

The thesis is organized as follows. Chapter II establishes the background for the FFH/MFSK systems and also discusses the configuration of the jammer and its geometric restrictions in reactive or follower jamming mode. Chapter III presents the theoretical analysis of the jamming mode's performance for an uncoded noncoherent FFH/MFSK system with a square–law linear combining receiver. Chapter IV analyzes the performance of the FFH/MFSK system with a square–law linear combining receiver in a

Rayleigh fading channel under the influence of AWGN and BNJ. Chapter V presents the simulation models, the simulation results corresponding to the theoretical analysis of Chapter III and a comparison of the simulation and theoretical results where these are available. Chapter VI presents the simulation models and simulation results that correspond to the theoretical analysis of Chapter IV. Finally, Chapter VII presents a summary with conclusions and proposes prospective developmental work in this area.

THIS PAGE INTENTIONALLY LEFT BLANK

II. BACKGROUND IN FREQUENCY–HOPPING SYSTEMS

A. IMPORTANCE OF EFFECTIVE ECM IN FHSS SYSTEMS

Frequency–hopping spread–spectrum protects against a hostile jammer by increasing the bandwidth that the information signal occupies far more than required. By increasing the system's bandwidth, the hostile jammer spreads its power over a wide frequency band W_T, which makes the jammer less effective.

B. FUNDAMENTAL CONCEPTS OF FREQUENCY HOPPING SYSTEMS

The main idea of frequency–hopping spread–spectrum is simply based on the multiplication of a conventional MFSK signal–prior to transmission–by an intermediate frequency. This frequency is generated by a frequency synthesizer [1] of the form:

$$p(t) = 2\cos(2\pi f_i t) = 2\cos\left\{2\pi\left[f_1 + (i-1)\Delta f_h\right]\cdot t\right\},\ i = 1,2,...,N \tag{2.1}$$

where N is the maximum number of possible frequency hop bins, Δf_h is the separation between the carrier frequencies of adjacent bins, and i changes pseudorandomly every T_h seconds. By doing this, the entire spectrum of the MFSK signal transmitted is shifted from its initial carrier frequency f_c to the new carriers frequencies:

$$f_{c_i} = f_c + f_1 + (i-1)\cdot\Delta f_h\,. \tag{2.2}$$

In Equation (2.1), there are N different frequency hop bins, each of bandwidth Δf_h. The value of i is changed periodically every T_h seconds according to some predetermined (but apparently random to a third–party observer) noiselike spreading code, called a "pseudorandom" or "pseudonoise sequence."

A simplified block diagram of the transmitter of the FH/MFSK system is shown in Figure 1.

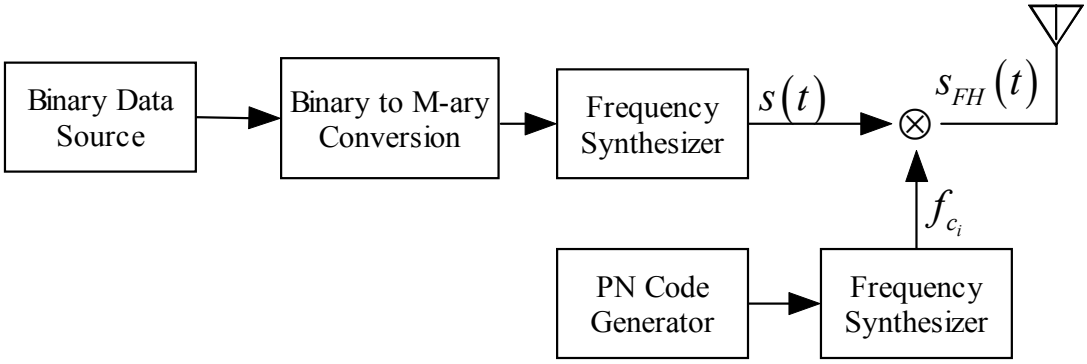

Figure 1. Transmitter of FH/MFSK System.

On a given hop, the signal bandwidth is identical to conventional MFSK, which is typically much smaller than W_T ; however, averaged over many hops, the FH/MFSK spectrum occupies the entire W_T bandwidth.

It is difficult to maintain phase coherence from hop to hop between the transmitter and the receiver, primarily because of frequency–dependent multipath and Doppler shifts [4]. Consequently, unless the hopping rate is very low compared to the transmitted symbol rate, practical frequency–hopping systems almost always require noncoherent or differentially coherent demodulation. For the rest of this thesis a non–coherent MFSK will be examined.

A conventional MFSK signal is described by

$$s(t) = \sqrt{2}A_c \cdot \cos\left\{2\pi\left[f_s + (m-1)\Delta f\right]\cdot t + \theta_i\right\}, m = 1,2,..,M \qquad (2.3)$$

where M is the modulation order of the signal, θ_i is the symbol phase , and Δf is the frequency separation between each of the *M* signaling tones. The step Δf is chosen to be an integer multiple of the symbol rate R_s in order to achieve orthogonality. So, multiplying this signal by the frequency from the synthesizer (2.1) the signal becomes:

$$
\begin{aligned}
s'(t) &= 2\sqrt{2}A_c \cos\left\{2\pi\left[f_s + (m-1)\Delta f\right]t + \theta_i\right\}\cos(2\pi f_i) \\
&= \sqrt{2}A_c \cos\left\{2\pi\left[f_i + f_s + (m-1)\Delta f\right]t + \theta_i\right\} + \sqrt{2}A_c \cos\left\{2\pi\left[f_i - f_s - (m-1)\Delta f\right]t - \theta_i\right\}.
\end{aligned} \tag{2.4}
$$

The carrier frequencies of the first term are

$$
f_i + f_s + \left(m-1\right)\Delta f = f_1 + \left(i-1\right)\Delta f_h + f_s + \left(m-1\right)\Delta f \ , \tag{2.5}
$$

which is smallest for $i = 1$ and $m = 1$. In this case, the carrier frequency becomes $f_s + f_1$.

The carrier frequencies for the second term are

$$
f_i - f_s - \left(m-1\right)\Delta f = f_1 + \left(i-1\right)\Delta f_h - f_s - \left(m-1\right)\Delta f \ , \tag{2.6}
$$

which is largest for $i = N$ and $m = 1$. In this case, the carrier frequency becomes

$$
f_1 + \left(N-1\right)\Delta f_h - f_s \, . \tag{2.7}
$$

If the smallest frequency of the first term is greater than the largest frequency of the second term, then from [1] the following condition has to be satisfied :

$$
f_s > f_1 + B + \frac{N-1}{2}\Delta f_h \tag{2.8}
$$

where B is the required guardband above and below the high– and the low–frequency signaling tones, respectively. In this case, a high–passed filter is used to remove the frequency difference contribution, and the frequency–hopped MFSK signal becomes

$$
s_{FH}\left(t\right) = \sqrt{2}A_c \cdot \cos\left\{2\pi\left[f_i + f_s + \left(m-1\right)\Delta f\right]\cdot t + \theta_i\right\} . \tag{2.9}
$$

The major advantage of frequency–hopping systems against non–sophisticated jammers is that the jammer cannot jam the specific hop bin where the FH system operates at any instant time. The reason is the lack of information about the hopping pattern that the transmitter uses.

The frequency hopping technique also allows portions of the frequency band containing known narrowband interference to be avoided.

Another advantage of an FH system is that the power spectral density of the frequency–hopped signal is identical to that of the conventional MFSK signal in a specific hop bin. However, since the signal hops from bin to bin, and assuming that the probability that any bin is occupied is equal to (1/*N*), the average power spectral density is

$$PSD = \frac{1}{N}\sum_{i=1}^{N} S_{FSK}(f \mid f_c = f_{c_i}). \tag{2.10}$$

One of the most popular jammers against frequency–hopping systems is the follower jammer [8]. The follower jammer is a sophisticated jammer that has the ability to intercept –with an acceptable probability– the instantaneous frequency of the FH system, and then it can generate an appropriate jamming in a narrow range about this frequency. A follower jammer and its limitations will be analyzed in a later section.

C. FAST FREQUENCY–HOPPING TECHNIQUE

In order to mitigate the effects of a follower jammer an anti–jam (AJ) application is employed called the Fast Frequency Hopping (FFH) technique. The role of this technique is to prevent the follower jammer from having sufficient time to intercept the frequency and retransmit it along with adjacent frequencies so as to create interfering signal components.

The term "fast" has nothing to do with the actual rate of frequency hopping. It indicates that the hop rate R_h is an integer multiple of the MFSK symbol R_s, while the term "slow" Frequency Hopping denotes the reverse condition.

Synthesizer technology is progressing so rapidly that in the past it was common for FH systems to operate at several hundreds hops/sec and 10 to 20 Khops/sec were considered to be state–of–the–art [3]. Yet synthesizer implementations have now been developed that deliver rates of the order of Mhops/sec.

The relation between the hop rate and symbol rate for the FFH is described by:

$$R_h = L \cdot R_s = \frac{L \cdot R_b}{k}, \tag{2.11}$$

where L indicates that every symbol is subdivided in L subsymbols and k is the number of bits per *M*–ary symbol.

Fast Frequency Hopping (FFH) is actually a form of frequency/time diversity. Diversity is a form of repetition coding that is used to introduce data redundancy in an effort to improve performance, under some conditions.

As previously mentioned each *M*–ary symbol is partitioned into L subsymbols with energy:

$$E_h = \frac{k \cdot E_b}{L}, \tag{2.12}$$

where E_b is the energy of a bit. Each subsymbol is transmitted on a different hop according with the pseudorandom sequence. The intention is that each subsymbol comprising an *M*–ary symbol will have an independent chance of being jammed.

Figure 2 presents a Frequency Hop Diversity example for a FFH/MFSK system where the modulation order $M = 4$, the diversity $L = 3$ and a 4–ary symbol 3 is followed by 1. Each subsymbol is transmitted at a different frequency.

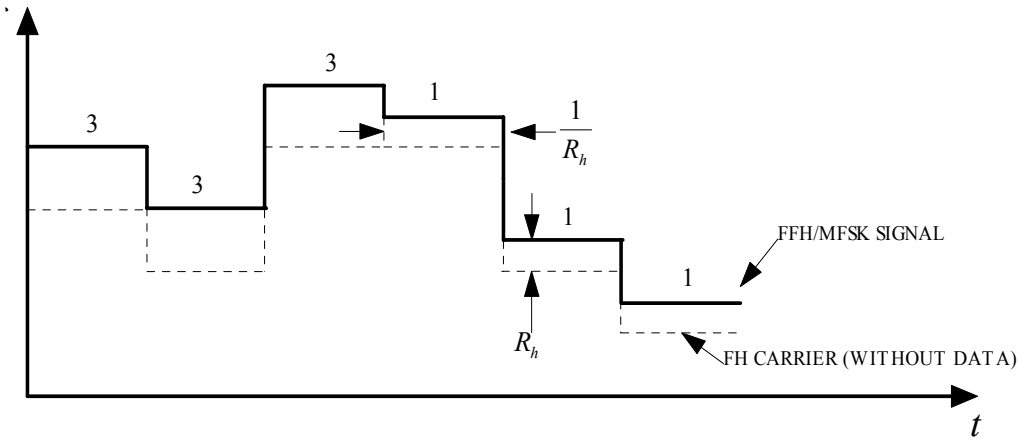

Figure 2. Diversity for a FFH/4FSK Communication System.

However, there is a penalty incurred in subdividing a signal into several FH elements because the energy from these separate elements is combined noncoherently. Consequently, the demodulator of the receiver incurs a penalty in the form of a noncoherent combining loss, as will be described at Chapter III.

For FFH/MFSK with diversity order $L > 1$ there are a number of ways in which the various diversity receptions can be combined depending on the type of the demodulator.

One method is implementing a "hard decision" majority vote where every diversity reception is demodulated individually, yielding a "1" for the signal present or "0" for no signal for each of the *M* branches of the noncoherent receiver. The individual symbols for every branch are summed and the branch with the largest number is chosen as corresponding to the received symbol.

Another combining method called "soft decision" is to sample the analog outputs of each square–law detector for each diversity every T_h and then adding them prior to deciding whether the signal corresponds to a particular branch or not. The decision for the received symbol is made according to which branch has the greatest value

If the hops of a symbol are combined linearly, then in case of jamming interference, the jammed hops have just as much weight in the overall decision statistics as do the unjammed hops, leading to a major degradation in performance of this system. This is considered one of the major disadvantages of the linear combining technique.

In order to overcome this disadvantage, other combining methods involving soft decision demodulation were discovered. In these methods, every diversity reception can be some how weighted or eliminated according to some criteria.

Numerous proposals have been made for improving performance by means of "side information, " where the receiver of the FFH/MFSK system attempts to decide if each hop has been jammed or not. This information is used to either discard the "jammed" hops entirely, or to assign a "weighted" value to the hop.

There are some disadvantages to the use of side information as Reference [5] indicates. First, the side information tends to be unreliable and can complicate the overall system quite considerably. Secondly, the "side information" methods can leave the system vulnerable to simple jammer methods that could make performance worse than if side information were not used.

Additionally, in the presence of large jamming, all hops tend to be jammed, thereby rendering side information is useless or, worse, causes the information on every hop to be erased, as all hops concerned as contaminated.

For all the above reasons, the simplest and easier receiver to implement is the Square–Law Linear Combining Soft Decision receiver in which we do not have any information regarding which hops are jammed and which are not (side information).

This is the system that will be examined in the next chapters against different jamming strategies as Barrage Noise Jamming, Partial Band Noise Jamming, and Multitone Band Jamming.

D. REPEATER JAMMER CONFIGURATION AND GEOMETRICAL LIMITATIONS IN REPEAT MODE OF OPERATION

The benefits of frequency hopping are potentially neutralized by a repeater jammer, also known as a follower jammer, which as mentioned before is a device that intercepts a signal, processes it, and then transmits the jamming signal at the same center frequency.

The geometrical configuration for a follower jammer appears in Figure 3 where D_{tr} is the distance between the transmitter and the receiver, D_{tj} is the distance between the transmitter and the jammer and D_{jr} is the distance between the jammer and the receiver. The hop period for the communication system is $T_h = \frac{1}{R_h}$.

Reference [4] notes that for the jammer to be effective against a frequency–hopping system, the arrival–time delay of the jamming relative to the authorized signal must not exceed a certain fraction of the dwell time as described by:

$$\frac{D_{tj} + D_{jr}}{c} + T_{pr} \le \frac{D_{tr}}{c} + n \cdot T_d \tag{2.13}$$

where c is the velocity of light, T_{pr} is the processing time required from the follower jammer, n is a fraction, and T_d is the dwell time, which is the duration of a frequency–

hopping pulse and is less than or equal to the hop duration T_h. A rearrangement of Equation (2.13) yields:

$$D_{tj} + D_{jr} \le \left(n \cdot T_d - T_{pr}\right) \cdot c + D_{tr}. \tag{2.14}$$

If the right–hand side of this inequality is regarded as a constant, then equating the two sides defines an ellipse with the transmitter and the receiver located at the "foci" of the ellipses. If the follower jammer is outside this area, the jammer cannot be effective.

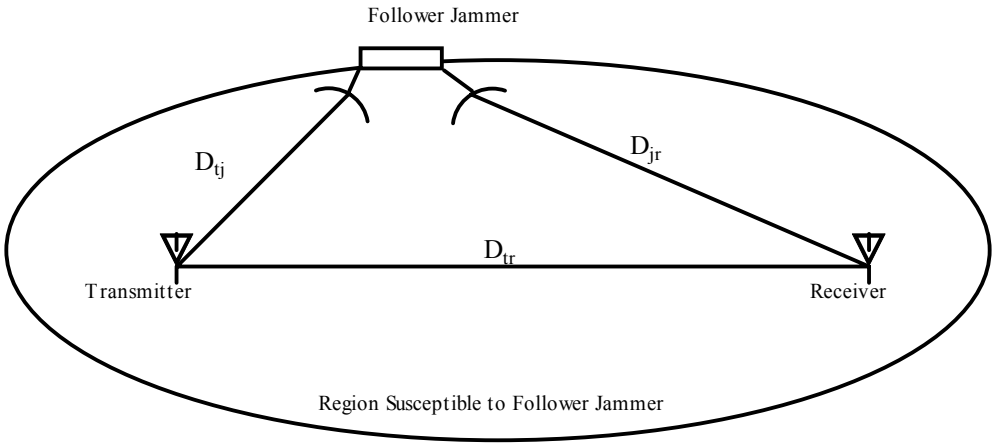

Figure 3. A Representation of the Transmitter–Jammer–Receiver Geometry.

Assuming that the jammer is located at the same level as the receiver and the transmitter, then the following equation gives the location that the jammer has to be placed in order to be effective:

$$\frac{4\left(x - \frac{D_{tr}}{2}\right)^2}{\left(D_{tr} + c \cdot \left(n \cdot T_d - T_{pr}\right)\right)^2} + \frac{4 \cdot y^2}{\left(D_{tr} + c \cdot \left(n \cdot T_d - T_{pr}\right)\right)^2 - {D_{tr}}^2} = 1 \tag{2.15}$$

where the *x* and *y* axis are centered on the transmit antenna, as in Figure 3.

Based on Reference [4], the quantity $\left(n \cdot T_d - T_{pr}\right)$ can be considered equal to the hop period T_h, so Equation (2.15) can be rewritten as:

$$\frac{4\left(x-\frac{D_{tr}}{2}\right)^2}{\left(D_{tr}+c\cdot T_h\right)^2}+\frac{4\cdot y^2}{\left(D_{tr}+c\cdot T_h\right)^2-D_{tr}^{\ 2}}=1. \qquad (2.16)$$

It is obvious that if the hop rate increases, then the area where the jammer can be effective becomes smaller.

On a real battlefield, the jammer's distance from the receiver is of vital importance for the jammer's survival. The closer the jammer is to the link between the transmitter and the receiver, the more vulnerable it is to the enemy's fire power.

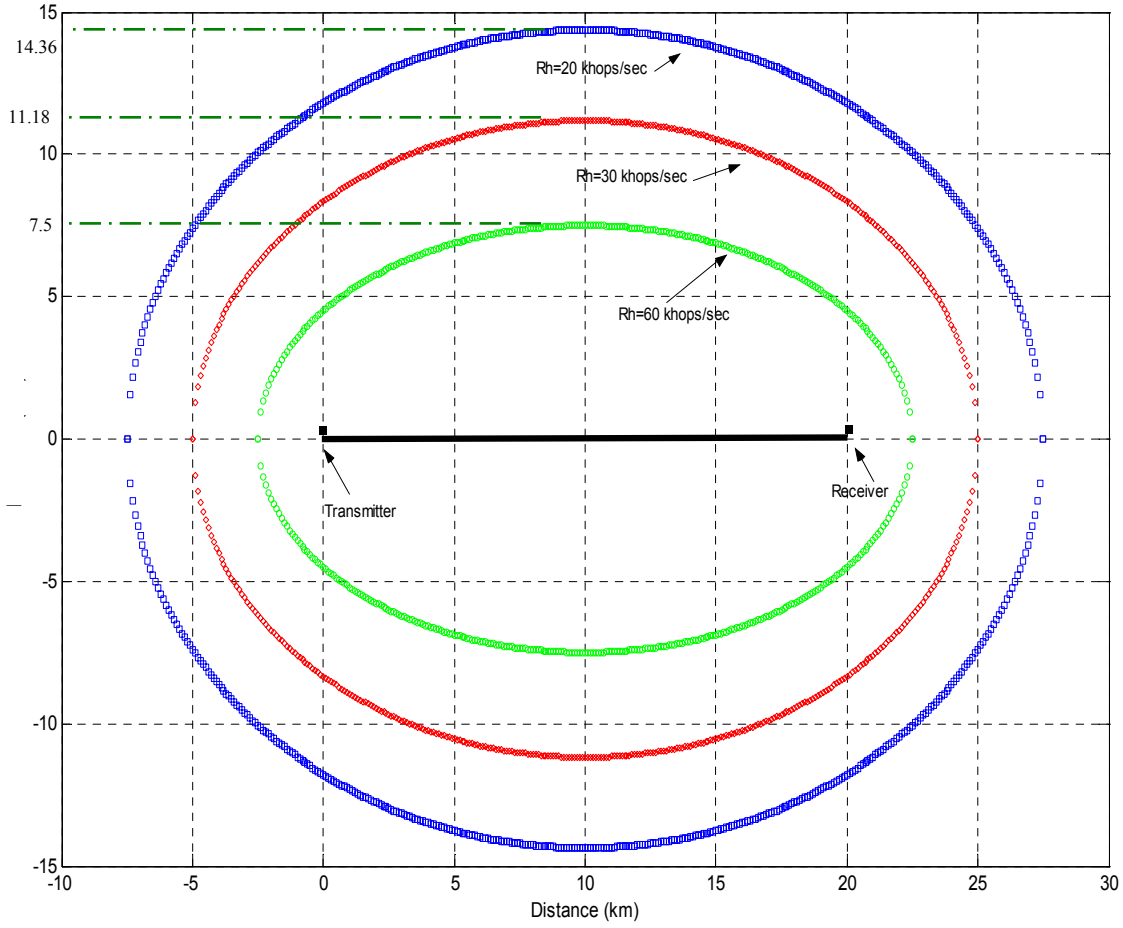

Figure 4. Boundary Ellipses for Operation of the Follower Jammer for Various R_h.

In Figure 4 a realistic example of the geometrical limitations for a follower jammer is given for different hop rates. The distance between the transmitter and receiver is set at a 20 km distance, which is typical on a real battlefield.

It is clear how small the area of the jammer operation becomes for higher hop rates. For example for $R_h = 20$ khops/sec the distance of the follower jammer from the link is 14.36 km compared to the distance of 7.5 km for the higher rate $R_h = 60$ khops/sec . This distance is considered unacceptable for a jammer on the real battlefield.

The limitation in distance is the reason that other jamming strategies must be devised so that the jammer can degrade the performance of a fast frequency–hopping system.

The drawback to using higher hop rates is that synchronization between the transmitter and receiver becomes more difficult and demands complicated synchronization techniques.

III. THEORETICAL ANALYSIS FOR DIFFERENT JAMMING STRATEGIES AGAINST AN FFH/MFSK SYSTEM

This chapter presents the different jamming strategies against an FFH/MFSK communication system. Examining each jamming strategy, describing the basic characteristics of a FFH/MFSK system, the channel model, and the symbology is very important, so that one can understand the system better.

A. FFH/MFSK SYSTEM DESCRIPTION, CHANNEL MODEL, AND SYMBOLOGY USED

The fundamental requirement of a FFH/MFSK communication system is to transmit binary source information over the channel by means of MFSK. An *M*–ary symbol is represented by one of the *M* orthogonal tones where

$$M = 2^k , \tag{3.1}$$

and k represents the number of bits per transmitted symbol. The binary input data have a rate R_b, which is related to the bit duration by :

$$R_b = \frac{1}{T_b} , \tag{3.2}$$

and the symbol rate R_s is related to the bit rate by:

$$R_s = \frac{R_b}{k} . \tag{3.3}$$

As previously mentioned, the hop rate R_h is related to the bit rate by:

$$R_h = \frac{L}{T_s} = \frac{L \cdot R_b}{k} . \tag{3.4}$$

At the receiver, shown in Figure 5, the received signal is mixed with the output of a local frequency synthesizer driven by the same "pseudorandom" sequence used at the transmitter. For the *K*–th hop, the output of the low pass filter is then a tone of frequency f_m of duration T_h. This tone is passed through a bank of M square law linear detectors. The outputs are the samples V_{mk} for m=1,…,M and k=1,2,…,L, where m denotes the

frequency bin and k denotes the hop period. The diversity combiners form the decision statistics V_m by summing the L samples, V_{mk}, in each bin. A decision is then made as to which symbol was sent by choosing the largest V_m. The M–ary symbols are then converted to binary.

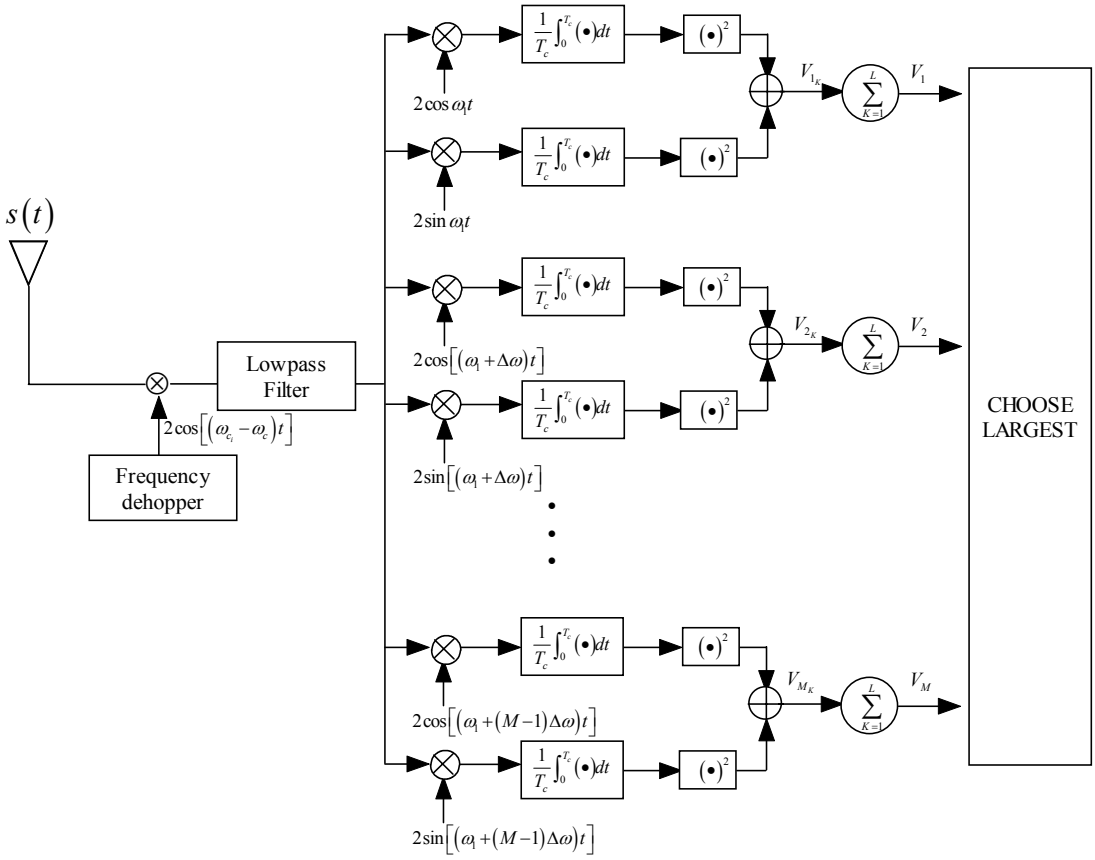

Figure 5. FFH/MFSK Linear Combining Square–Law Receiver [7].

The total bandwidth W_T of the FFH/MFSK system can be divided into N FH bands (W_{band}) and each band can be further divided into M bins as illustrated in Figure 6. Therefore, the signal's bandwidth is

$$W_T = N \cdot W_{Band} = M \cdot N \cdot \Delta f \,, \tag{3.5}$$

where

$$\Delta f = p \cdot R_h = p \cdot \frac{1}{T_h} \,, \tag{3.6}$$

and p is an integer number. The value of Δf must satisfy Equation (3.6) in order to achieve orthogonal signaling [7].

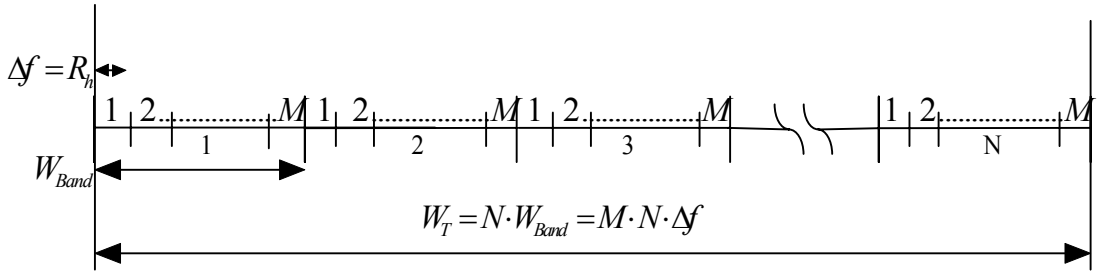

Figure 6. Bandwidth Representation of the FFH/MFSK System.

B. JAMMING STRATEGIES AGAINST FFH/MFSK SYSTEM IN A AWGN CHANNEL

This section presents different jamming strategies against a FFH/MFSK system. In these types of jamming, the jammer has no information about the transmitting frequency of the signal.

The strategies that will be presented are barrage noise jamming, partial band jamming, and multitone band jamming. Before analyzing all of the above methods, it is necessary to show the performance of the system without any interference, except for AWGN. This is important in order to clarify the concept of diversity in an FFH/MFSK system.

1. Performance of Uncoded FFH/MFSK in AWGN

When AWGN is present, the total received signal in the receiver of the FFH/MFSK is the transmitted signal (2.9) plus the AWGN $n(t)$ with PSD $N_0/2$ [8]. Thus, the received signal is

$$s_T(t) = \sqrt{2} A_c \cos\left\{2\pi\left[f_i + f_s + (m-1)\Delta f\right]t + \theta_i\right\} + n(t). \tag{3.7}$$

By combining Equation (3.6), this becomes

$$s_T(t) = \sqrt{2}A_c \cos\left\{2\pi\left[f_i + f_s + (m-1)\,pR_h\right]t + \theta_i\right\} + n(t). \tag{3.8}$$

Reference [7] notes that the probability of symbol error is

$$\begin{aligned} P_s &= \Pr(\text{error}\,|\,1)\Pr(1) + \Pr(\text{error}\,|\,2)\Pr(2) + ... + \Pr(\text{error}\,|\,M)\Pr(M) \\ &= \sum_{m=1}^{M} \Pr(\text{error}\,|\,m)\Pr(m). \end{aligned} \tag{3.9}$$

The transmitted symbols, without loss of generality, are assumed equally likely thus

$$\Pr(1) = \Pr(2) = \Pr(3) = ...\Pr(M) = \frac{1}{M}. \tag{3.10}$$

As a consequence of the symmetric nature of the receiver structure and the noise,

$$\Pr(\text{error}\,|\,1) = \Pr(\text{error}\,|\,2) = ... = \Pr(\text{error}\,|\,M). \tag{3.11}$$

By combining Equations (3.9), (3.10) and (3.11) the expression for symbol error becomes:

$$\begin{aligned} Ps &= \frac{1}{M}\sum_{m=1}^{M} \Pr(\text{error}\,|\,m) = \frac{1}{M} M \Pr(\text{error}\,|\,m) \\ &= \Pr(\text{error}\,|\,m)\,,\ m = 1,2,....,M\,. \end{aligned} \tag{3.12}$$

In Figure 5 the random variables V_m, $m = 1,2,3,...M$ represent the outputs of branches 1,2,…M, respectively. Without a loss of generality, it is assumed that the symbol "1" represented by the frequency tone f_1 is transmitted. In order not to have an error, the output of branch one (f_1) must be greater than the outputs of all the other branches. The opposite condition causes an error situation. Reference [7] notes that the probability of symbol error becomes:

$$
\begin{aligned}
P_s &= 1 - P_{\text{correct}} \\
&= 1 - \Pr(V_1 \rangle V_2 \bigcap V_1 \rangle V_3 \bigcap V_1 \rangle V_4 ..... \bigcap V_1 \rangle V_M \mid 1) \\
&= 1 - \int_0^\infty \left[\int_0^{v_1} \int_0^{v_1} .... \int_0^{v_1} f_{V_1 V_2 ... V_M} \left(v_1, v_2 ..., v_M \mid 1 \right) dv_2 dv_3 ... dv_M \right] dv_1 \qquad (3.13) \\
&= 1 - \int_0^\infty f_{V_1} \left(v_1 \mid 1 \right) \left[\int_0^{v_1} f_{V_2} \left(v_2 \mid 1 \right) dv_2 \int_0^{v_1} f_{V_3} \left(v_3 \mid 1 \right) dv_3 .... \int_0^{v_1} f_{V_M} \left(v_M \mid 1 \right) dv_M \right] \\
&= 1 - \int_0^\infty f_{V_1} \left(v_1 \mid 1 \right) \left[\int_0^{v_1} f_{V_2} \left(v_2 \mid 1 \right) dv_2 \right]^{M-1} dv_1 ,
\end{aligned}
$$

where according to Reference [2], $f_{V_1}\left(v_1 \mid 1\right)$ and $f_{V_2}\left(v_2 \mid 1\right)$ are the conditional probability density functions (PDFs) for the $V_{1,2}$ when the signal along with the AWGN is present and only the AWGN is present respectively.

Reference [2] indicates that the PDF at the output of a square law detector when a signal is present is the PDF of the square of the envelope of a sine wave with random phase plus a narrowband Gaussian process. The result is a special case of the non–central chi–squared distribution. Assuming that the signal is present in channel "1," the PDF for the random variable V_{1_k} will be

$$
f_{V_{1_k}}\left(v_{1_k} \mid 1\right) = \frac{1}{2\sigma_k^2} \cdot e^{\left(-\frac{v_{1_k} + 2\alpha_c^2}{2\sigma_k^{\,2}} \right)} \cdot I_0 \left(\frac{A_c \cdot \sqrt{2 v_{1_k}}}{\sigma_k^2} \right) \cdot u\left(v_{1_k}\right), \qquad (3.14)
$$

where $u\left(v_{1_k}\right)$ is the unit step function, $I_0\left(\bullet\right)$ is the modified Bessel function of the first kind and zero order, and

$$
\sigma_k^2 = \frac{N_0}{T_h} \qquad (3.15)
$$

represents the noise power of each hop.

The PDF at the output of the square law detector for each of the M–1 channels with only Gaussian noise present is a special case of (3.14) when $A_c \to 0$. Thus, the PDF for the random variable V_{2_k} will be

$$f_{V_{2_k}}\left(v_{2_k}\,|1\right) = \frac{1}{2\sigma_k^2}\cdot e^{\left(-\frac{v_{1_k}}{2\sigma_k{}^2}\right)}\cdot u\left(v_{1_k}\right). \tag{3.16}$$

Since each hop is assumed to be independent, after the summation of diversity hops, the PDFs become [7]:

$$f_{V_1}\left(v_1\,|1\right) = f^{\otimes L}{}_{V_{1_k}}\left(v_{1_k}\,|1\right) = \frac{v_1{}^{\frac{L-1}{2}}}{2\sigma_k{}^2\left(2LA_c{}^2\right)} e^{\frac{-\left(v_1+2LA_c^2\right)}{2\sigma_k{}^2}} I_{L-1}\left(\frac{A_c\sqrt{2Lv_1}}{\sigma_k{}^2}\right), \tag{3.17}$$

and

$$f_{V_2}\left(v_2\,|1\right) = f^{\otimes L}{}_{V_{2_k}}\left(v_{2_k}\,|1\right) = \frac{v_2{}^{L-1}}{\left(2\sigma_k{}^2\right)^L\left(L-1\right)!} e^{\frac{-v_2}{2\sigma_k{}^2}}, \tag{3.18}$$

where $\otimes L$ defines L–1 convolutions.

The result of the replacement of (3.17) and (3.18) into (3.13) gives:

$$P_s = 1-\int_0^\infty \frac{v_1{}^{\frac{L-1}{2}}}{2\sigma_k{}^2\left(2LA_c{}^2\right)} e^{\frac{-\left(v_1+2LA_c^2\right)}{2\sigma_k{}^2}} I_{L-1}\left(\frac{A_c\sqrt{2Lv_1}}{\sigma_k{}^2}\right)\left[\int_0^{v_1}\frac{v_2{}^{L-1}}{\left(2\sigma_k{}^2\right)^L\left(L-1\right)!}e^{\frac{-v_2}{2\sigma_k{}^2}}dv_2\right]^{M-1} dv_1. \tag{3.19}$$

Using the results from Reference [9] this becomes:

$$P_s = 1-\int_0^\infty \frac{v_1{}^{\frac{L-1}{2}}}{2\sigma_k{}^2\left(2LA_c{}^2\right)^{\frac{L-1}{2}}} e^{\frac{-\left(v_1+2LA_c^2\right)}{2\sigma_k{}^2}} I_{L-1}\left(\frac{A_c\sqrt{2Lv_1}}{\sigma_k{}^2}\right)\left[1-e^{\frac{-v_1}{2\sigma_k{}^2}}\sum_{n=0}^{L-1}\frac{v_1^n}{\left(2\sigma_k{}^2\right)^n n!}\right]^{M-1} dv_1. \tag{3.20}$$

Rearranging the terms, Equation (3.20) becomes:

$$P_s = 1 - \left[\int_0^{\infty} \frac{\left(\frac{v_1}{2\sigma^2}\right)^{\frac{L-1}{2}}}{\left(\frac{2LA_c^2}{2\sigma^2}\right)^{\frac{L-1}{2}}} e^{-\left(\frac{v_1}{2\sigma^2}+\frac{2LA_c^2}{2\sigma^2}\right)} I_{L-1}\left(\sqrt{\frac{4LA_c^2 v_1}{2\sigma^2\sigma^2}}\right)\left[1 - e^{-\frac{v_1}{2\sigma^2}} \sum_{n=0}^{L-1}\left(\frac{v_1}{2\sigma^2}\right)^n \frac{1}{n!}\right]^{M-1} \frac{dv_1}{2\sigma^2} \right]. \quad (3.21)$$

Substituting $x = \frac{v_1}{2\sigma^s}$ and $dx = \frac{dv_1}{2\sigma^2}$ into Equation (3.21) results in

$$P_s = 1 - \left[\int_0^{\infty} \frac{(x)^{\frac{L-1}{2}}}{\left(\frac{LA_c^2}{\sigma_k^2}\right)^{\frac{L-1}{2}}} e^{-\left(x+\frac{LA_c^2}{\sigma_k^2}\right)} I_{L-1}\left(\sqrt{\frac{4LA_c^2 \cdot x}{\sigma_k^2}}\right)\left[1 - e^{-x} \sum_{n=0}^{L-1}(x)^n \frac{1}{n!}\right]^{M-1} dx \right]. \quad (3.22)$$

There are two possibilities to consider according to Reference [7]: constant bit rate systems and constant hop rate systems. For constant hop rates systems, R_h remains fixed. So, the hop energy E_h will also remain fixed. According to Equation (2.12), the increase of diversity order *L* leads to the increase of bit energy E_b. This also implies that the system has constant bandwidth since the bandwidth derives from Equation (3.5).

The other possibility is to implement a constant bit rate. Consequently, the bit energy E_b remains fixed and the hop energy E_h decreases as the diversity order *L* increases. This generates a system with variable bandwidth as the diversity order *L* is changed.

For the rest of the analysis, a constant bit rate system will be considered since this case is the conventional method for comparing diversity systems. Consequently, Equation (2.12) can be rewritten as

$$E_b = \frac{L \cdot E_h}{k} = \frac{L \cdot A_c^2 \cdot T_h}{k} \Rightarrow L \cdot A_c^2 = \frac{k \cdot E_b}{T_h}, \quad (3.23)$$

so the probability of symbol error based on Equations (3.15) and (3.23) is rewritten as:

$$P_s = 1 - \left[\int_0^{\infty} \frac{(x)^{\frac{L-1}{2}}}{\left(\frac{k \cdot E_b}{N_0}\right)^{\frac{L-1}{2}}} e^{-\left(x + \frac{k \cdot E_b}{N_0}\right)} I_{L-1}\left(\sqrt{\frac{4 \cdot k \cdot E_b \cdot x}{N_0}}\right) \left[1 - e^{-x} \sum_{n=0}^{L-1} (x)^n \frac{1}{n!} \right]^{M-1} dx \right]. \quad (3.24)$$

For orthogonal signaling, the average probability of bit error is related to the average probability of symbol error [2] by:

$$P_b = \frac{2^{k-1}}{2^k - 1} \cdot P_s . \quad (3.25)$$

The combination of Equations (3.25) and (3.24) results in the probability of bit error for the noncoherent FFH/MFSK system in the AWGN. Finally, the probability of bit error for a noncoherent FFH/MFSK system derives from

$$P_b = \frac{2^{k-1}}{2^k - 1} \cdot \left\{ 1 - \left[\int_0^{\infty} \frac{(x)^{\frac{L-1}{2}}}{\left(\frac{k \cdot E_b}{N_0}\right)^{\frac{L-1}{2}}} e^{-\left(x + \frac{k \cdot E_b}{N_0}\right)} I_{L-1}\left(\sqrt{\frac{4 \cdot k \cdot E_b \cdot x}{N_0}}\right) \left[1 - e^{-x} \sum_{n=0}^{L-1} (x)^n \frac{1}{n!} \right]^{M-1} dx \right] \right\}. \quad (3.26)$$

The analytical solution of Equation (3.26) is very complicated and the best way to proceed is by numerical evaluation.

Figure 7 indicates the loss in performance due to the noncoherent combination of the received hops. Specifically, notice the values of the four curves for $P_b = 10^{-5}$ that have been marked. It becomes apparent that as the diversity order increases the performance of the system degrades.

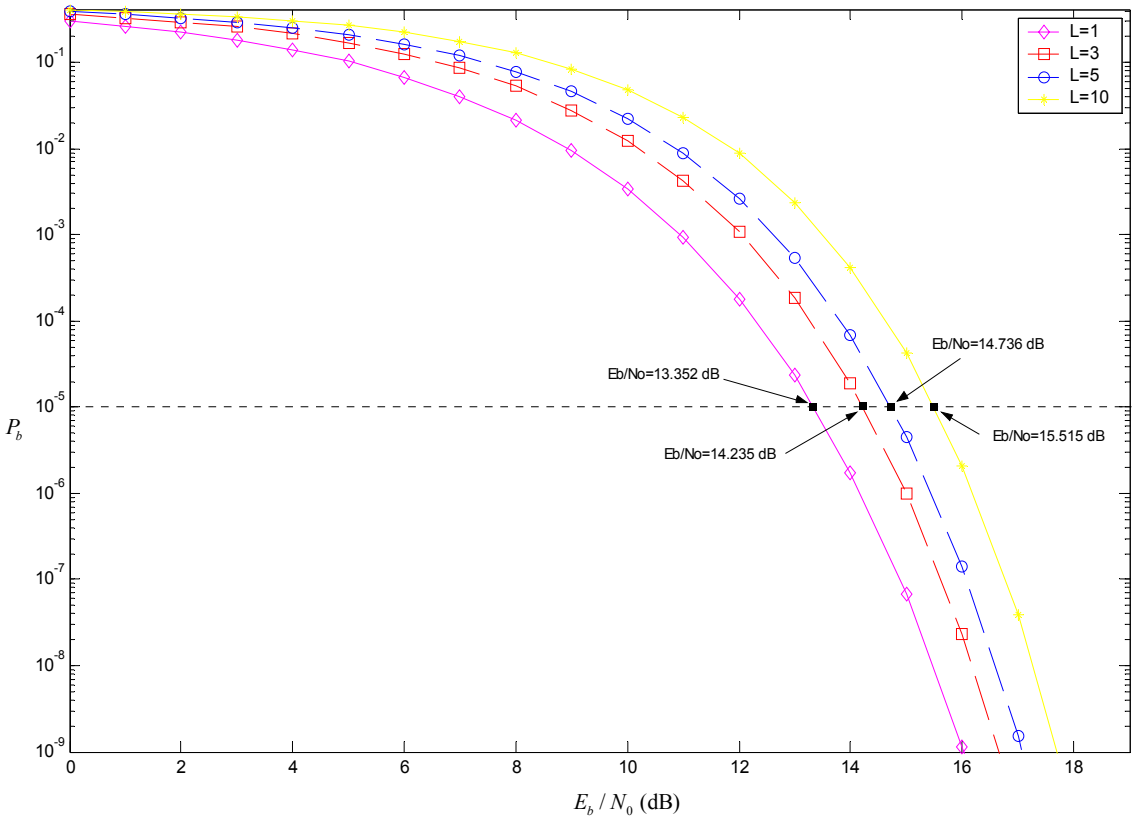

Figure 7. Performance of FFH/BFSK System in an AWGN for L=1,3,5,10.

In Figure 8, the values of the three curves for $E_b / N_0 = 13.35\ dB$ have also been marked. This is the signal–to–noise ratio (SNR) value that will be considered for the future simulation models. As was expected, the performance of the system significantly improves as the modulation order M increases.

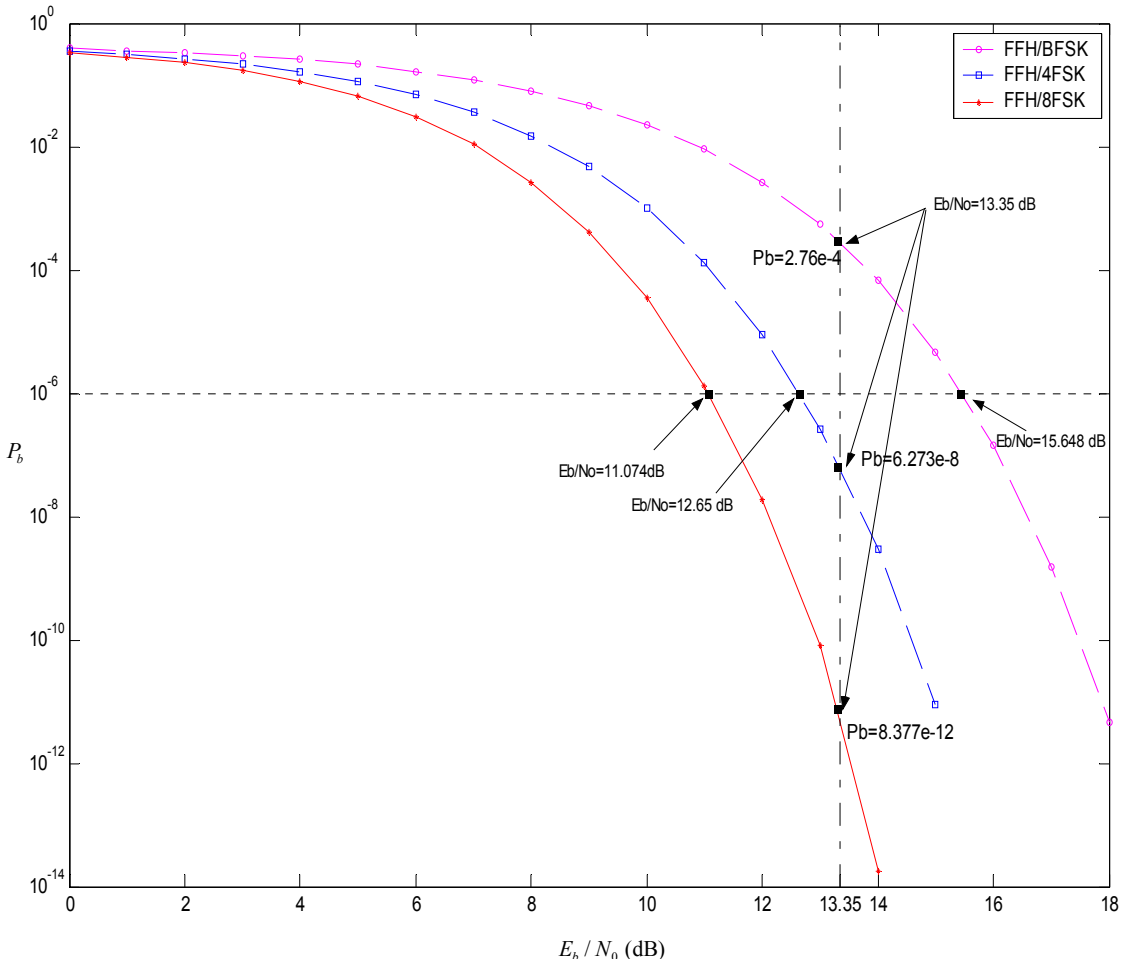

Figure 8. Performance of the FFH/MFSK System in the AWGN for L=5 and M=2,4,8.

The next sections discuss the performance of different jamming strategies, such as barrage noise, partial band and multitone band jamming.

2. Barrage Noise Jamming Against an FFH/MFSK System

Barrage noise jamming (BNJ) is considered the simplest and least sophisticated form of jamming. In BNJ, the jammer knows by observation only the occupied region of spectrum for the FFH/MFSK system.

In BNJ, the jammer attacks a FFH/MFSK system injecting a bandlimited noise–like signal $n_I(t)$ with PSD $S_{n_I}(f)$. Since the $n_I(t)$ and the $n(t)$ are independent random processes, the total PSD becomes:

$$N_T(f) = \frac{N_0}{2} + S_{n_I}(f), \tag{3.27}$$

where $S_{n_I}(f)$ is $N_I / 2$ across the bandwidth W_T, which the FH system occupies, and zero elsewhere.

The barrage noise is flat across the bandwidth of the receiver, so it affects the receiver just as if it is were AWGN. The PSD of the total noise will be

$$N_T(f) = \frac{N_0}{2} + \frac{N_I}{2}. \tag{3.28}$$

Replacing the noise power from Equation (3.26) with the total noise power N_T from Equation (3.28), the performance of the BNJ can be calculated as:

$$P_b = \frac{2^{k-1}}{2^k - 1} \cdot \left\{ 1 - \left[\int_0^\infty \frac{(x)^{\frac{L-1}{2}}}{\left(\frac{k \cdot E_b}{N_0 + N_I} \right)^{\frac{L-1}{2}}} e^{-\left(x + \frac{k \cdot E_b}{N_0 + N_I} \right)} I_{L-1}\left(\sqrt{\frac{4 \cdot k \cdot E_b \cdot x}{N_0 + N_I}} \right) \left[1 - e^{-x} \sum_{n=0}^{L-1} (x)^n \frac{1}{n!} \right]^{M-1} dx \right] \right\}. \tag{3.29}$$

Rearranging Equation (3.29), the probability of bit error becomes:

$$P_b = \frac{2^{k-1}}{2^k - 1} \left\{ 1 - \left[\int_0^\infty \frac{(x)^{\frac{L-1}{2}}}{\left(\frac{k}{\left(\frac{E_b}{N_0}\right)^{-1} + \left(\frac{E_b}{N_I}\right)^{-1}} \right)^{\frac{L-1}{2}}} e^{-\left(x + \frac{k}{\left(\frac{E_b}{N_0}\right)^{-1} + \left(\frac{E_b}{N_I}\right)^{-1}} \right)} I_{L-1}\left(\sqrt{4 \frac{k}{\left(\frac{E_b}{N_0}\right)^{-1} + \left(\frac{E_b}{N_I}\right)^{-1}} x} \right) \left[1 - e^{-x} \sum_{n=0}^{L-1} (x)^n \frac{1}{n!} \right]^{M-1} dx \right] \right\}. \tag{3.30}$$

The interference power with BNJ for the conventional MFSK is

$$P_I = B_{nn} \cdot \left(\frac{N_I^{'}}{2} + \frac{N_I^{'}}{2} \right) = B_{nn} \cdot N_I^{'}, \tag{3.31}$$

where B_{nn} is the null–to–null bandwidth of the conventional MFSK signal and $N_I^{'}$ is the PSD across the bandwidth B_{nn}.

The interference power with BNJ for FFH/MFSK is

$$P_I^{'} = W_T \cdot \left(\frac{N_I}{2} + \frac{N_I}{2} \right) = W_T \cdot N_I \quad . \tag{3.32}$$

In both cases, the available jammer's power is the same for this type of jammer. Thus, the second part of Equations (3.31) and (3.32) are equal. So

$$B_{nn} \cdot N_I^{'} = W_T \cdot N_I \Rightarrow N_I = \frac{B_{nn} \cdot N_I^{'}}{W_T} \quad . \tag{3.33}$$

According to Reference [2], the null–to–null bandwidth for the noncoherent MFSK system is

$$B_{nn} = \frac{\left(2^k + 1\right) \cdot R_b}{k}. \tag{3.34}$$

The bandwidth that the FFH/MFSK occupies derives from Equation (3.5) where

$$W_T = N \cdot W_{Band} = M \cdot N \cdot \Delta f, \tag{3.35}$$

and since $\Delta f = R_h = L \cdot R_s = \frac{L \cdot R_b}{k}$ then

$$W_T = N \cdot W_{\text{Band}} = 2^k \cdot N \cdot \frac{L \cdot R_b}{k}. \tag{3.36}$$

Combining Equations (3.34) and (3.36) with Equation (3.33), the power density of the BNJ for the FFH/MFSK system will be

$$N_I = \lambda \cdot N_I^{'}, \tag{3.37}$$

where $\lambda = \frac{1}{N}\frac{\left(2^k+1\right)}{2^k \cdot L}$. Replacing N_I in Equation (3.29) with the result from Equation (3.37) reveals that the influence of barrage noise jamming mode in a FFH/MFSK system is

$$P_b = \frac{2^{k-1}}{2^k-1}\cdot\left\{1-\left[\int_0^{\infty}\frac{(x)^{\frac{L-1}{2}}}{\left(\frac{k}{\left(\frac{E_b}{N_0}\right)^{-1}+\lambda\cdot\left(\frac{E_b}{N_I}\right)^{-1}}\right)^{\frac{L-1}{2}}}e^{-\left(x+\frac{k}{\left(\frac{E_b}{N_0}\right)^{-1}+\lambda\left(\frac{E_b}{N_I}\right)^{-1}}\right)}I_{L-1}\left(\sqrt{4\cdot\frac{k}{\left(\frac{E_b}{N_0}\right)^{-1}+\lambda\cdot\left(\frac{E_b}{N_I}\right)^{-1}}\cdot x}\right)\left[1-e^{-x}\sum_{n=0}^{L-1}(x)^n\frac{1}{n!}\right]^{M-1}dx\right]\right\}. \tag{3.38}$$

When AWGN is not considered negligible, a usual value for the signal–to–noise ratio E_b / N_0 is 13.35 dB. Equation (3.38) has some parameters that can control the performance of the system. The signal to interference ratio, $E_b / N_I^{'}$ is the only parameter that the jammer can control dynamically. The other three parameters that Equation (3.38) depends on is the modulation order, the diversity, and the number of channels *N*.

In Figure 9, the performance of the FFH/MFSK system for *M*=1,2,3 has been plotted keeping the diversity order *L* as a constant and defining the number of channels *N* as the variable parameter.

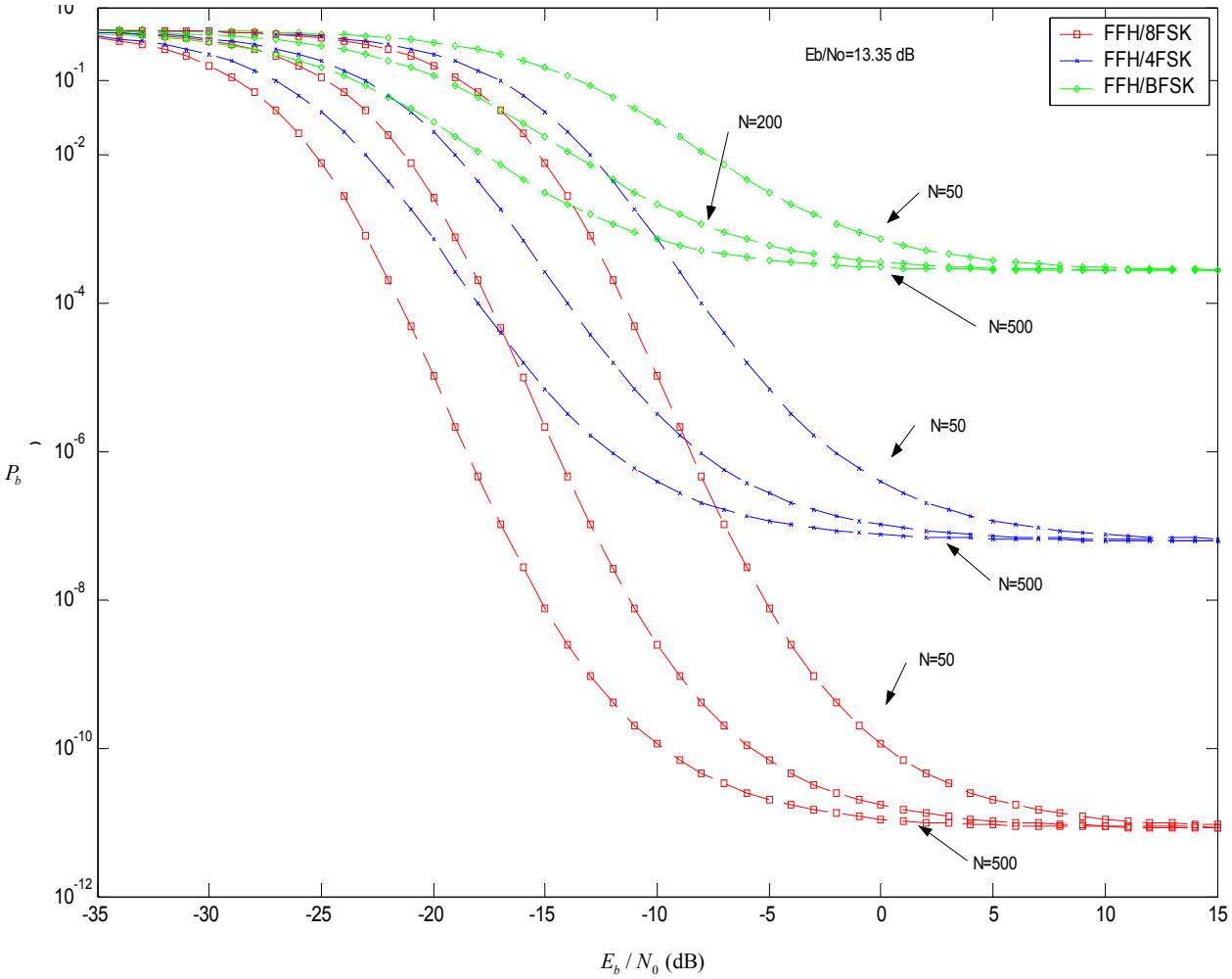

Figure 9. Effect of the BNJ in the Performance of a FFH/MFSK System for Various Number of Hopping Bands N.

Figure 9 clearly shows that as the number of channel N increases, the performance of the jammer decreases. The performance of the BNJ also decreases as the modulation order M increases. The value of parameter λ controls the processing gain of the spread spectrum system. In Table 1, different values of λ have been calculated keeping the diversity order L as a constant.

	$N=50$	$N=100$	$N=200$	$N=500$
$k=1$	22.21(dB)	25.22 (dB)	28.23 (dB)	32.21 (dB)
$k=2$	23.01 (dB)	26.02 (dB)	29.03 (dB)	33.01 (dB)
$k=3$	23.46 (dB)	26.47 (dB)	29.48 (dB)	33.46 (dB)

Table 1. Possible Values of $1/\lambda$ (dB) for Different k and N with Diversity Order $L=5$.

Finally, it becomes apparent that the smaller the value of λ the worst the performance of the barrage noise jammer is.

Figure 10 also illustrates the results from Equation (3.38) for $E_b / N_0 = 13.35$ dB with diversity order L and modulation order M as parameters. It is very interesting to observe that as the diversity order increases, the performance of the jammer for higher values $E_b / N_I^{'}$ (above –15 dB) actually improves.

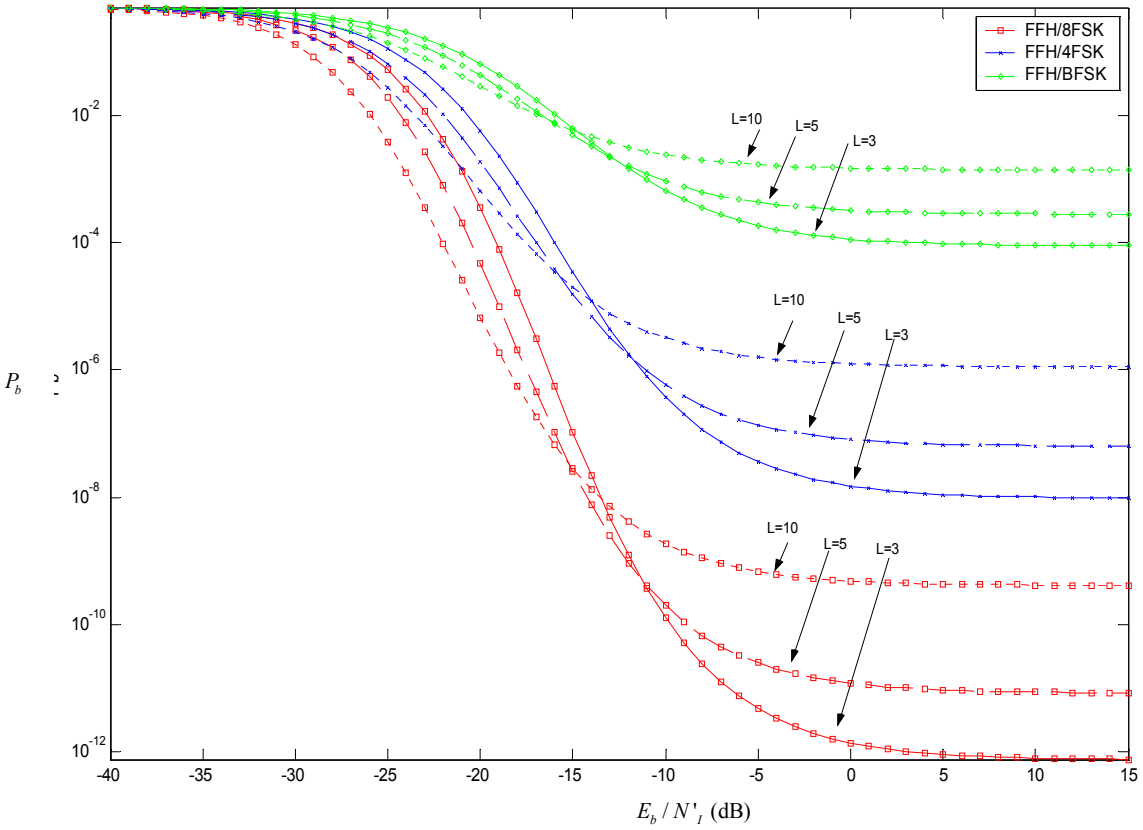

Figure 10. Effect of the BNJ in the Performance of a FFH/MFSK System for L=3,5,10 and N=400.

In order to be consistent with the examination of other jamming strategies and to have comparable results, the total SS bandwidth of the system will remain constant for all the modulation orders M. The noise will be considered as $N_I / 2$ for the given bandwidth. In that case Equation (3.30) can be used, as it is independent from the number of frequency hop bands N.

In Figure 11 the performance of the BNJ is presented for different modulation orders M and for a constant PSD for the given bandwidth. The results will be compared with the simulation results in Chapter V.

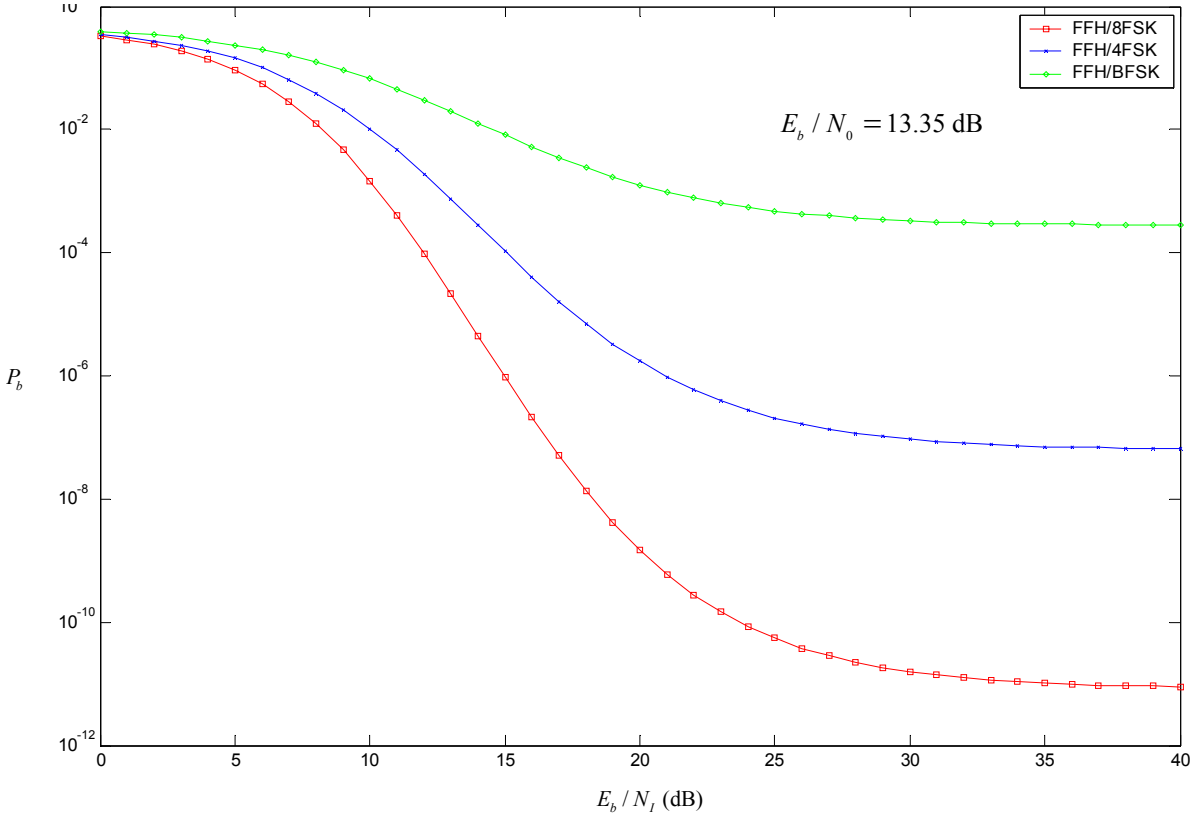

Figure 11. Effect of the BNJ in the Performance of a FFH/MFSK System for Modulation Order M=2,4,8, Diversity Order L=5 and the Same SS Bandwidth.

In order to have the same bandwidth for all modulation orders, we use the same number of frequency hop bands for FFH/BFSK and FFH/4FSK, but a different number of frequency hop bands for the FFH/8FSK. The assumption of fixed SS bandwidth is more realistic because military communications systems have specific frequency bands that are allocated and can be utilized.

In conclusion, the BNJ strategy for the FFH/MFSK systems is considered the least effective jamming technique. The reason is that the jammer does not have any information about the instantaneous frequency of the frequency hop pulse. This forces the jammer to distribute its power to all the frequency spectrum that the SS system uses. As

the number of hop bands and the modulation order increases, the performance of the jammer decreases. The performance of BNJ will be used as a benchmark against more intelligent jammers.

In the following sections the two principal types of intelligent but non–adaptive FH jamming threats [3], namely partial–band noise and multitone band jamming, will be presented. For these types of intelligent jammers, it is assumed that they have a priori knowledge of all relative signal parameters, with the critical exception of real–time PN spreading sequence synchronization. Specifically the jammer has the ability to optimize its strategy to exploit information about W_T, M, N, R_b, R_h, the location of the FH tones, the detection metric, the signal power, and the nominal P_b.

3. Partial Band Jammer Against a FFH/MFSK Communication System

In partial–band noise jamming strategy (PBJ), the jammer spreads its available power over a portion of the entire spread spectrum bandwidth. This strategy is considered moreeffective than BNJ because the jammer uses less bandwidth and more power for the given bandwidth.

Usually jammers can produce, with the help of a waveform generator, pulses containing noise with variable bandwidth.

The partial–band interference is modeled as additive Gaussian noise and is assumed to corrupt only a fraction ρ, where $1 \geq \rho > 0$, of the entire spread–spectrum bandwidth at one time. The partial–band interference is assumed to be present in each branch of the MFSK receiver. In addition, the fraction of the spread–spectrum bandwidth experienced partial–band interference is assumed to be the same for all hops of a symbol.

One major advantage of the frequency–hopping technique is that it can avoid certain frequency bands that it determines as particularly noisy [3]. Consequently, it is assumed (seen in Figure 12) that the intelligent jammer hops the jammed band over W_T. This transition is slow relative to the FH hop rate R_h, but fast enough to deny the FH system the chance to detect that it is being jammed and to take remedial action. Also, to

simplify the analysis, it is assumed that the shifts in the jammed band coincide with carrier hop transitions, so the channel is considered stationary over each hop. Furthermore, on a given hop, each N hop band lies entirely inside or outside W_T.

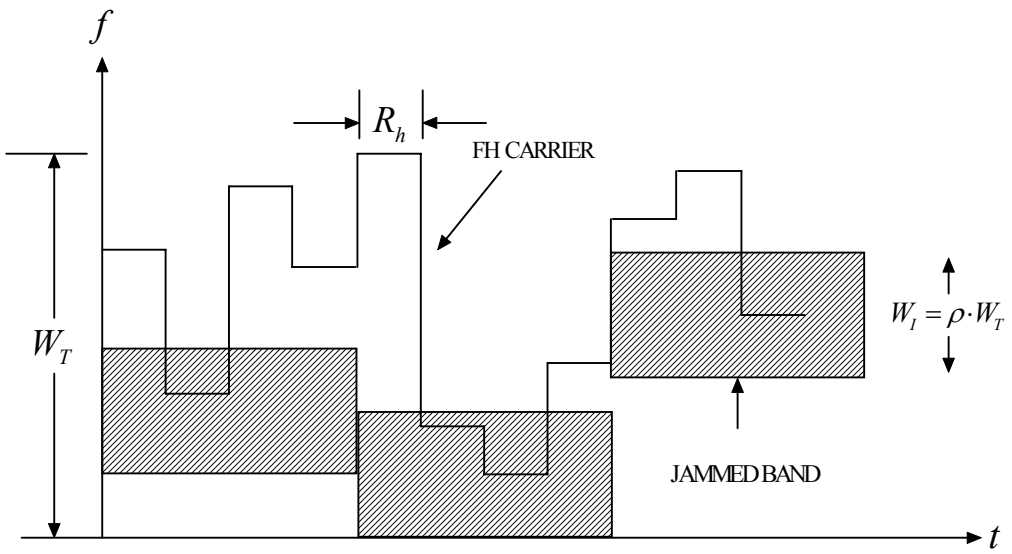

Figure 12. Partial–Band Noise Jamming of FFH System Where Jammer Hops the Noise Band to Prevent FFH Band Avoidance Countermeasure.

From the previous analysis for BNJ it was defined that the average power spectral density of narrowband interference for the entire bandwidth is $N_I / 2$. Then the power spectral density of the partial–band jamming for the given jamming bandwidth is

$$S'_{n_I}(f) = \frac{N_I}{2 \cdot \rho}. \tag{3.39}$$

The total jamming power is considered the same whether the jammer is using a barrage or a partial–band jamming technique.

This analysis also includes thermal and other wideband noises that corrupt the channel and modeled as AWGN. The power spectral density of the noise was previously defined as $N_0 / 2$. Thus, the power spectral density of the total noise is $\frac{N_I}{2 \cdot \rho} + \frac{N_0}{2}$ when partial–band jamming is present and is $N_0 / 2$ otherwise.

According to Reference [1], there is a practical limitation in PBJ because the jammer may not be able to transmit the peak power $\frac{N_I}{2 \cdot \rho}$ then ρ is too small. One other limitation is that the jammer cannot jam less than one frequency hop band. This leads to

$$1 \geq \rho \geq \frac{1}{N}. \tag{3.40}$$

For the case of a square–law linear combining receiver, there is no information for the jamming state (side information). In that case, the jammed hops have just as much weight in the overall decision statistics as unjammed hops do, and in case of partial–band noise jamming, the system behaves worse [7] without the appropriate error control coding scheme.

This becomes apparent for the case of FFH/BFSK with a square–law linear combining receiver. Reference [10] indicates that the error performance of FFH is worsened when the bit energy is fixed and diversity L is increased. This happens due to the dominance of increased noncoherent combining losses for higher values of L for this type of receiver. Figure 13 shows the improvement in performance for the jammer for different values of L, assuming that $E_b / N_0 = 13.35$ dB. This is the value of energy bit–to–noise ratio that will be used in the simulation model in Chapter V.

The only parameters that a PBJ can control are the E_b / N_I and the jammed fraction ρ. The partial–band noise jammer may select the fraction ρ and E_b / N_I in order to optimize the effect on the communication system.

The analytical performance of PBJ against the FFH/MFSK system is beyond the scope of this thesis. The results from Reference [10] will be used in order to confirm the simulation results from Chapter V.

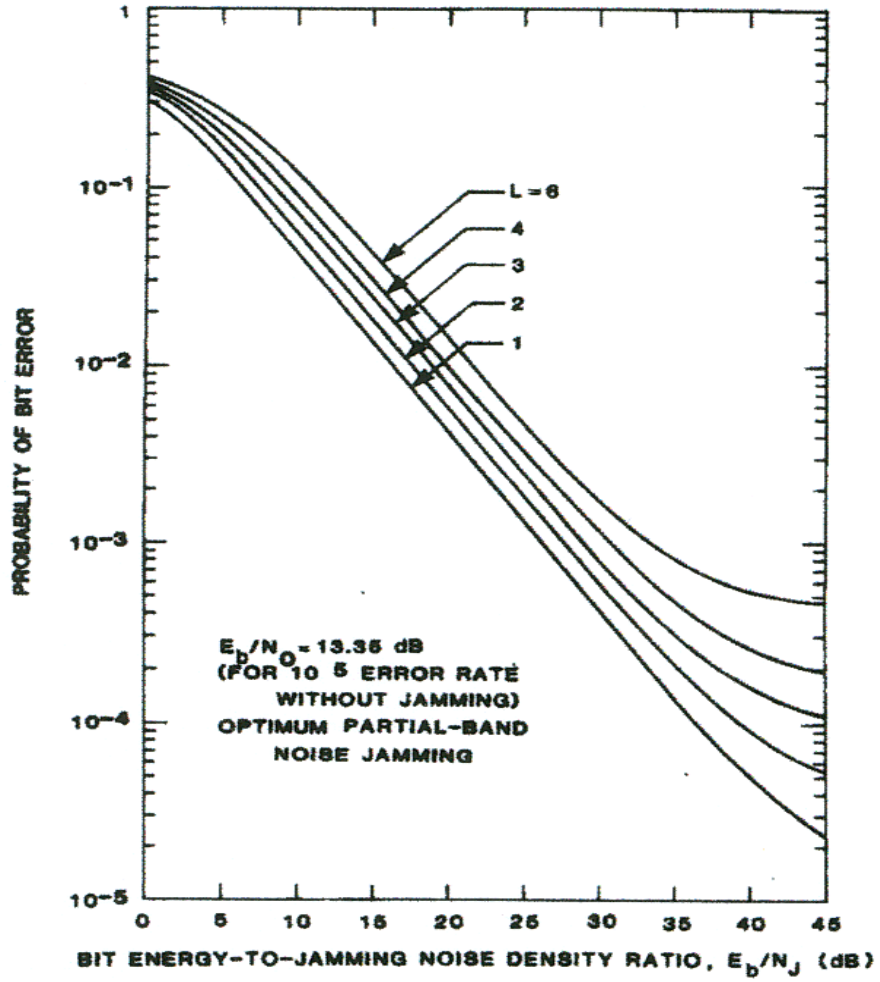

Figure 13. Optimal Performance of PBJ in a FFH/BFSK System for Different Diversity Order L from Reference [10].

Figure 14 illustrates the optimum fraction ρ for the PBN jammer for different L. Note that for $L > 3$, the optimum fraction remains fairly constant for a given ratio of signal–to–jamming power.

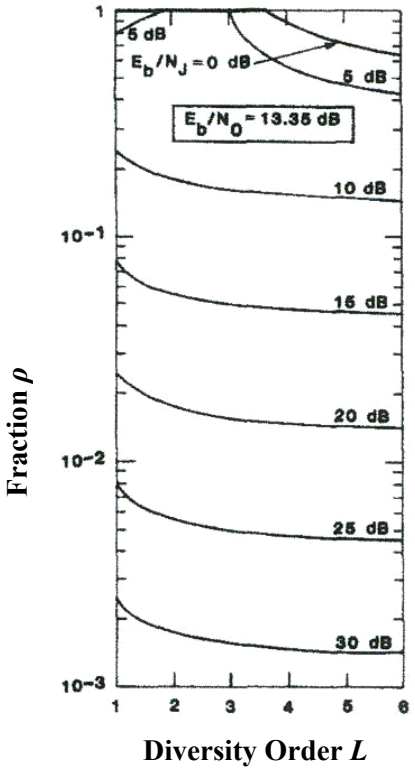

Figure 14. Optimum Fraction ρ versus Diversity Order L when $E_b / N_0 = 13.35$ dB with E_b / N_I as a Parameter from Reference [10]

Table 2 also presents the values of optimum fraction ρ for different values of E_b / N_I given that the number of frequency hop bands $N = 483$. This is the number of frequency hop bands that will be used in the simulation model of the FFH/BFSK system.

The parameter μ also defines the closest integer value of the $\rho \cdot N$ given that it must be $1 \le \mu \le N$.

$E_b / N_I \quad (dB)$	ρ	$\rho \cdot N$	μ
0	0.8	386.4	386
5	0.45	217.35	217
10	0.16	77.28	77
15	$5.6 \cdot 10^{-2}$	27.048	27
20	$1.5 \cdot 10^{-2}$	7.245	7
25	$5 \cdot 10^{-3}$	2.415	2
30	$1.5 \cdot 10^{-3}$	0.7245	1

Table 2. Optimum Fraction ρ for FFH/BFSK System for N=483.

Reference [10] indicates that in an FFH system, the noncoherent "combining losses," play a predominant role and, hence, when the bit energy is constrained, the error performance is further degraded as L increases. This conclusion is also valid for all modulation orders. As expected, in the general case, where both jamming noise and thermal noise were present, the "bottoming out" effect was observed in the region where the jamming power was weaker than the signal power.

In conclusion, the PBN jammer has better performance than the BNJ and the FFH/MFSK system provides no diversity improvement for this type of receiver.

4. Multitone Band Jammer Against an FFH/MFSK Communication System

The second class of intelligent jammers is the multitone or CW tone interference jammers. In this category, the jammer divides its total power P_I into q distinct, equal power, random phase CW tones. Every jamming tone can be expressed as

$$J(t) = \sqrt{2}a_I \cdot \cos\left(2\pi f_I t + \phi_I\right), \tag{3.41}$$

where a_I is the amplitude of the tone and ϕ_I is again the random phase. Each of the jamming tones [7] will then have power:

$$P_{I_T} = \frac{P_I}{q}, \tag{3.42}$$

where P_I is the total available power of the jammer. Every jamming tone is spaced from the other at least by W_{Band} Hz. An equivalent MTJ power spectral density is defined as:

$$N_I = \frac{P_I}{W_T}. \tag{3.43}$$

There are two types of multitone jamming strategies: the band multitone and the independent multitone jamming. The independent multitone jamming (IMTJ) technique distributes the jamming tones randomly across the entire frequency–hopped bandwidth with the number of jamming tones within the hop band varying from zero to M.

In multitone band jamming (MTBJ), the jamming tones are distributed randomly across the entire SS signal bandwidth W_T with at most only one jamming tone per frequency hop bin. So

$$1 \le q \le N . \tag{3.44}$$

This thesis examines the MTBJ case because it is considered more effective than the IMTJ [7].

The frequency f_I of the jamming tones are assumed to coincide exactly with one of the hopping frequencies at the *M*–ary band, as Figure 15 indicates. In order for the jammer to be effective, it must understand the structure of the signal. If the jammer cannot verify the structure of the system, then this jamming strategy is worthless in an FFH system.

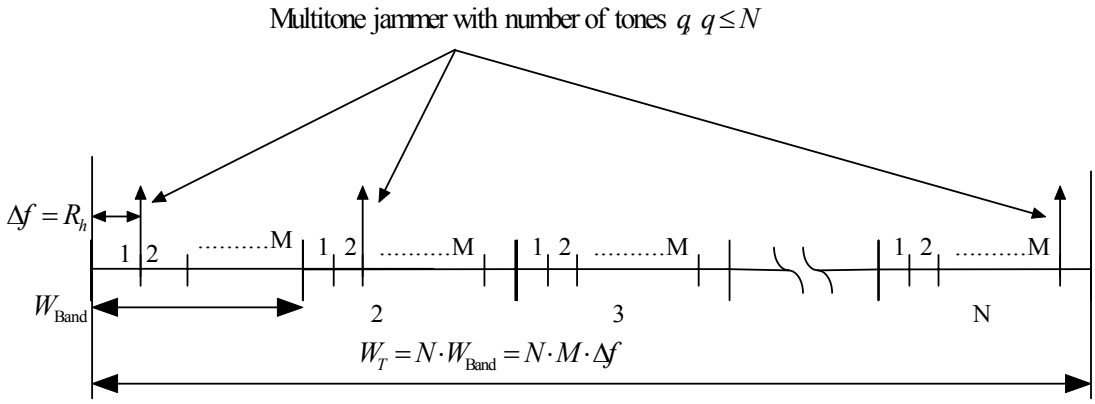

Figure 15. Multitone Band Jamming Representation in an FFH/MFSK System.

Again, for this type of jamming, the receiver does not know if the transmitted hop frequencies are jammed or not. The symbol energy E_s for the FFH/MFSK system is also considered as a constant.

In our analyses the thermal noise is modeled again as additive white Gaussian noise (AWGN) with two–sided spectral density $N_0 / 2$.

As in the previous section, the probability of bit error for the optimum case of MTBJ against the FFH/BFSK system derives from Reference [11].

In Figure 16 the performance of the jammer for different diversity level L is illustrated with the signal–to–noise ratio $E_b / N_0 = 13.35$ dB.

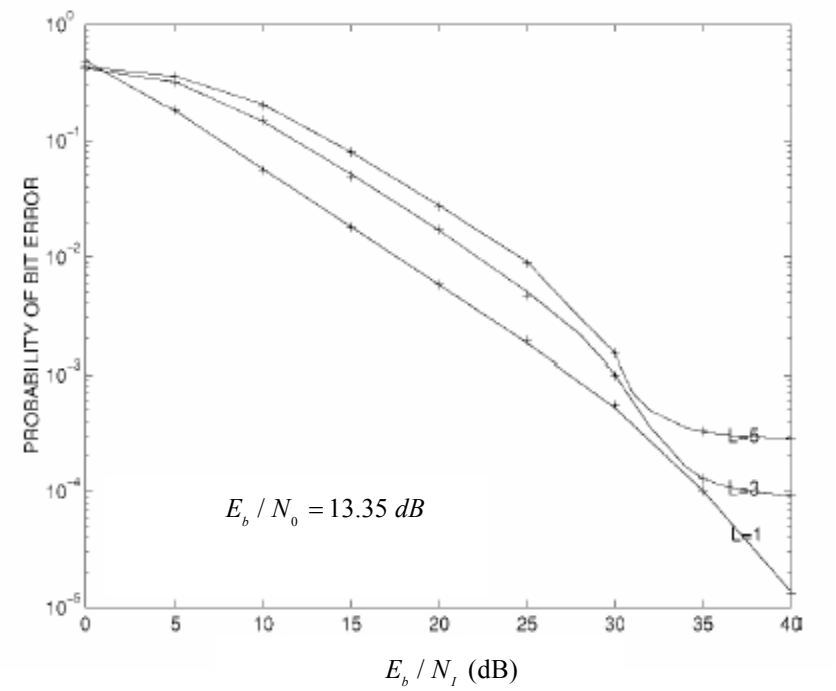

Figure 16. Optimal Performance of MTBJ in a FFH/BFSK System for Different Diversity Order *L* [11].

Again it is observed that as the diversity level L increases, the performance of the jammer improves for the optimum case of multitone band jamming.

Comparing Figures 13 and 16 for the FFH/BFSK system, the optimum MTBJ strategy appears to have a slightly better performance than the optimum PBJ strategy.

The disadvantage of the MTBJ technique is that the jammer must know the signal's full structure in order to interfere with the system.

In all strategies, the performance of the jammer improves as the diversity order also increases, due to the dominance of the noncoherent "combining losses," assuming that the interference noise density remains constant for the SS bandwidth.

A full comparison for all jamming strategies and different modulation orders is examined in Chapter V using simulation software.

IV. THEORETICAL ANALYSIS FOR AN FFH/MFSK SYSTEM IN A RAYLEIGH FADING CHANNEL

The previous chapter described the performance of different jamming strategies against a an FFH/MFSK system in a Gaussian channel. The primarily impairment in the Gaussian channel model was noise which is characterized as AWGN.

This chapter describes the performance of an FFH/MFK system with a square–law linear combining receiver in a fading multipath channel.

Generally, the fading channels can significantly degradate the performance of a communication system. The fast frequency–hopping technique that involves diversity is one of the methods that is used to overcome the consequences of a fading channel.

A. CHANNEL MODEL DESCRIPTION AND SYMBOLOGY USED

The received signal's amplitude, in a fading channel, fluctuates and can no longer be modeled as a deterministic parameter but only as a random variable [7].

There are two widely used channel models for a fading channel. The first is the Ricean fading channel and the other is the Rayleigh fading channel. The Rayleigh channel is considered a special case of the Ricean channel.

The Ricean channel model is used in a line–of–sight case between the transmitter and the receiver, where a portion of the received signal power is due to multipath. In the Rayleigh channel model there is no line–of–sight between the transmitter and the receiver, and the entire received signal's power is due to multipath.

In this chapter the smallest spacing between the frequency hop bands is larger than the coherence bandwidth of the channel. As a result, each hop of a symbol experiences independent fading.

In addition, the channel for each hop of a symbol is modeled as a frequency–nonselective, slowly fading Rayleigh process. This implies that the signal bandwidth is much smaller than the coherence bandwidth of the channel and that the hop duration T_h is much smaller than the coherence time of the channel [12]. The latter assumption is

equivalent to requiring the hop rate to be large compared to the Doppler spread of the channel. As a result, the signal amplitude can be modeled as a Rayleigh random variable that remains fixed at least for the duration of a single hop.

The PDF of the received amplitude for the Rayleigh channel derives from

$$f_{A_{C_k}}\left(a_{C_k}\right)=\frac{a_{C_k}}{{\sigma_R}^2}\cdot e^{\left(-\frac{a^2{}_{C_k}}{2{\sigma_R}^2}\right)}\cdot u\left(a_{C_k}\right), \tag{4.1}$$

where $2{\sigma_R}^2$ is the power of the diffuse signal component of the respective tone.

B. PERFORMANCE OF AN FFH/MFSK SYSTEM IN A RAYLEIGH FADING CHANNEL WITH AWGN

From the previous analysis for the Gaussian channel the probability of a symbol error from Equation (3.13) is given:

$$\begin{aligned} P_s &= 1-P_c \\ &= 1-\int_0^{\infty} f_{V_1}\left(v_1\,|\,1\right)\left[\int_0^{v_1} f_{V2}\left(v_2\,|\,1\right)dv_2\right]^{M-1} dv_1. \end{aligned} \tag{4.2}$$

This is the general case for both fading and non–fading channels as long as the noise of the channel is characterized as AWGN.

As before, a derivation of the PDFs $f_{V_1}\left(v_1\,|\,1\right)$ and $f_{V_2}\left(v_2\,|\,1\right)$ must be made in the output of the diversity combiner for every branch before the decision of which symbol has been transmitted.

From the previous analysis, the PDF of the random variable that represents the output of the branch not containing the signal is described by:

$$f_{V_2}\left(v_2\,|\,1\right)=\frac{{v_2}^{L-1}}{\left(2\sigma_k^2\right)^L\left(L-1\right)!}e^{-\frac{v_2}{2\sigma_k^2}}\cdot u\left(v_2\right). \tag{4.3}$$

The channel fading has no effect on the output of branches that do not contain the signal [12]. Therefore Equation (4.3) of the PDF can be used in our primary Equation (4.2) without modification.

The probability density function $f_{V_1}\left(v_1 \mid 1\right)$, before diversity combining, is now conditioned upon the received hop's amplitude α_{C_k}. This conditional PDF can be expressed as:

$$f_{V_{1_k}}\left(v_{1_k} \mid 1, a_{C_k}\right) = \frac{1}{\left(2\sigma_k^2\right)} e^{-\frac{v_{1_k}+2a^2{}_{C_k}}{2\sigma_k^2}} \cdot I_0\left(\frac{a_{C_k} \cdot \sqrt{2v_{1_k}}}{\sigma_k^2}\right) \cdot u\left(v_{1_k}\right), \tag{4.4}$$

where $u(\bullet)$ is the unit step function and $I_0(\bullet)$ is the modified Bessel function of the first kind and order zero. The conditioning on a_{C_k} must be removed by evaluating:

$$f_{V_{1_k}}\left(v_{1_k} \mid 1\right) = \int_0^\infty f_{V_{1_k}}\left(v_{1_k} \mid 1, a_{C_k}\right) \cdot f_{A_{C_k}}\left(a_{C_k}\right) da_{C_k}. \tag{4.5}$$

The average received signal power is

$$\overline{s^2(t)} = \overline{a_{C_k}{}^2} = 2\sigma_R{}^2. \tag{4.6}$$

The ratio of the average energy per diversity reception–to–noise power spectral density is given in Reference [7]:

$$\overline{\gamma_h} = \frac{2\sigma_R^2}{\sigma_k^2}. \tag{4.7}$$

Inserting Equations (3.15) and (4.6) into (4.7) gives:

$$\overline{\gamma_h} = \frac{\overline{a_{C_k}^2}}{N_0} T_h. \tag{4.8}$$

Reference [2] indicates that the average energy per bit–to–noise ratio is

$$\overline{\gamma_b} = \frac{L}{\log_2 M}\overline{\gamma_h}, \tag{4.9}$$

where M indicates the modulation order.

Inserting Equations (4.1) and (4.4) into Equation (4.5) and rearranging the terms gives the following expression for the PDF:

$$f_{V_{1_k}}\left(v_{1_k}\,|1\right) = \frac{1}{2\sigma_k^2\cdot{\sigma_R}^2}\cdot e^{\left(-\frac{v_{1_k}}{2{\sigma_k}^2}\right)}\int_0^\infty a_{C_k}\cdot e^{\left[-\alpha_{c_k}^2\cdot\left(\frac{1}{{\sigma_k}^2}+\frac{1}{2{\sigma_R}^2}\right)\right]}\cdot I_0\left(\frac{a_{c_k}\cdot\sqrt{2v_{1_k}}}{\sigma_k^2}\right)da_{C_k}. \tag{4.10}$$

According to Reference [7] the PDF expression simplifies as follow:

$$f_{V_{1_k}}\left(v_{1_k}\,|1\right) = \frac{1}{2\left(\sigma_k^2+2{\sigma_R}^2\right)}\cdot e^{\left[-\frac{1}{2}\left(-\frac{v_{1_k}}{{\sigma_k}^2+2{\sigma_R}^2}\right)\right]}u\left(v_{1_k}\right). \tag{4.11}$$

Equation (4.11) has the same form as Equation (3.16) if we substitute $\sigma_k^2+2{\sigma_R}^2$ for σ_k^2 and v_{1_k} for v_{2_k} respectively. Exploiting this similarity, the PDF for the branch that contains the signal–in the output of diversity combining–can derive substituting in Equation (3.18) again $\sigma_k^2+2{\sigma_R}^2$ for σ_k^2 and v_{1_k} for v_{2_k} respectively.

Following this substitution the conditional PDF for the random variable v_1 becomes:

$$f_{V_1}\left(v_1\,|1\right) = f^{\otimes L}{}_{V_{1_k}}\left(v_{1_k}\,|1\right) = \frac{{v_1}^{L-1}}{\left[2\left({\sigma_k}^2+2\sigma_R^2\right)\right]^L\left(L-1\right)!}e^{\frac{-v_1}{2\left({\sigma_k}^2+2\sigma_R^2\right)}}\cdot u\left(v_1\right). \tag{4.12}$$

By combining Equations (3.46), (3.55) and (4.2) the symbol error probability can be expressed as:

$$P_s = 1 - \int_0^{\infty} \frac{{v_1}^{L-1}}{\left[2\left({\sigma_k}^2 + 2\sigma_R^2\right)\right]^L (L-1)!} e^{\frac{-v_1}{2\left({\sigma_k}^2+2\sigma_R^2\right)}} \left[\int_0^{v_1} \frac{{v_2}^{L-1}}{\left(2{\sigma_k}^2\right)^L (L-1)!} e^{\frac{-v_2}{2{\sigma_k}^2}} dv_2\right]^{M-1} dv_1$$

$$= 1 - \int_0^{\infty} \frac{{v_1}^{L-1}}{\left[2\left({\sigma_k}^2 + 2\sigma_R^2\right)\right]^L (L-1)!} e^{\frac{-v_1}{2\left({\sigma_k}^2+2\sigma_R^2\right)}} \left[1 - e^{\frac{-v_1}{2{\sigma_k}^2}} \sum_{n=0}^{L-1} \frac{v_1^n}{\left(2{\sigma_k}^2\right)^n n!}\right]^{M-1} dv_1. \tag{4.13}$$

Regrouping the terms of Equation (4.13) results in:

$$P_s = 1 - \int_0^{\infty} \frac{\frac{{v_1}^{L-1}}{\left(2{\sigma_k}^2\right)^L}}{\left[1 + \frac{2\sigma_R^2}{{\sigma_k}^2}\right]^L (L-1)!} e^{\frac{-\left(\frac{v_1}{2{\sigma_k}^2}\right)}{1+\frac{2\sigma_R^2}{{\sigma_k}^2}}} \left[1 - e^{\frac{-v_1}{2{\sigma_k}^2}} \sum_{n=0}^{L-1} \frac{v_1^n}{\left(2{\sigma_k}^2\right)^n n!}\right]^{M-1} dv_1$$

$$= 1 - \int_0^{\infty} \frac{\left(\frac{v_1}{2{\sigma_k}^2}\right)^{L-1}}{\left[1 + \frac{2\sigma_R^2}{{\sigma_k}^2}\right]^L (L-1)!} e^{\frac{-\left(\frac{v_1}{2{\sigma_k}^2}\right)}{1+\frac{2\sigma_R^2}{{\sigma_k}^2}}} \left[1 - e^{\frac{-v_1}{2{\sigma_k}^2}} \sum_{n=0}^{L-1} \left(\frac{v_1}{2{\sigma_k}^2}\right)^n \cdot \frac{1}{n!}\right]^{M-1} \frac{dv_1}{2{\sigma_k}^2}. \tag{4.14}$$

By setting

$$\frac{v_1}{2{\sigma_k}^2} = x \Rightarrow \frac{dv_1}{2{\sigma_k}^2} = dx, \tag{4.15}$$

and combining Equations (4.8) and (4.9) with Equation (4.15), the probability of symbol error is expressed as [2]:

$$P_s = 1 - \int_0^{\infty} \frac{(x)^{L-1}}{\left[1 + \frac{\log_2 M \cdot \overline{\gamma_b}}{L}\right]^L (L-1)!} e^{\frac{-(x)}{1+\frac{\log_2 M \cdot \overline{\gamma_b}}{L}}} \left[1 - e^{-x} \sum_{n=0}^{L-1} (x)^n \cdot \frac{1}{n!}\right]^{M-1} dx. \tag{4.16}$$

The symbol error rate P_s may be converted to an equivalent bit error rate by using Equation (3.25). This results in a probability of bit error as follows:

$$P_b = \frac{M}{2(M-1)}\left\{1 - \int_0^{\infty} \frac{(x)^{L-1}}{\left[1+\frac{\log_2 M \cdot \overline{\gamma_b}}{L}\right]^L (L-1)!} e^{\frac{-(x)}{1+\frac{\log_2 M \cdot \overline{\gamma_b}}{L}}} \left[1 - e^{-x}\sum_{n=0}^{L-1}(x)^n \cdot \frac{1}{n!}\right]^{M-1} dx\right\}. \quad (4.17)$$

The resulting analytic expression is extremely complicated, so a numerical evaluation is preferable to an analytical solution.

Figures 17 and 18 illustrate the performance of an FFH/MFSK system for different diversity level $L = 3,5,10$ and different modulation order $M = 2,4,8$ respectively. The bit rate remains fixed and consequently the energy of every transmitted bit also remains fixed for the different examined cases.

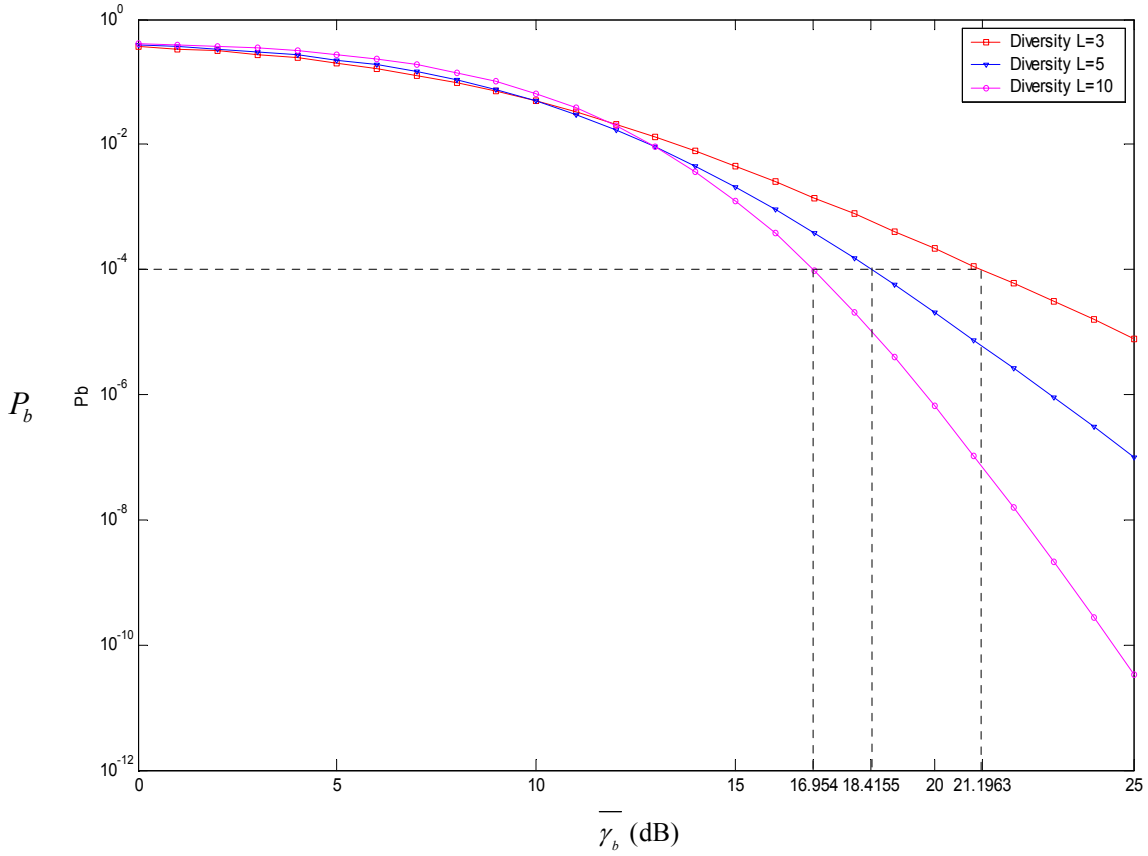

Figure 17. Performance of an FFH/BFSK System in a Rayleigh Channel for Diversity Order *L*=3,5,10.

The FFH/MFSK system behaves differently in a nonselective slow fading Rayleigh channel as compared to a channel with no fading (AWGN only).

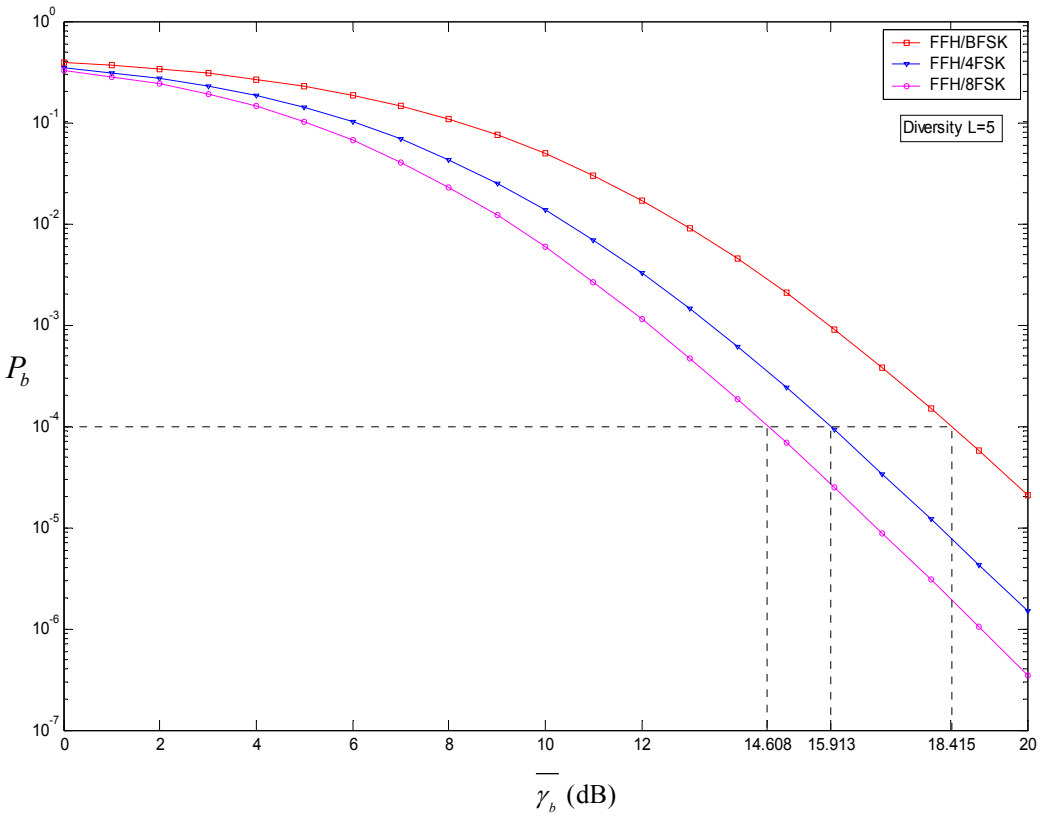

Figure 18. Performance of an FFH/MFSK for Modulation Order *M*=2,4,8 and Diversity Order *L*=5.

As can be concluded from Figures 17 and 18, performance improves significantly when the diversity order L and the modulation order M is increased [2]. For example, when the diversity order L is increased from 3 to 5 for a probability of bit error $P_b = 10^{-4}$, a gain of 2.78 dB for the average energy per bit–to–noise ratio can be obtained. This is a significant gain for an FFH/MFSK system using diversity.

Another important observation is that as the modulation order *M* increases, performance can be improved. For example, in order to achieve a bit error rate of $P_b = 10^{-4}$ a FFH/4FSK system needs 2.5 dB less than the corresponding FFH/BFSK system for the same diversity order *L*.

Generally, an increase in diversity order L seems more efficient than a corresponding increase in the modulation order M, as Reference [2] indicates.

The next section presents the performance of an FFH/MFSK system under the influence of barrage jamming in a nonselective slow fading Rayleigh channel. This analysis will serve as a benchmark for other jamming techniques in future work.

C. PERFORMANCE OF BARRAGE NOISE JAMMER AGAINST AN FFH/MFSK SYSTEM IN A RAYLEIGH FADING CHANNEL

In BNJ, the jammer has knowledge only about the portion of the frequency spectrum that an FFH/MFSK system occupies. This information can be easily derived after observing the spread spectrum signal's behavior.

This method is considered the least efficient jamming method because the jammer is forced to spread its power to the entire bandwidth of the fast frequency–hopping system. This method, as before, is the initial step for the comparison with other jamming techniques.

In BNJ, the jammer increases the total noise power that corrupts each received hop pulse. Thus, the noise power at the integrator output for each hop can be expressed as:

$$\sigma_k^2 = \sigma_0^2 + \sigma_I^2, \tag{4.18}$$

where σ_k^2 is the noise power of a jammed hop, σ_0^2 is the AWGN noise power and σ_I^2 is the jamming noise power. Analytically these can be expressed as:

$$\sigma_0^2 = \frac{N_0}{T_h}, \tag{4.19}$$

and

$$\sigma_I^2 = \frac{N_I}{T_h}, \tag{4.20}$$

where N_0 and N_I are the noise PSDs of the AWGN and the jamming signal respectively.

Combining Equations (3.25), (4.14) and (4.15) gives the following expression for the probability of bit error:

$$P_b = \frac{M}{2(M-1)}\left\{1-\int_0^{\infty}\frac{(x)^{L-1}}{\left[1+\frac{2\sigma_R^2}{\sigma_k^2}\right]^L (L-1)!}e^{\frac{-(x)}{1+\frac{2\sigma_R^2}{\sigma_k^2}}}\left[1-e^{-x}\sum_{n=0}^{L-1}(x)^n\cdot\frac{1}{n!}\right]^{M-1}dx\right\}. \quad (4.21)$$

Inserting Equations (4.6) and (4.19) into (4.22) the expression for the probability of bit error becomes:

$$P_b = \frac{M}{2(M-1)}\left\{1-\int_0^{\infty}\frac{(x)^{L-1}}{\left[1+\frac{\overline{\alpha_{C_k}^2}T_h}{(N_0+N_I)}\right]^L (L-1)!}e^{\frac{-(x)}{1+\frac{\overline{\alpha_{C_k}^2}T_h}{(N_0+N_I)}}}\left[1-e^{-x}\sum_{n=0}^{L-1}(x)^n\cdot\frac{1}{n!}\right]^{M-1}dx\right\}. \quad (4.22)$$

Rearranging the terms of (4.23) in a more convenient way we can express the P_b as:

$$P_b = \frac{M}{2(M-1)} \times\left\{1-\int_0^{\infty}\frac{(x)^{L-1}}{\left[1+\frac{\log_2 M}{L}\left(\left(\overline{\gamma_b}\right)^{-1}+\left(\overline{\gamma_I}\right)^{-1}\right)^{-1}\right]^L (L-1)!}e^{\frac{-(x)}{1+\frac{\log_2 M}{L}\left(\left(\overline{\gamma_b}\right)^{-1}+\left(\overline{\gamma_I}\right)^{-1}\right)^{-1}}}\left[1-e^{-x}\sum_{n=0}^{L-1}(x)^n\frac{1}{n!}\right]^{M-1}dx\right\}, \quad (4.23)$$

where

$$\overline{\gamma_b} = \frac{L}{\log_2 M}\frac{\overline{a_{C_k}^2}T_h}{N_0}, \quad (4.24)$$

and

$$\overline{\gamma_I} = \frac{L}{\log_2 M}\frac{\overline{a_{C_k}^2}T_h}{N_I}, \quad (4.25)$$

since $\overline{\gamma_b}$ is the average energy per bit–to–noise ratio and $\overline{\gamma_I}$ is the average energy per bit –to–jamming power ratio for the FFH/MFSK system.

The power density of the BNJ for the conventional MFSK, $N_I^{'}$, is related with the corresponding jamming power density for the FFH/MFSK, N_I, by Equation (3.37):

$$N_I = \lambda \cdot N_I^{'}, \tag{4.26}$$

where

$$\lambda = \frac{1}{N}\frac{(M+1)}{M \cdot L}. \tag{4.27}$$

Combining Equations (4.26) and (4.27) into Equation (4.24) results in:

$$P_b = \frac{M}{2(M-1)} \times \left\{ 1 - \int_0^{\infty} \frac{(x)^{L-1}}{\left[1 + \frac{\log_2 M}{L}\left(\left(\overline{\gamma_b}\right)^{-1} + \lambda\left(\overline{\gamma'_I}\right)^{-1}\right)^{-1}\right]^{L} (L-1)!} e^{\frac{-(x)}{1+\frac{\log_2 M}{L}\left(\left(\overline{\gamma_b}\right)^{-1} + \lambda\left(\overline{\gamma'_I}\right)^{-1}\right)^{-1}}} \left[1 - e^{-x}\sum_{n=0}^{L-1}(x)^n \frac{1}{n!}\right]^{M-1} dx \right\}, \tag{4.28}$$

where $\overline{\gamma'_I}$ is the average energy per bit –to–jamming power spectral density for the conventional MFSK system.

Equation (4.28) indicates the highly dependence of the FFH/MFSK from the number of frequency hop bins *N*, the diversity order L, and the modulation order M.

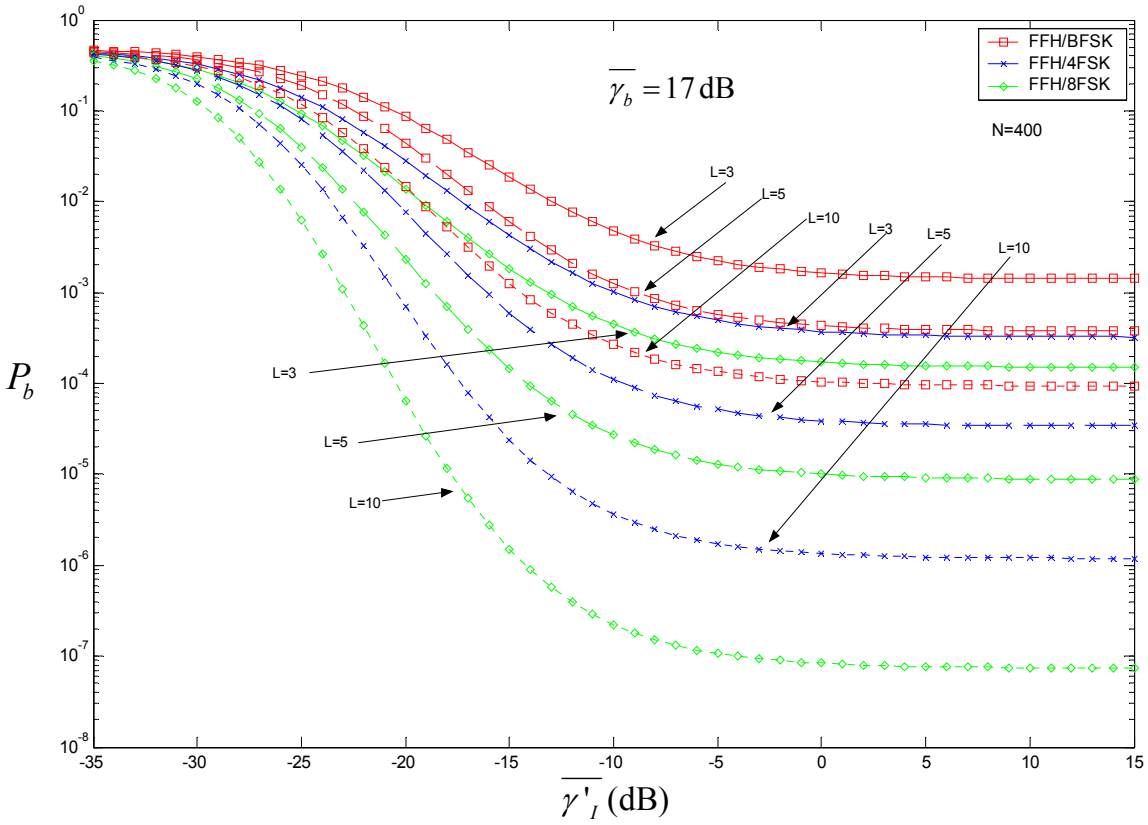

Figure 19. Effect of the BNJ in the Performance of a FFH/MFSK System in a Rayleigh Channel for L=3,5,10 and N=400.

In Figure 19, the probability of bit error has been plotted with L and M as parameters for the same number of frequency hop bands N. It is obvious that higher modulation order M and greater diversity order L deteriorates the performance of the jammer and improves the performance of the FFH/MFSK system.

The drawback for greater values of L, M and N is the necessary increase of the signal's bandwidth because the system uses orthogonal signaling and a fixed bit rate R_b. Table 3 presents the necessary SS bandwidth for a different modulation order M and diversity L, assuming that the frequency hop bands N and the R_b remain fixed. These calculations were made according to Equation (3.36) giving:

$$W_T = M \cdot N \cdot \frac{L \cdot R_b}{\log_2 M}. \tag{4.29}$$

	L=3	L=5	L=10
M=2	28,800,000 Hz	48,000,000 Hz	96,000,000 Hz
M=4	28,800,000 Hz	48,000,000 Hz	96,000,000 Hz
M=8	38,400,000 Hz	64,000,000 Hz	128,000,000 Hz

Table 3. Bandwidth of the FFH/MFSK System with $R_b = 12$ kbits/sec and N=400.

Figure 20 shows that as the numbers of frequency hop bands N increases, the performance of the jammer decreases. For a large average energy per bit–to–jamming ratio the P_b remains stable independently from the number of frequency hop bands N. The performance of the jammer is also influenced by the modulation order. As M increases, the ability of the jammer to jam the signal decreases.

Table 3 and Figure 20 reveal that the bandwidth for the same diversity order L and number of hop bands N is the same for the FFH/BFSK and FFH/4FSK system. The probability of bit error in that case decreases, improving the performance of the system without increasing the bandwidth of the signal.

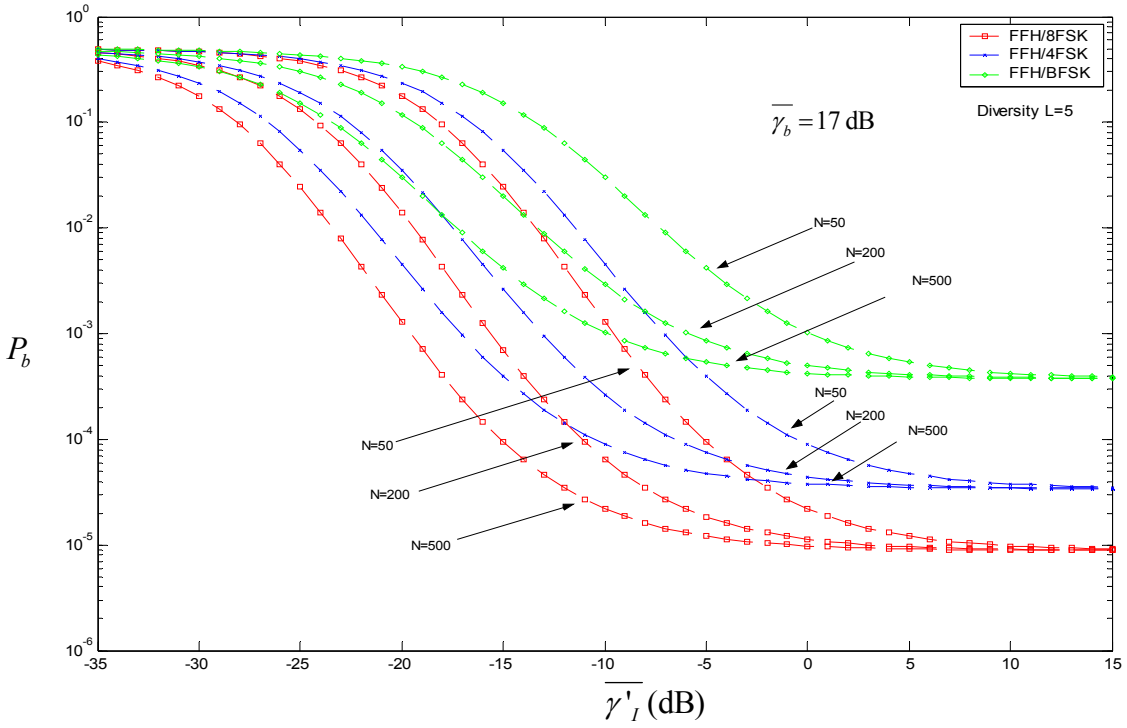

Figure 20. Effect of the BNJ in the Performance of an FFH/MFSK System in a Rayleigh Channel for N=50,200,500.

In order to compare the results from the mathematical analysis and the simulation analysis, we use Equation (4.23) to calculate the probability of bit error. Using this equation is also a necessity in order to compare the BNJ strategy with others jamming strategies in a future work.

Equation (4.23) is not dependent upon the number of frequency hop bands N because it is assumed that the SS bandwidth remains the same for all the modulation orders M. With this assumption, the SS bandwidth of the system remains fixed for every modulation order M.

The only difference between the curves of Figure 20 and Figure 21 is that there is a movement of the curves by $10 \cdot \log\left(\frac{1}{\lambda}\right)$ dB.

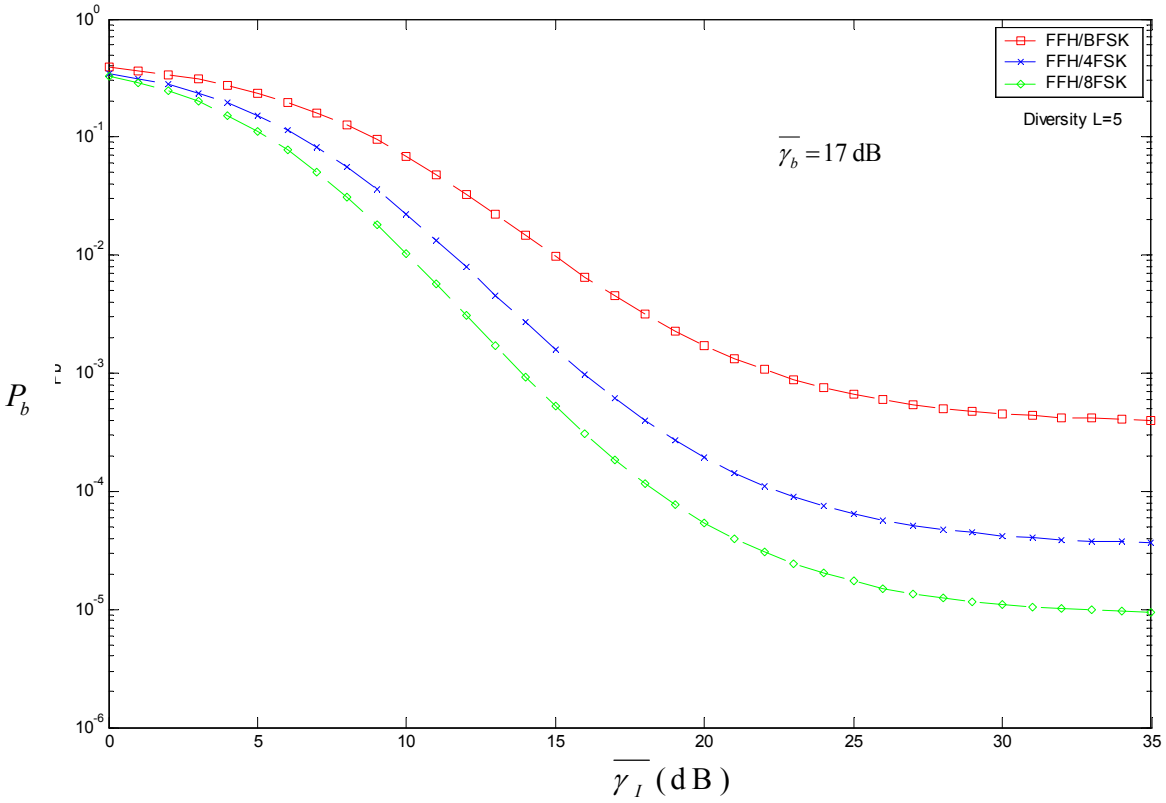

Figure 21. Effect of BNJ in an FFH/MFSK System for a Rayleigh Channel Independently from the Number of Hop Bands N.

To summarize, the BNJ strategy cannot be considered efficient enough because it does not degrade the system enough. The system can improve itself using greater

diversity order, a greater number of frequency hop bands and a greater modulation order. These disadvantages for the jammer will lead to the investigation of other forms of jamming, such as partial–band jamming and multitone band jamming.

Chapter V introduces the creation of two simulation channel environments. The first one is an FFH/MFSK system in a Gaussian channel, which is under the influence of different jamming strategies. The second simulation model environment is the FFH/MFSK system in a Rayleigh fading channel, which is used to investigate and to verify the results in Chapter IV. The simulation environments were created by using a relatively new software called SystemView.

V. SIMULATION RESULTS OF AN UNCODED NONCOHERENT FFH/MFSK SYSTEM UNDER THE INFLUENCE OF DIFFERENT JAMMING STRATEGIES

This chapter presents the simulation results for the FFH/MFSK system performance under the influence of different jamming strategies for a Gaussian channel model. A comparison will be made to determine which method degrades the system most.

The jamming modes that are simulated are the Barrage Noise Jamming (BNJ), the Partial Band Noise Jamming (PBJ), and the Multitone Band Jamming (MTBJ). The simulation results will be compared with the theoretical values only when available. As mentioned in Chapter III, the theoretical analysis of the performance of the FFH/MFSK under the influence of partial–band jamming and multitone band jamming is extremely complicated, so we are restricted to the simulation analysis.

All the simulations were generated with the help of a software package, which is called SystemView. SystemView is a comprehensive dynamic systems analysis environment for the design and simulation of engineering systems. It provides real–time signal analysis in the time and/or frequency domain.

The FFH/MFSK simulation scheme is used as a platform upon each type of jamming strategy is represented by adding the appropriate tokens.

A. UNCODED NONCOHERENT FFH/MFSK SIMULATION MODEL

The FFH/MFSK model was based on the model for slow frequency–hopping system from Reference [13]. This model was modified appropriately in order to support a fast frequency–hopping technique with a square–law linear combining receiver involving soft decision.

The construction of the FFH/MFSK model was made based on the assumptions that were made in the previous chapters.

The parameters of the FFH/MFSK were chosen under two basic assumptions. The first assumption was that the system has the same bandwidth as the VHF combat radios, which is approximately 60 MHz. The second assumption was that the information bit rate $R_b = 12000$ bits/s is very close to 16000 bits/sec, which is the usual bit rate for the combat radios.

	R_s	R_h	Δf	N	W_T	Frequency Range
FFH/BFSK	12000 bit/s	60000 h/s	60 kHz	483	57.960 MHz	31.14–89.1 MHz
FFH/4FSK	6000 sym/s	30000 h/s	30 kHz	483	57.960 MHz	31.14–89.1 MHz
FFH/8FSK	4000 sym/s	20000 h/s	20 kHz	363	58.080 MHz	31.1–89.18 MHz

Table 4. Operational Characteristics of the FFH/MFSK Simulation Model for Diversity Order L=5 and Bit Rate $R_b = 12000$ bits/s .

The overall block diagrams of the noncoherent FFH/BFSK and FFH/4FSK is shown in Figures 22 and 23, respectively.

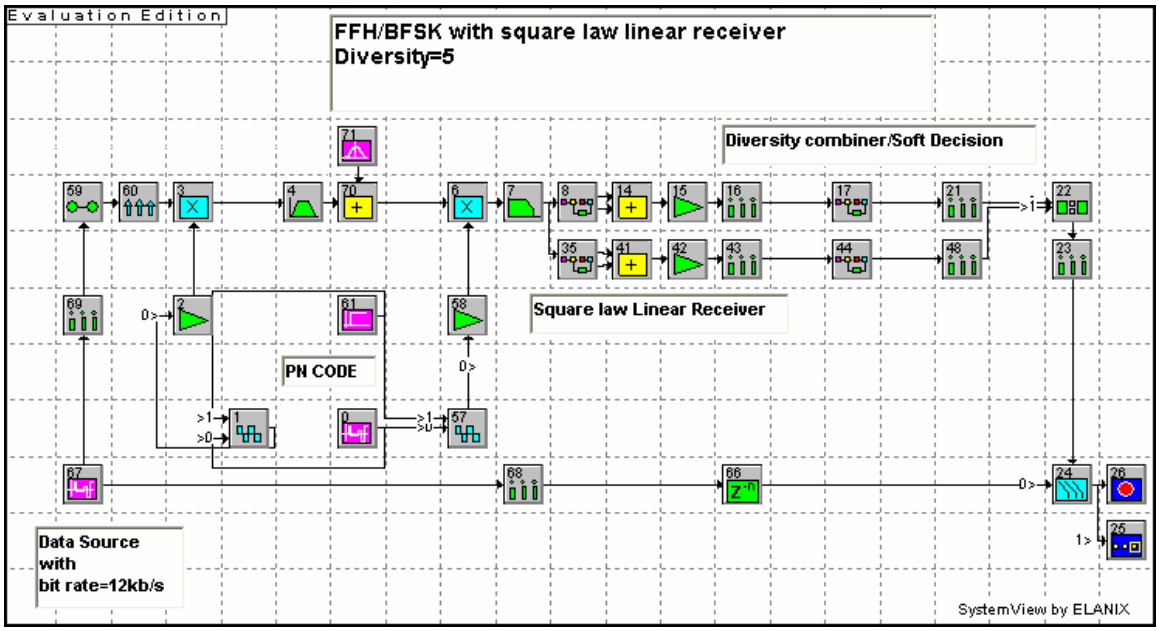

Figure 22. Noncoherent FFH/BFSK Simulation Model.

The noncoherent FFH/8FSK model is similar to the FFH/4FSK model, and therefore is not presented here.

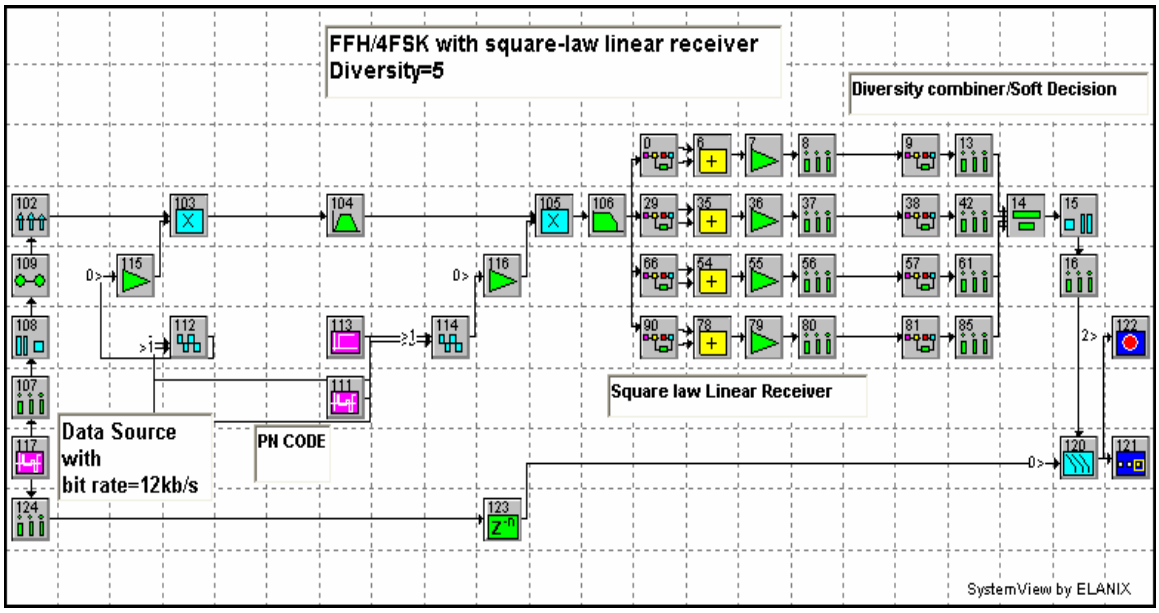

Figure 23. Noncoherent FFH/4FSK Simulation Model.

The 12 kbps data source (token 67) is first modulated in the MFSK modulator (token 60). The frequency separation Δf of modulated tones is set $\Delta f = R_h$ in order to achieve orthogonal signal. The modulated signal is multiplied with the output from the frequency synthesizer, which consists of a numerical controlled oscillator (token 1) and a PN code generator (token 0). The PN code generator generates the 483 frequencies of the FFH system with a hop rate $R_h = 60$ kh/s . The multiplication generates the FFH signal with diversity $L = 5$ as the bit rate R_b is related with the hop rate R_h with $R_h = 5R_b$. This subdivides every BFSK symbol into *L*=5 subsymbols. Token 4 represents the spread bandwidth W_T of the system, which is referenced in Table 4. This token also defines the sample rate of the specific SystemView model because the system's sample rate must be at least twice the cut–off frequency of the filter.

As assumed in the theoretical analysis, the interference of the channel is characterized as AWGN with a signal–to–noise ratio $E_b / N_0 = 13.35$ dB . The AWGN inserts to the system with the form of token 71.

Considering perfect synchronization, the frequency synthesizer (token 57) is driven by the same PN sequence as it was in the transmitter. The multiplication in token 6 achieves the perfect dehopping of the signal. The dehopped signal is filtered out in order to move the high frequency components with token 7.

After the successful defiltering, the signal passes through the square–law detectors (tokens 8 and 35) and is sampled with a sample rate (token16) equal to a hop rate $R_h = 60\ kh/s$ (seen Figure 24). We used this improvised module instead of the regular MFSK demodulator that SystemView has because the output of the regular MFSK demodulator does not provide the voltage of every diversity reception for every branch. This voltage is necessary in order to make the soft decision when adding the diversity receptions.

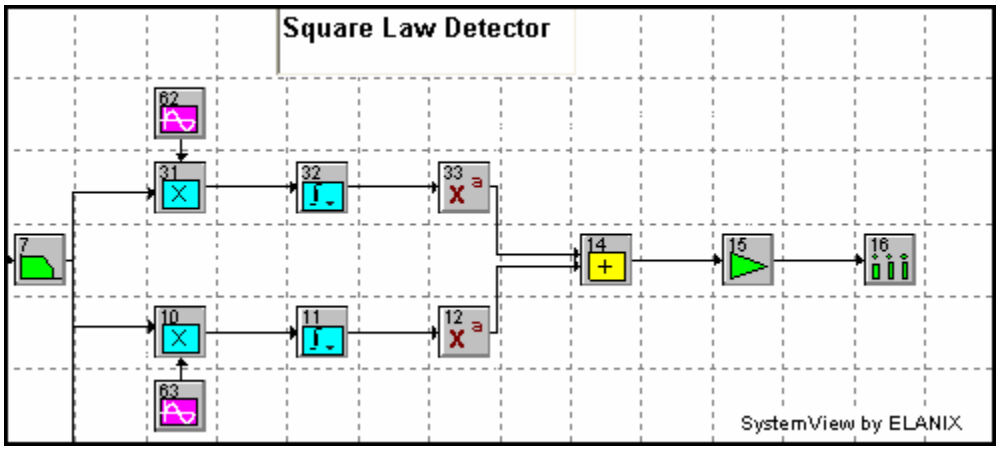

Figure 24. Square–Law Detector for FFH/MFSK (Token 8 and 25).

The next step is to add all the diversity receptions (token 17) using the method as it appears in Figure 25. SystemView does not provide a token to combine diversity receptions, so we improvised again using a combination of delay tokens (27, 28, 29, and 30) and an adder (token 19). This improvised method corresponds to the soft decision method. The output of the combiner was again sampled with a rate equal to symbol rate $R_s = R_b = 12$ kbps (token 21).

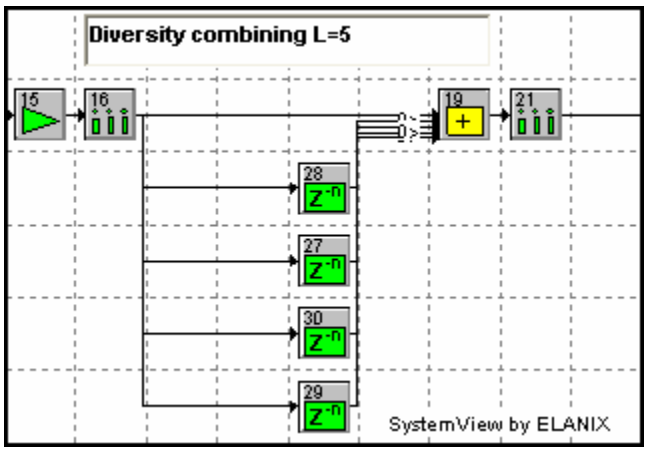

Figure 25. Linear Diversity Combiner.

The final step is performed by using token 22 (or token 14 for FFH/4FSK), which we used in order to make a decision about what symbol was sent.

Finally token 24 compares the transmitted data with the received data and extracts the probability of the bit error of the system.

SystemView software estimates the probability of error by comparing the transmitted bit with the received one. The probability of error for the SystemView model is generated from the equation:

$$P_b = \frac{Er \cdot R_{sv}}{P_{sv} \cdot R_b} \tag{5.1}$$

where Er is the total number of errors of every simulation loop, P_{sv} is the number of samples of every loop for the corresponding Er, and R_{sv} is the sample rate of the SystemView model. The sample rate derives from secondary parameters as the cutoff frequencies of various filters in the system. So the smaller probability of bit error that the system can derive is when we have $Er = 1$ error to a loop and the maximum number of samples $P_{sv} = 2^{31}$ and this corresponds to $P_b(\min) = 6.98 \cdot 10^{-6}$.

The number of samples that will pass through the system, the sample rate, the variable token, and the number of frequency loops can be arranged from the time specifications of the software.

A usual limitation for software such as SystemView is that as the complexity of the system increases, the execution time also increases. For example, in the case of FFH/8FSK system under the influence of MTBJ, in order to calculate $P_{sv} = 2^{31}$ samples, the simulation time was approximately 17 hours. The execution time depends on the capabilities of the PC used (processor, RAM).

Before proceeding to the performance of different jamming methods, it is important to examine the above simulation under the effect of the AWGN only in order to verify that the models behave as expected.

B. UNCODED NONCOHERENT FFH/MFSK SIMULATION MODEL IN AWGN

The simulation model of the FFH/BFSK system in AWGN is illustrated in Figure 23. By adding Gaussian noise (token 71) and defining the density as a variable parameter, the simulation is executed nine times for the FFH/BFSK, seven times for the FFH/4FSK, and six times for the FFH/8FSK system. Every time the simulation was executed (loop), the value of the power density N_0 decreased. This reduction corresponds to a continuous increase of E_b / N_0.

It is very interesting to observe in Figure 26 and Figure 27 the outputs of the square–law detectors branches for the FFH/BFSK system before the linear diversity combining (tokens 16 and 40)

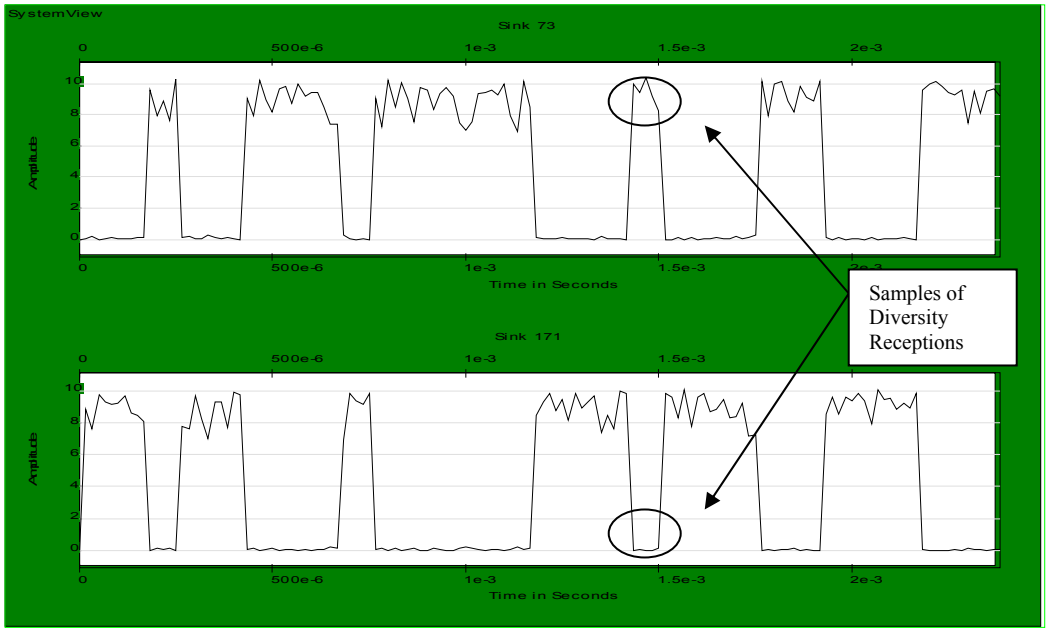

Figure 26. Square–law Detector Output before Diversity Combining without AWGN.

Specifically, Figure 27 presents the outputs from the sampler without AWGN and Figure 28 presents the sampler outputs under the influence of AWGN with $E_b / N_0 = 13.35$ dB.

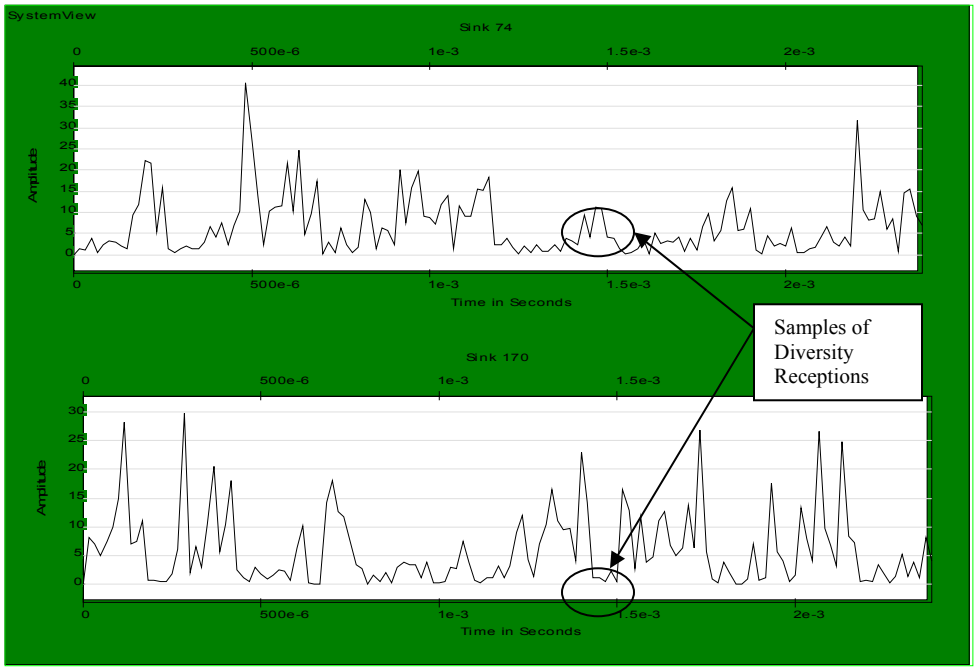

Figure 27. Square–law Detector Outputs before Diversity Combining under the Influence of AWGN with $E_b / N_0 = 13.35$ dB.

In order to verify that the above simulation model is an FH system, an oscilloscope is connected at the output of token 4. Figure 28 presents the frequency hop pulses for the FFH/BFSK system using N=483 frequency hop bands. It is apparent that the communication system is an FH system and its SS bandwidth is $W_T = 57.96$ MHz.

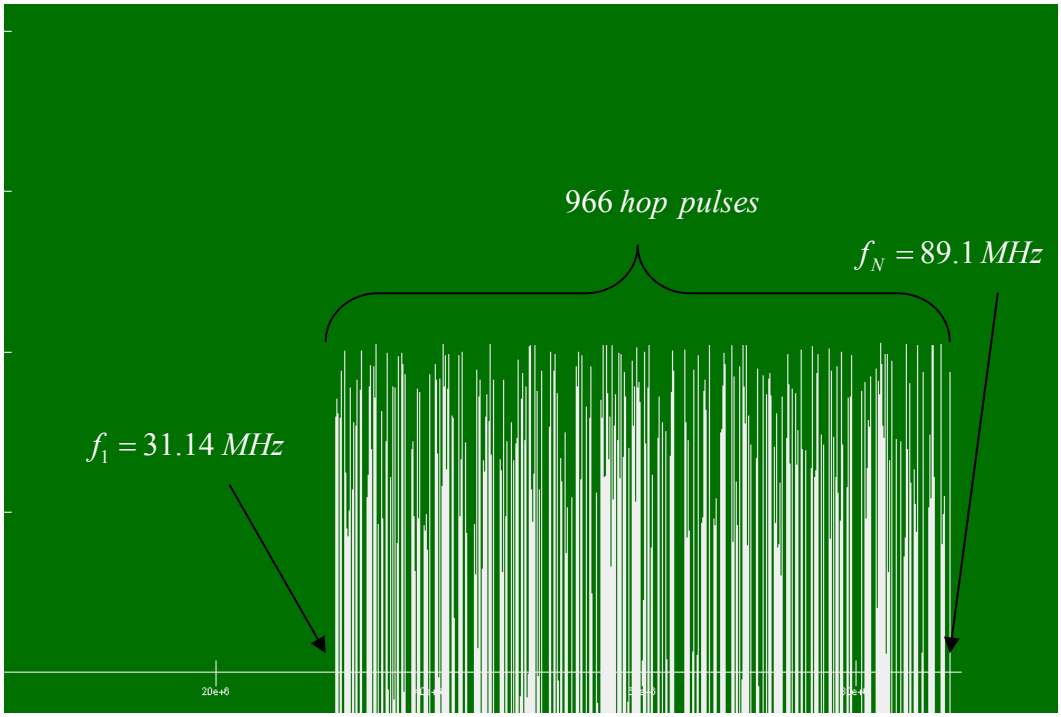

Figure 28. Spread–Spectrum Bandwidth of FFH/BFSK System.

Figure 29 presents the probability of bit error for a FFH/BFSK, FFH/4FSK and FFH/8FSK both simulated and theoretical according to Equation (3.26). The results verify that the simulation model results as expected with small variations for the FFH/BFSK system for larger values of E_b / N_0.

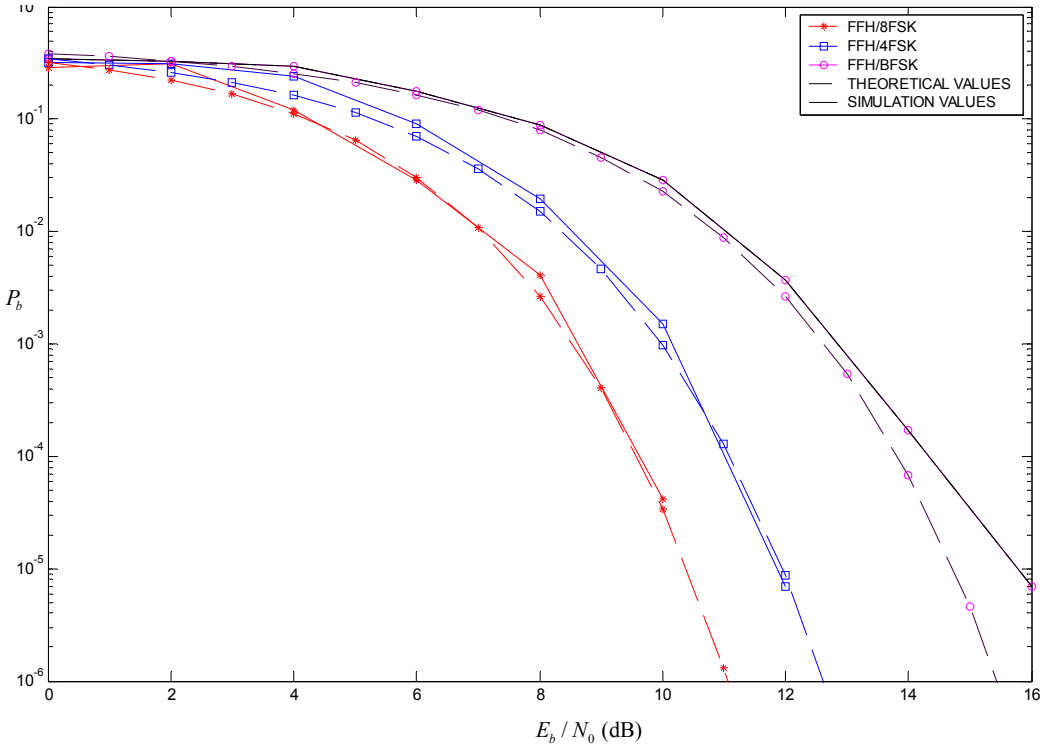

Figure 29. Simulation of Noncoherent FFH/MFSK Performance in AWGN as Compared to Theoretical Curves.

The next step is to generate the model for the first examined jamming strategy, the Barrage Noise Jamming.

C. UNCODED NONCOHERENT FFH/MFSK SIMULATION MODEL UNDER THE INFLUENCE OF THE BARRAGE NOISE JAMMING

The interference in the barrage noise jamming strategy is modeled as AWGN with noise density from Equation (3.32)

$$N_I = \frac{P_I}{W_T} \tag{5.2}$$

where P_I is the total available power of the jammer.

Figure 30 illustrates the BNJ strategy against an FFH/BFSK system. The combination of tokens 72 and 73 represents the barrage noise jammer that is jamming the total operational SS bandwidth of the system

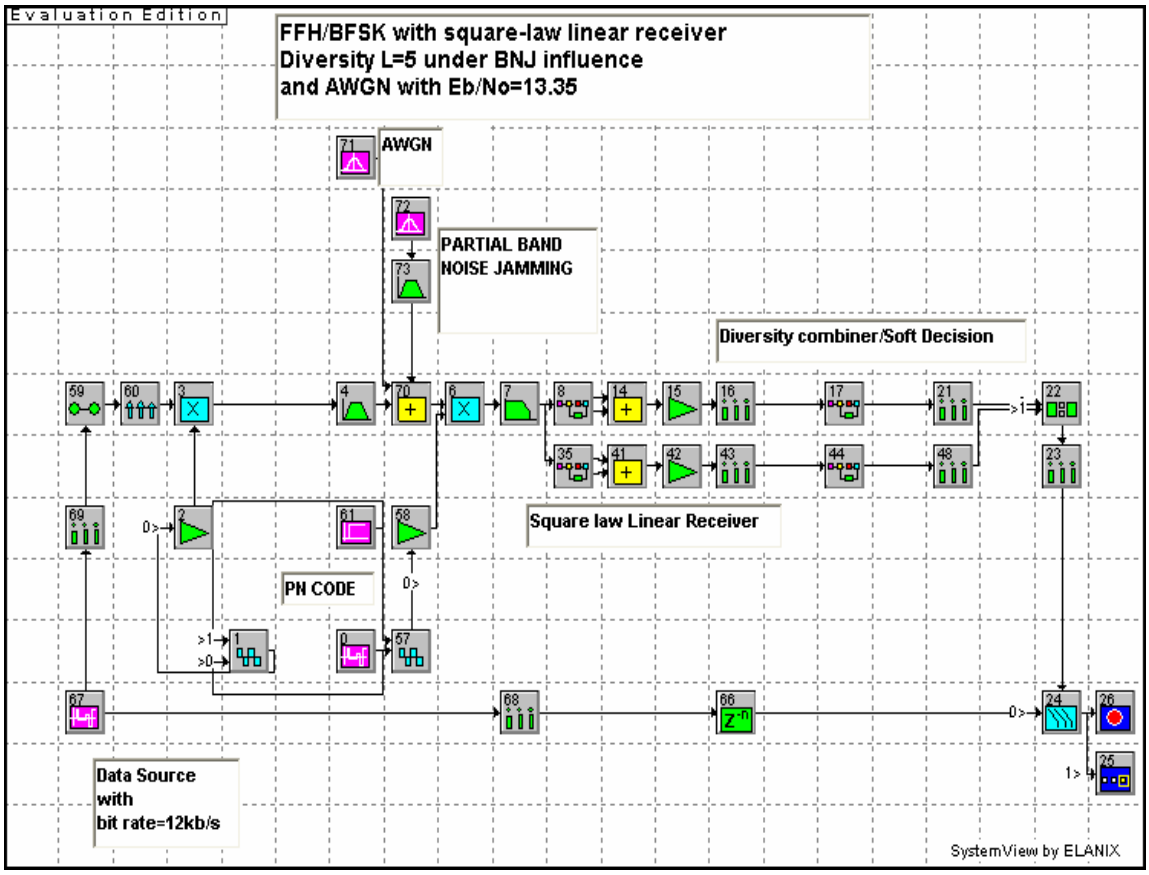

Figure 30. Barrage Noise Jamming Strategy Against an FFH/BFSK System.

The noise of the channel is modeled again as AWGN with $E_b / N_0 = 13.35$ dB. The only variable parameter to the system model is the noise density in token 72 that represents the available noise power of the jammer.

The results of the simulation for the FFH/BFSK, FFH/4FSK and FFH/8FSK system are illustrated along with the theoretical results in Figure 31.

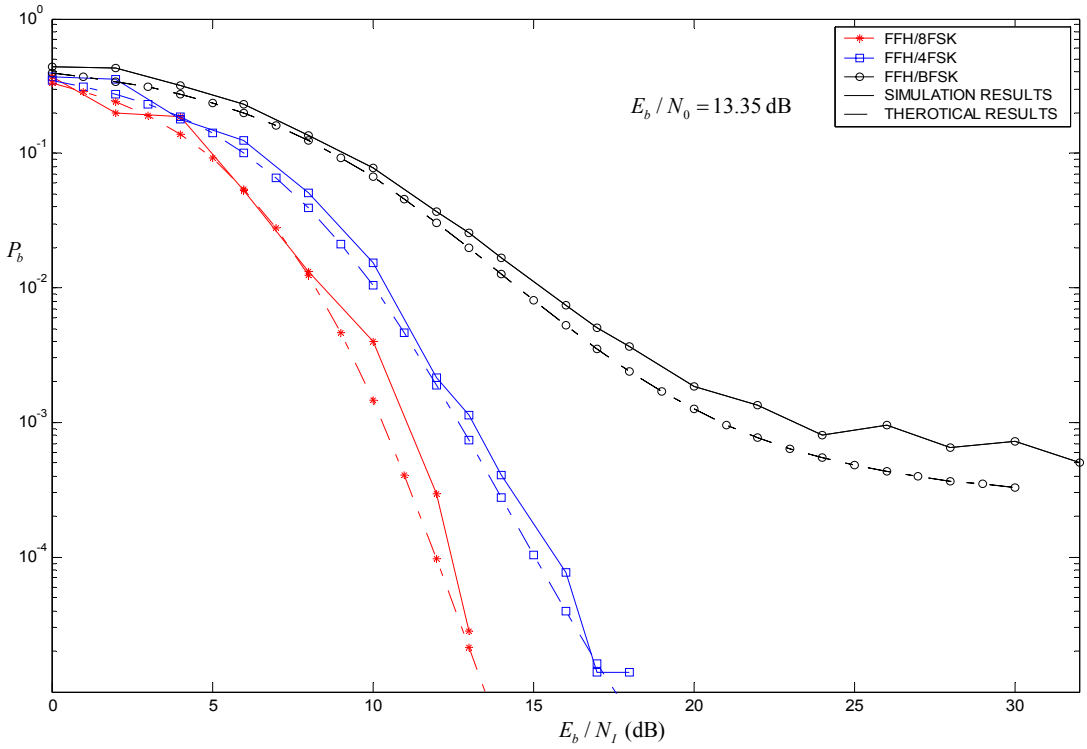

Figure 31. Simulation Results of the Effect of the BNJ on the Performance of an FFH/MFSK System Along with the Theoretical Results for Diversity Order L=5.

The simulation results verify the theoretical results with small variations in the case of the FFH/BFSK for greater values of E_b / N_I for which the "bottoming effect" takes place. Again SystemView cannot produce a probability of bit error less than $P_b < 6.98 \cdot 10^{-6}$.

D. UNCODED NONCOHERENT FFH/MFSK SIMULATION MODEL UNDER THE INFLUENCE OF THE PARTIAL–BAND JAMMING

The simulation model in the partial–band jamming case is the same as the BNJ model. The only difference is that now two variable parameters exist. The first, as before, is the noise density power that is represented by token 71 and is calculated from:

$$N_I^{"} = \frac{N_I}{\rho} \tag{5.3}$$

where N_I is the available noise power density of the BNJ and ρ is the ratio of the bandwidth of the filter (token 73) to total SS bandwidth W_T of the system.

The second variable parameter is the bandwidth of the filter (token 73) that controls the part of the SS bandwidth that will be jammed (fraction ρ).

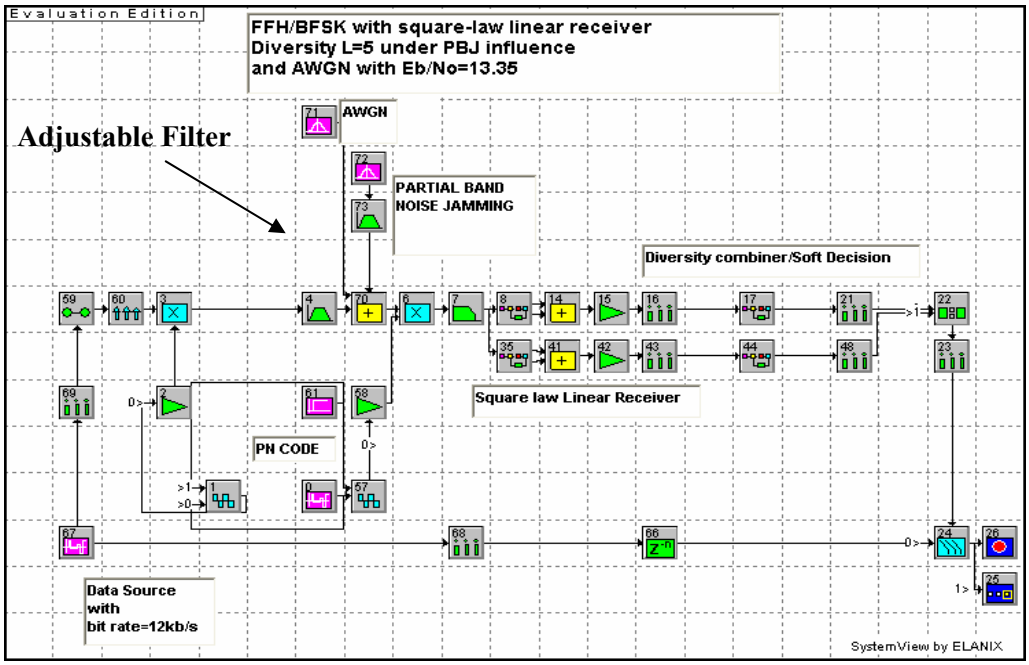

Figure 32. Partial–Band Noise Jamming Model over an FFH/BFSK Communication System.

It is very interesting to observe in Figure 33 the influence of the PBJ at the output of the samplers of the square–law detectors (token 15, 43).

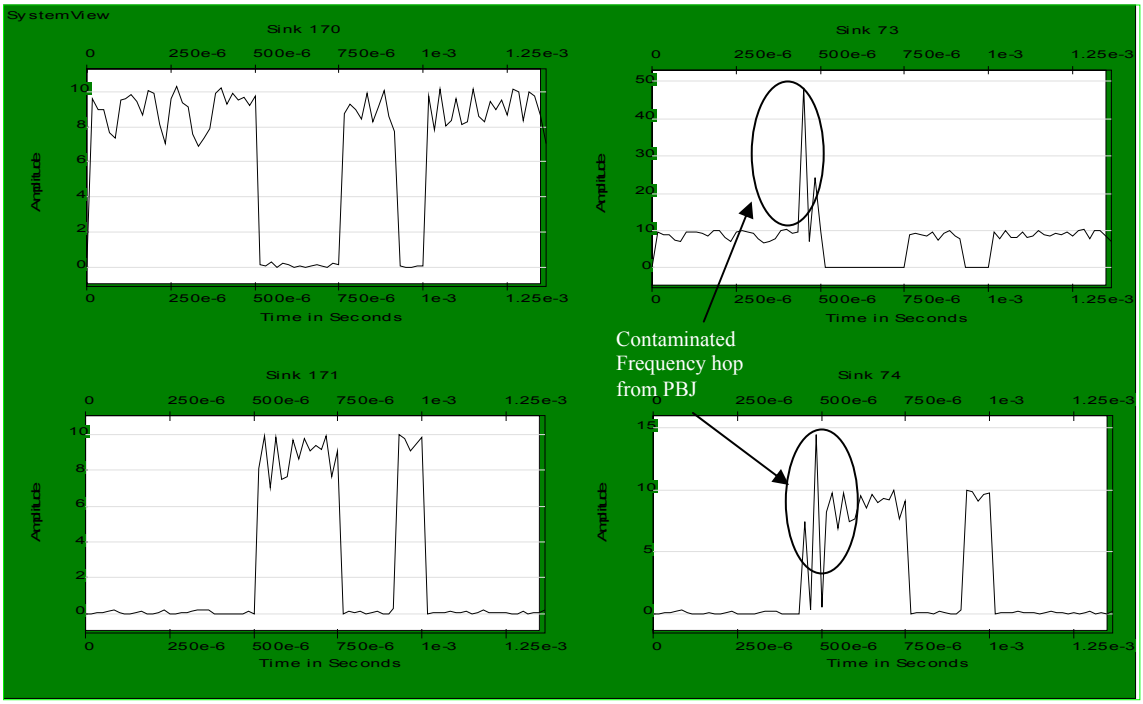

Figure 33. Square–Law Detectors Output without PBJ (Sink 170,171) and with PBJ (Sink 73, 74) in an FFH/BFSK System.

It is obvious that the jamming noise influences some of the diversity and not all receptions because every frequency hop is independent from the next one. In the specific case of Figure 33, the PBJ contaminates two of the five diversity receptions creating a bit error. The PBJ influences all the branches of the receiver when the frequency hop coincides with jammed fraction.

In Figure 34, with the help of the SystemView's oscilloscope, the presence of the partial–band jamming in the communication system for a particular value of fraction ρ can be observed.

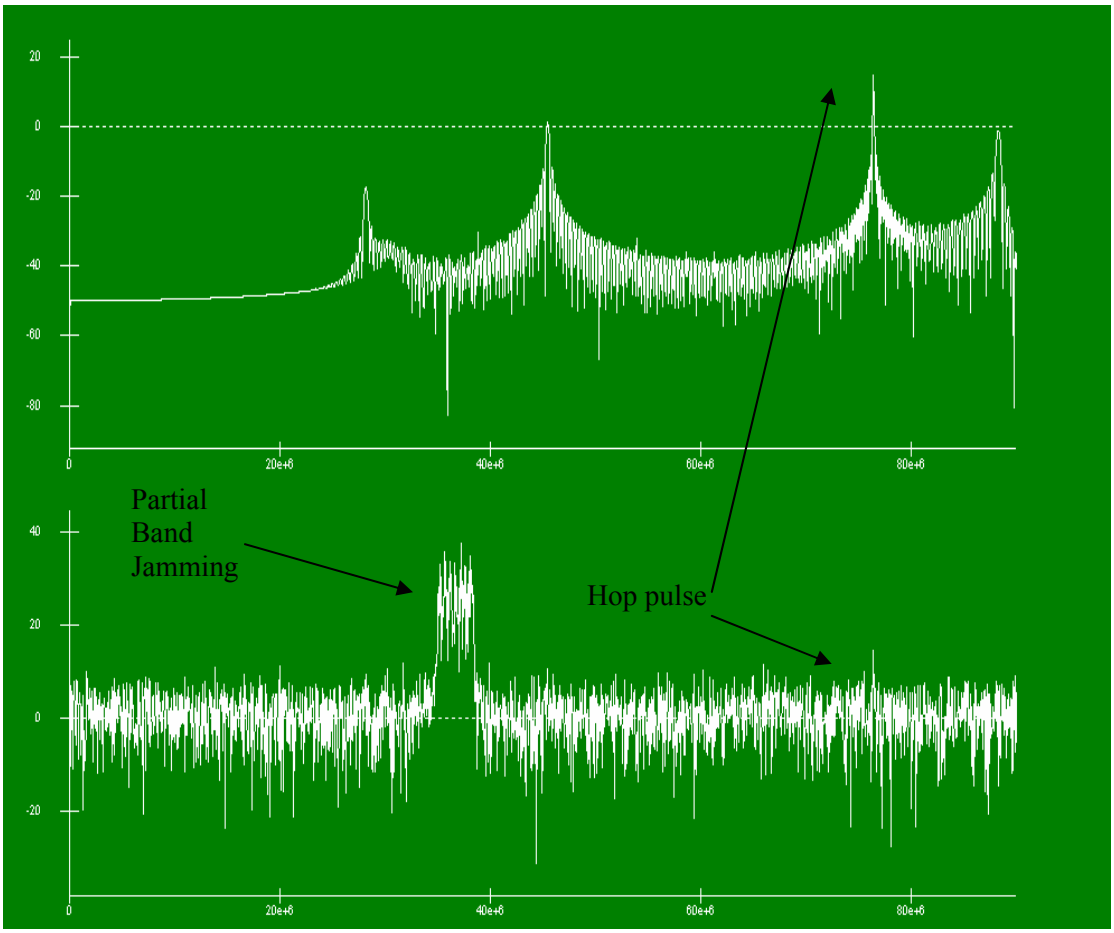

Figure 34. Influence of PBJ Along with AWGN in an FFH/BFSK System with Jamming Fraction $\rho = 5.6 \cdot 10^{-2}$.

In order to calculate the case of PBJ that degrades the FFH/MFSK system most, we used Table 2 as a guide to estimate the optimum fraction ρ_{oc}.

Even though the interference power can be set easily as a variable, the bandwidth of the filter cannot, since in SystemView there is no option for variable bandwidth. The only possible procedure is to plot a curve for a given fraction ρ, and a range of E_b / N_I and save the results. The next step is to change the bandwidth of the filter (fraction ρ), the noise power density N_I'' (according to Equation $N_I'' = N_I / \rho$) and plot the data again for the same range E_b / N_I, save the results, and so on.

Based on this iterative technique, several simulation curves were plotted for the FFH/BFSK, FFH/4FSK and FFH/8FSK modulation scheme, as illustrated in Figures 35, 36 and 37, respectively.

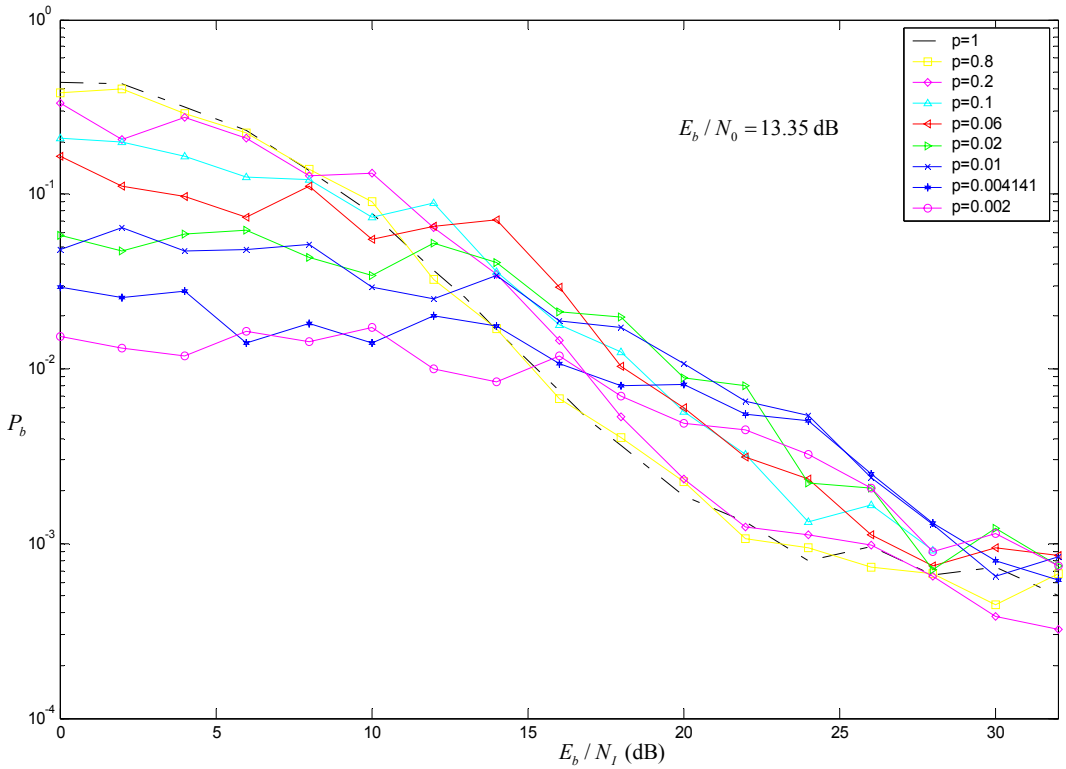

Figure 35. Simulation Results of the Effect of Partial–Band Jamming for Different Fractions ρ over an FFH/BFSK System.

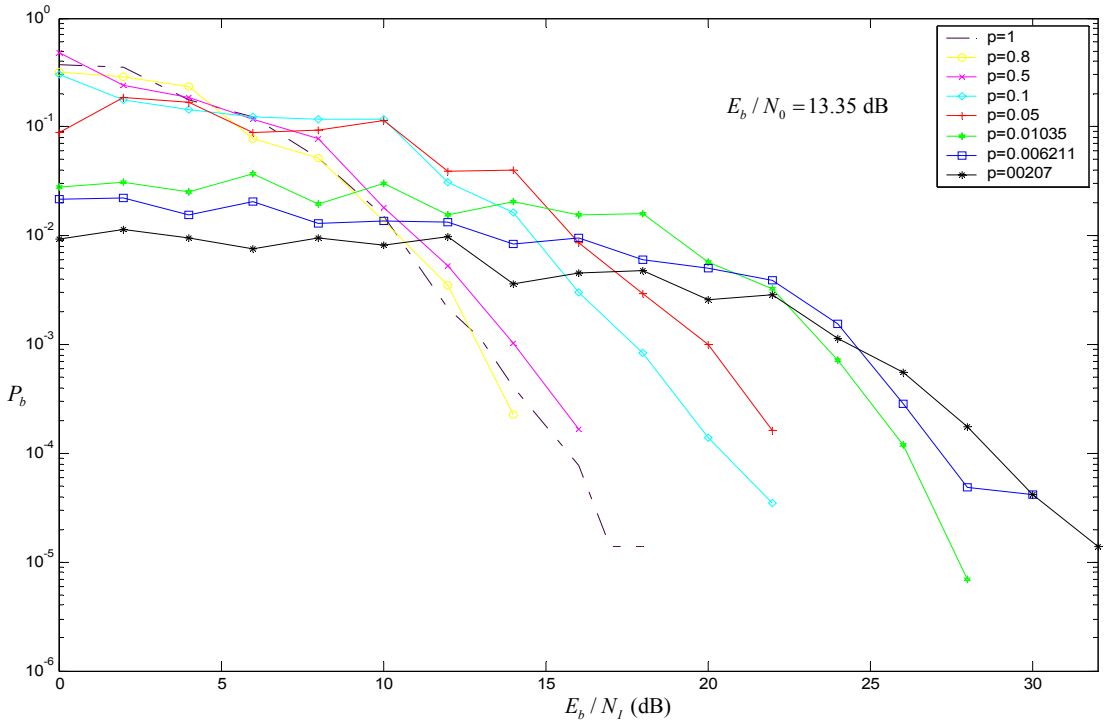

Figure 36. Simulation Results of the Effect of Partial–Band Jamming for Different Fractions ρ over an FFH/4FSK System.

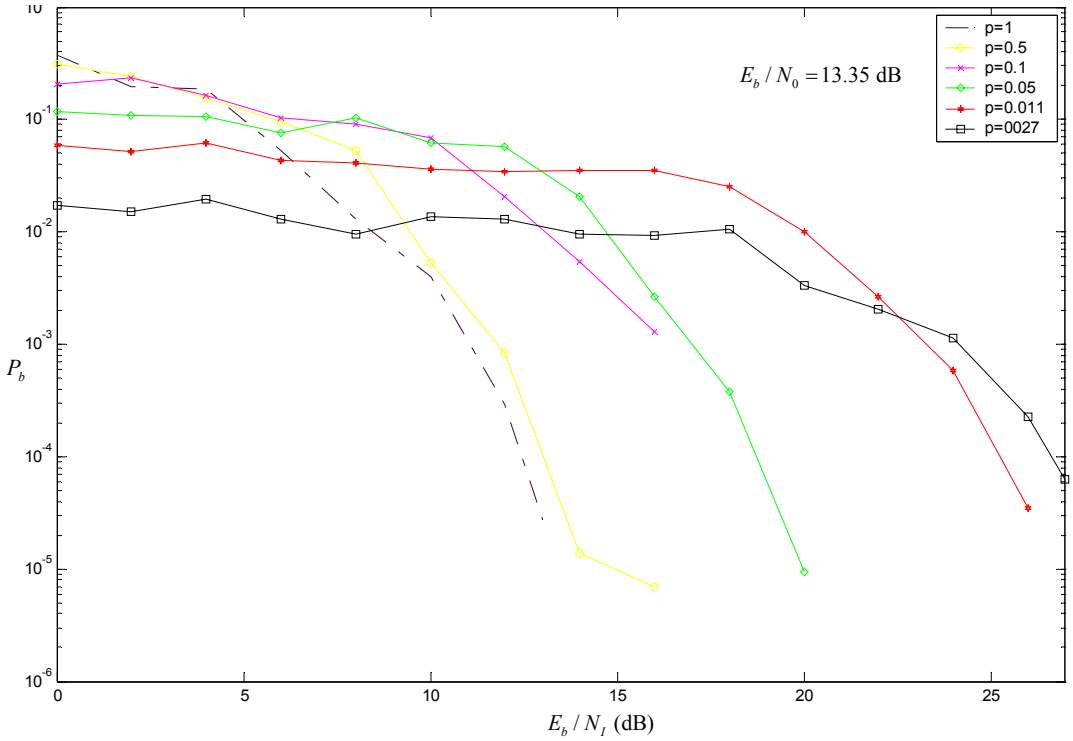

Figure 37. Simulation Results of the Effect of Partial–Band Jamming for Different Fractions ρ over an FFH/8FSK System.

The curves for different fractions appear to have a flat area and a break point. As the fraction ρ becomes smaller, this break point moves to the left for higher values of E_b / N_I.

As the signal–to–jamming ratio increases, the probability of error curves for all ρ tend forward the same value of P_b. This value is the error produced due to AWGN**.** This phenomenon can be observed better in the case of FFH/BFSK in which the P_b for different fractions ρ tends to become the same for higher values of E_b / N_I.

In general, for any value of E_b / N_I, there is an optimum value of ρ from the jammer's viewpoint that maximizes P_b, and this is denoted by ρ_{oc} (for an optimum case). The performance in an optimum case partial–band noise is the upper envelope (or supremum) of the family of P_b curves for fixed values of ρ [3]. Of course, in practice, it may be difficult for the jammer to match ρ to the actual E_b / N_I.

Finally, from the simulation results, the optimum performance for the partial–band jammer over the FFH/BFSK, FFH/4FSK and FFH/8FSK systems is illustrated in Figure 38.

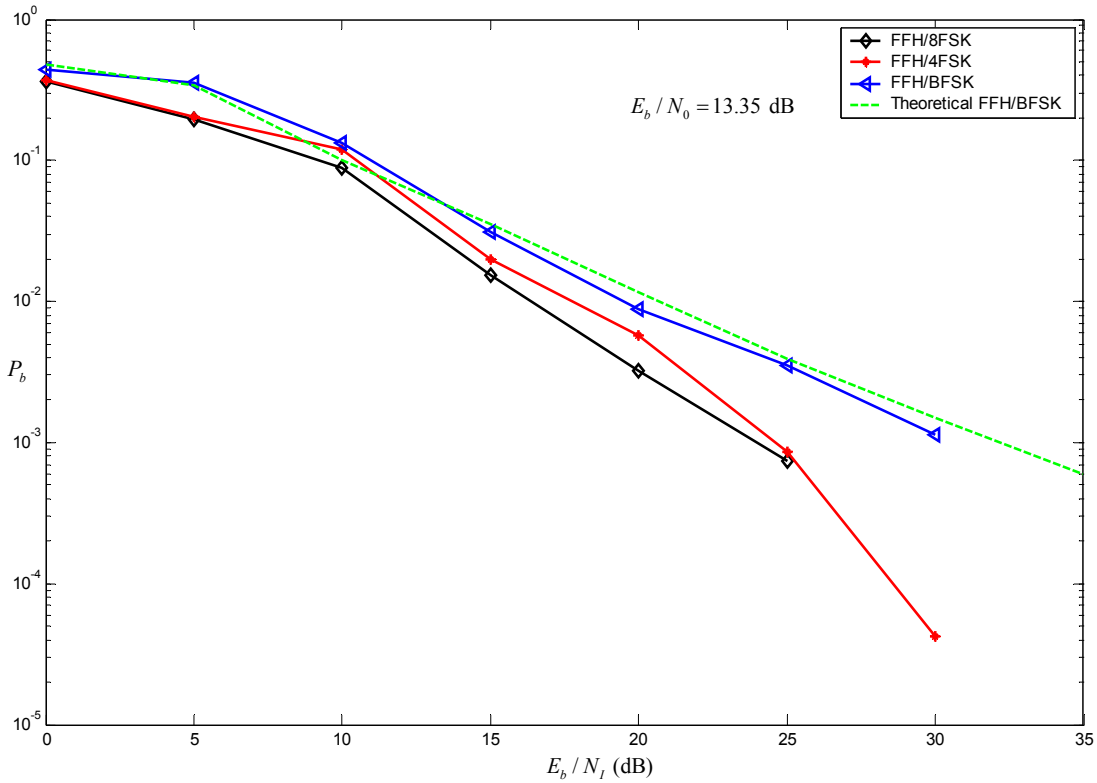

Figure 38. Optimum Performance of the Partial–Band Jammer Against an FFH/MFSK Communication System for Modulation Order M=2, 4, 8 and Diversity Order L=5.

Table 5 presents the simulation fraction ρ_{oc} that was used in order to calculate the optimum performance for the simulation model. There is a slight difference between the theoretical and the simulated optimum fraction ρ_{oc}. The reason is that the filter (token 73) that we used to limit the jamming power to the specific fraction of the SS bandwidth was not ideal. Therefore the jammer also influenced some of the adjacent frequency hop bands. This is an undesirable phenomenon, but this is something usual for real–time simulation systems.

E_b / N_I	FFH/BFSK		FFH/4FSK		FFH/8FSK	
	ρ_{oc}	int$(\rho \cdot N)$	ρ_{oc}	int$(\rho \cdot N)$	ρ_{oc}	int$(\rho \cdot N)$
0 dB	1	483	1	483	1	363
5 dB	0.8	386	0.8	386	0.5	181
10 dB	0.2	96	0.1	48	0.1	36
15 dB	0.06	29	0.05	24	0.05	18
20 dB	0.02	9	0.01035	5	0.011	4
25 dB	0.004141	2	0.00207	1	0.00207	1
30 dB	0.00207	1	0.00207	1	–	–

Table 5. Simulation Results for the Optimum Fraction ρ_{oc} and Number of Jammed Hop Bands of PBJ Against an FFH/MFSK System for *M*=2, 4, 8.

It is observed from Figure 38 that for the same bandwidth for all the modulation schemes (*M*=2, 4, 8) the FFH/8FSK has greater resistance to the optimum case of the partial–band jamming strategy than the other two modulation schemes.

In case of an FFH/BFSK system, the theoretical optimum performance of the PBJ given from Reference [10] is very close to the simulated one. This verifies the operation of the simulation model. It is also observed that for the same SS bandwidth the performance of the jammer decreases as the modulation order *M* increases.

The next step is to create the model of the multitone band jammer and observe its performance against the FFH/MFSK system.

E. UNCODED NONCOHERENT FFH/MFSK SIMULATION MODEL UNDER THE INFLUENCE OF THE MULTITONE BAND JAMMING

The simulation of the multitone band jamming can be achieved by using one of the existing channel models in the SystemView library, which is called *narrow band interferer* (NBI).

This specific token generates unmodulated (CW) tones over a prescribed frequency range [13]. The desired signal $x(t)$ after the influence of the NBI, becomes

$$y(t) = x(t) + \sum_{k=1}^{q} A_k \sin(2\pi f_k t + \varphi_k), \tag{5.4}$$

where q is the number of jamming tones, φ_k is the random phase of each NBI which is distributed uniformly between 0 and 2π. The amplitude A_k of each NBI is distributed between specific values that the user can set. A_k is also the variable in this specific simulation model. The frequency f_k of each NBI is chosen randomly over the communication bandwidth. This means that the jamming tones will be placed on frequencies separated by the frequency spacing parameter.

Figure 39 represents the simulation model for the multitone band jamming (MTBJ) case in which token 72 represents the influence of the multitone band jammer.

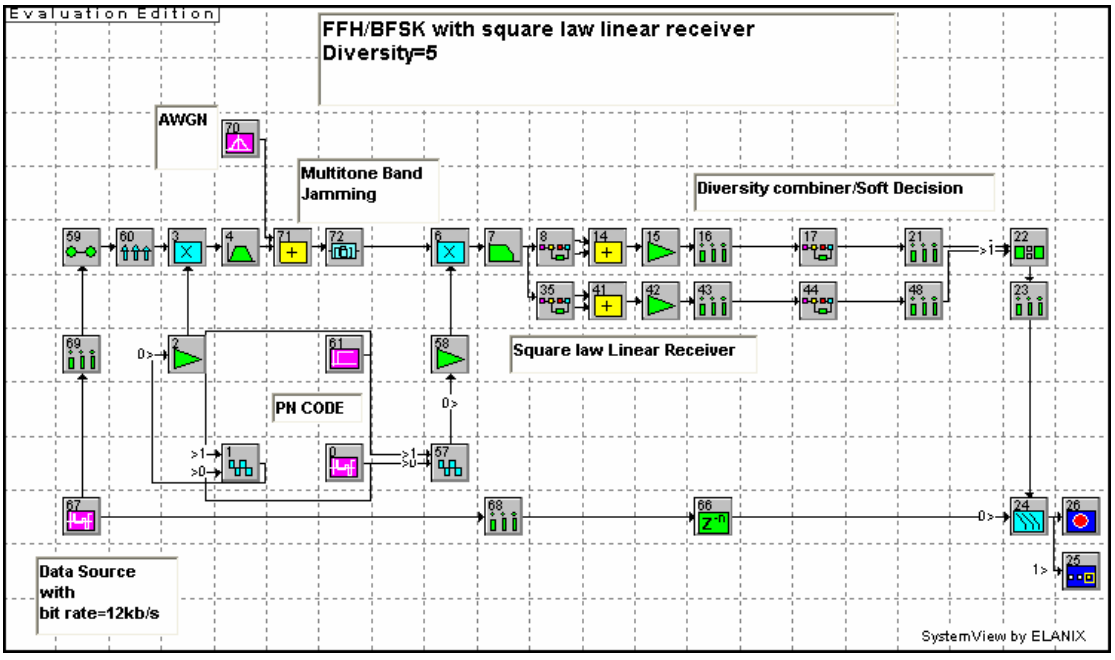

Figure 39. Multitone Jamming Model in the Noncoherent FFH/BFSK System.

In Figure 40, using the oscilloscope from SystemView, the influence of the jammer in multitone band jamming can be observed. In the specific case, the jammer distributes five jamming tones randomly in the SS bandwidth that do not coincide with the frequency hops.

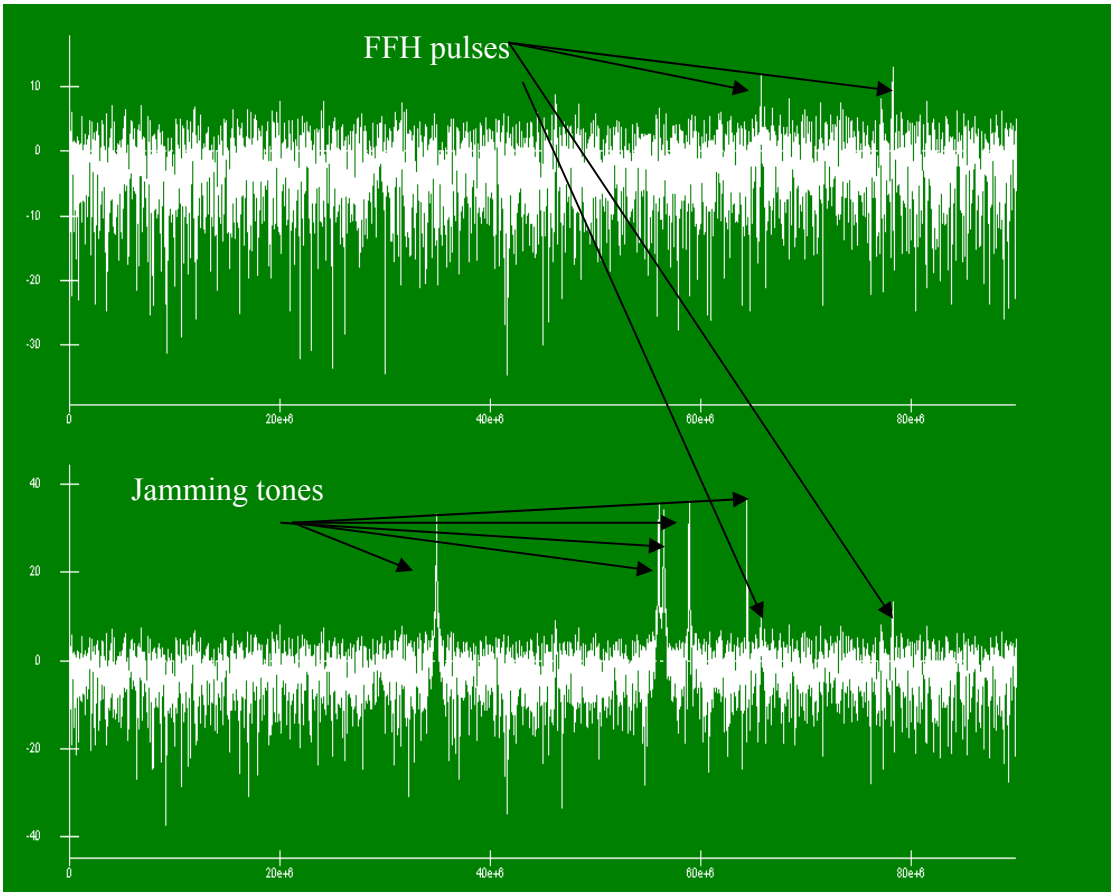

Figure 40. Influence of the MTBJ over an FFH/BFSK System with a Number of Jamming Tones $q = 5$.

Figure 41 also shows the influence of a jamming tone that coincides with a frequency hop in the output of the square–law detectors. It is obvious that the jamming tone influences only the branch that corresponds to the specific *M* frequency and not the other branch.

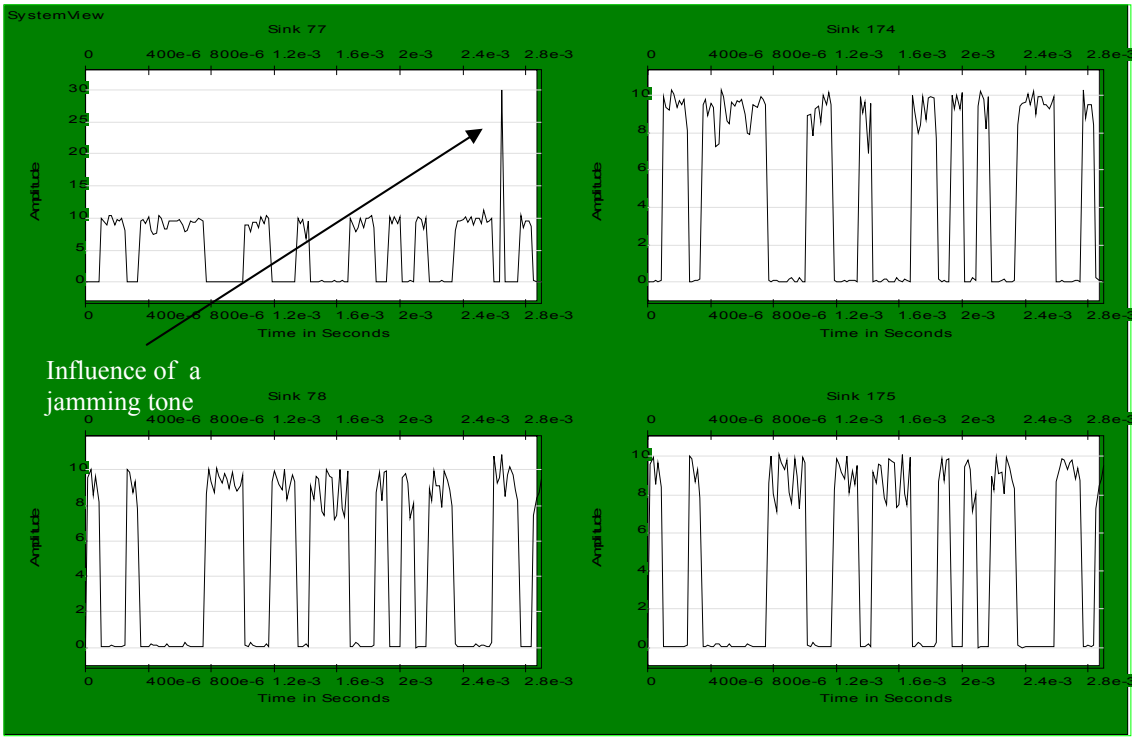

Figure 41. Square–Law Detectors Output without MTBJ (Sink 174,175) and with MTBJ (Sink 77,78) in an FFH/BFSK System.

In order to compare the multitone band jamming strategy with the partial–band noise jamming and barrage noise jamming strategy, we need to establish a common measurement. This measurement is the ratio E_b / N_I where N_I is the power density of the jammer, and it is the same for all strategies.

The available power for every jamming strategy derives from

$$P_I = N_I \cdot W_T . \tag{5.5}$$

In case of multitone band jamming the P_I is distributed to q equal power tones according to

$$P_{I_T} = \frac{P_I}{q} \tag{5.6}$$

where the q jamming tones coincide exactly with some of the N possible frequencies that the system can hop.

The power of every jamming tone can become a variable if we set the amplitude A_k of the jamming tone as a variable parameter (token 72). The power of every tone derives from $P_{I_T} = A_K^2 / 2 = P_I / q.$ The only way to proceed is to plot a curve for a specific number of jamming tones q by decreasing consecutively the amplitude by $\sqrt{10^{\frac{X\,(\mathrm{dB})}{10}}}$ where X (dB) corresponds to the increase in E_b / N_I (dB). When the simulation is completed, the results are saved. We repeat the same procedure for a different number of jamming tones and save the results in overlay plots.

In Figures 42, 43, and 44 the simulation results have been plotted for various numbers of jamming tones along with AWGN $E_b / N_0 = 13.35$ dB for modulation order $M = 2, 4, 8$ respectively.

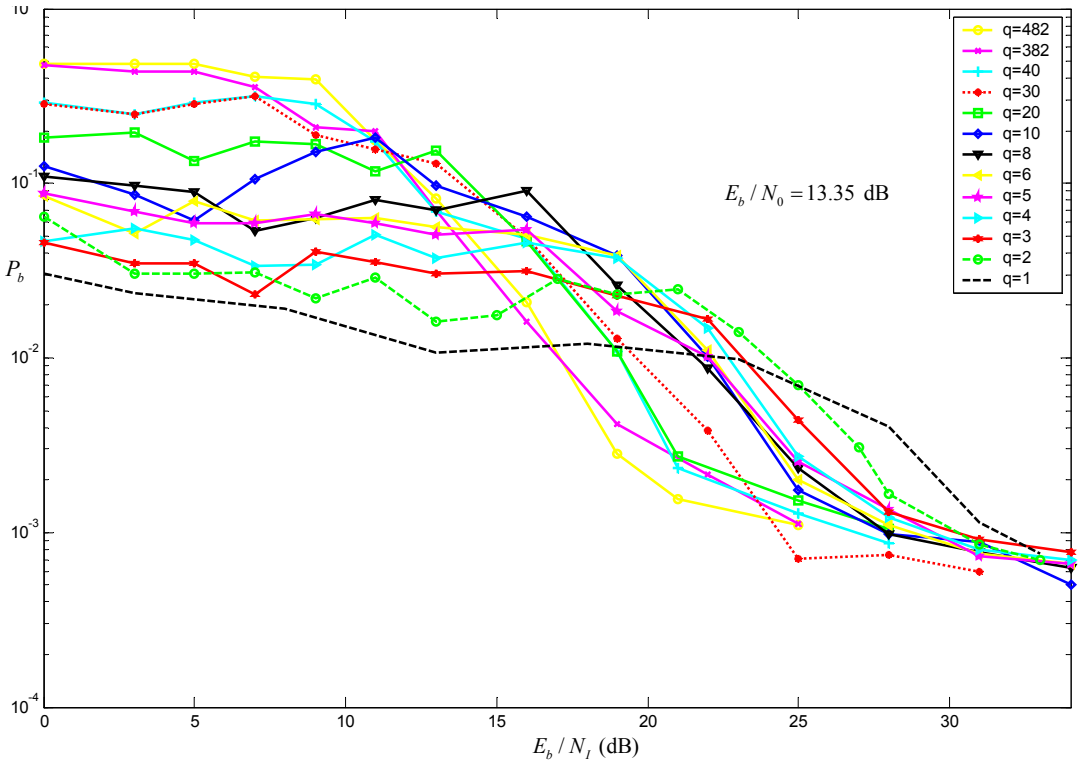

Figure 42. Simulation Results of the Effect of Multitone Band Jamming for a Different Number of Jamming Tones q over an FFH/BFSK System.

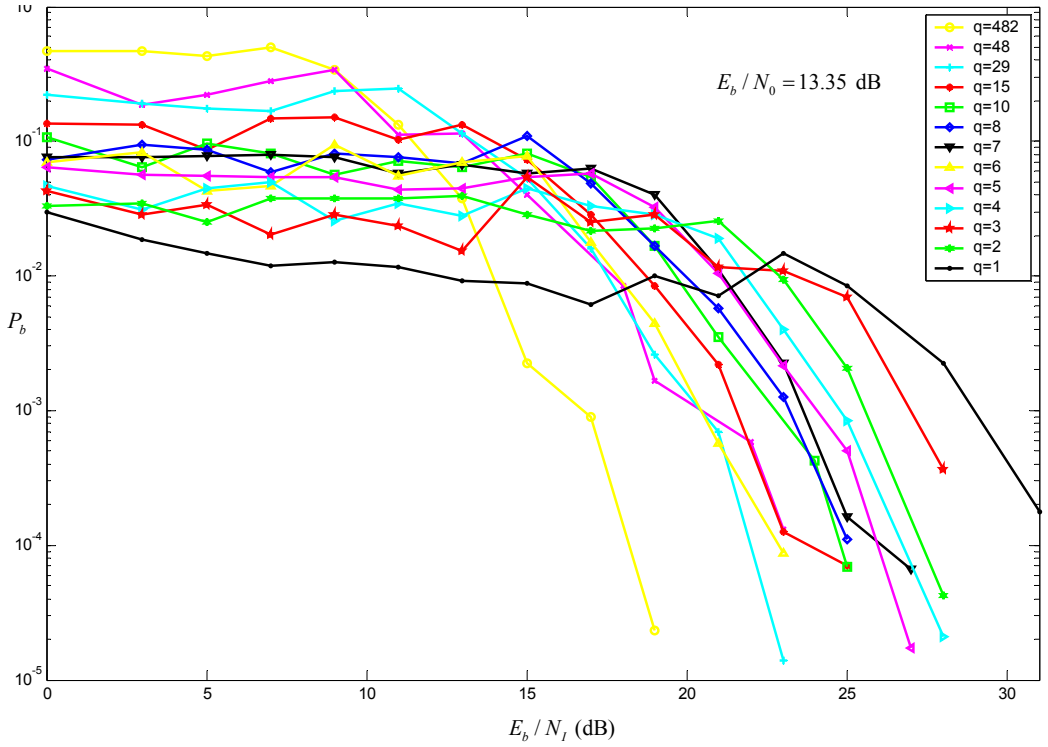

Figure 43. Simulation Results of the Effect of Multitone Band Jamming for a Different Number of Jamming Tones q over an FFH/4FSK System.

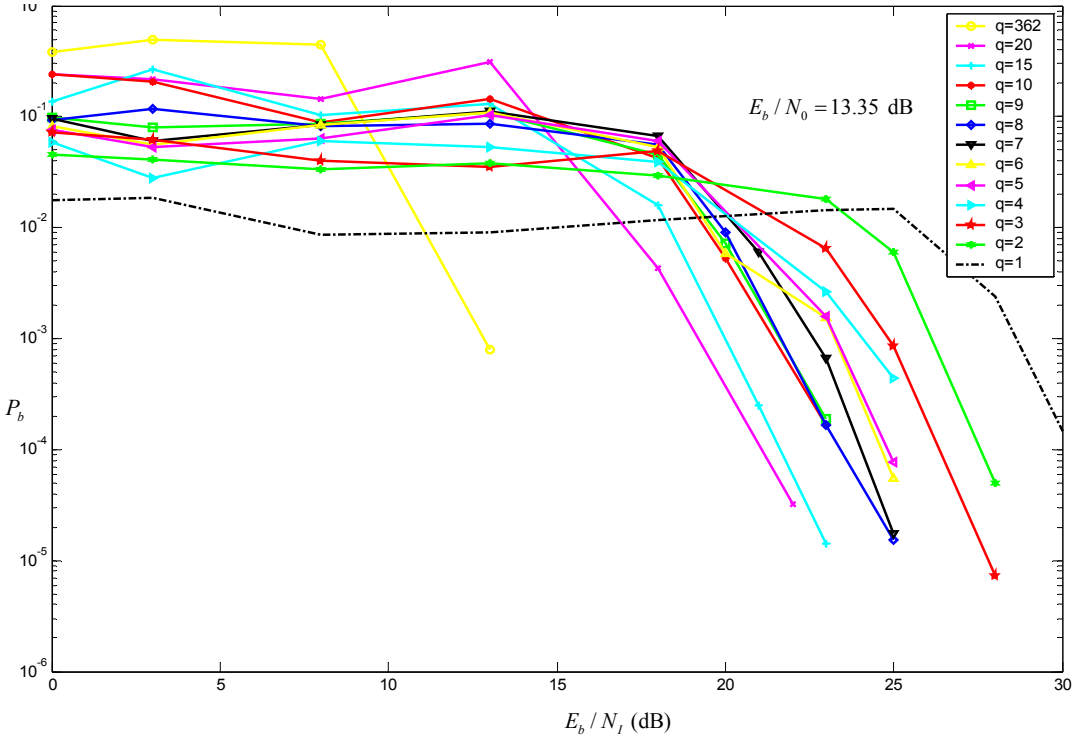

Figure 44. Simulation Results of the Effect of Multitone Band Jamming for a Different Number of Jamming Tones q over an FFH/8FSK System.

As before, in the analysis of the optimum case of partial–band jamming, for any value of E_b / N_I, there is an optimum value of q from the jammer's viewpoint that maximizes P_b, and this is denoted by q_{oc}. The performance in the optimum case MTBJ is the upper envelope of the overlay plots of P_b for fixed values of q.

Figure 45 presents the optimum performance of the MTBJ strategy over an noncoherent FFH/MFSK system along with AWGN $E_b / N_0 = 13.35$ dB.

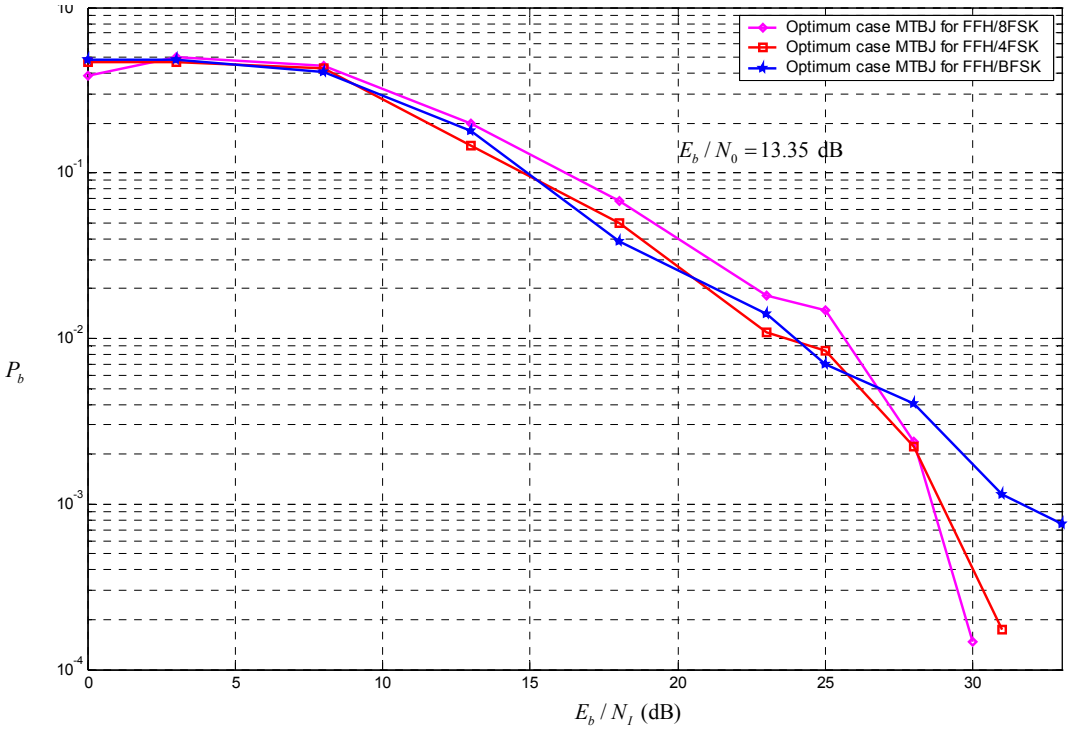

Figure 45. Optimum Performance of MTBJ over the FFH/MFSK System for Modulation Order M=2,4,8 and Diversity Order L=5

From the results of Figure 45 we see that the optimum MTBJ creates approximately the same probability of bit error for the modulation orders M =4, 8 assuming that the systems have the same SS bandwidth. For large values of E_b / N_I (above 25 dB) the FFH/BFSK system appears to be more sensitive than the other two modulation schemes in MTBJ.

In Table 6 the values of optimum number of tones are presented based on the simulation results. The power of every jamming tone P_{I_T} is calculated in relation to the total available jamming power P_I and the corresponding number of tones from Equation:

$$P_{I_T} = \frac{P_I}{q \cdot 10^{\frac{[E_b/N_I\,(\mathrm{dB})]}{10}}} \tag{5.7}$$

where P_I is the total available jamming power that corresponds to $N_I = E_b$.

E_b / N_I	**FFH/BFSK**		**FFH/4FSK**		**FFH/8FSK**	
	q_{oc}	P_{I_T}	q_{oc}	P_{I_T}	q_{oc}	P_{I_T}
0 dB	482	$0.002075 \cdot P_I$	482	$0.002075 \cdot P_I$	362	$0.002075 \cdot P_I$
3 dB	482	$0.00104 \cdot P_I$	482	$0.00104 \cdot P_I$	362	$0.001384 \cdot P_I$
8 dB	482	$0.000329 P_I$	482	$0.000329 P_I$	362	$0.000438 P_I$
13 dB	15	$0.003341 \cdot P_I$	29	$0.001728 P_I$	20	$0.002506 P_I$
18 dB	10	$0.001585 P_I$	7	$0.002264 P_I$	7	$0.002264 P_I$
23 dB	2	$0.002506 P_I$	3	$0.001671 P_I$	2	$0.002506 P_I$
25 dB	2	$0.001581 P_I$	1	$0.003162 P_I$	1	$0.003162 P_I$
28 dB	1	$0.001585 P_I$	1	$0.001585 P_I$	1	$0.001585 P_I$
30 dB	1	$0.001 P_I$	–		1	$0.001 P_I$
31 dB	1	$0.000794 P_I$	1	$0.000794 P_I$	–	–
33 dB	1	$0.0005 P_I$	–	–	–	–

Table 6. Simulation Results for the Optimum Number of Jamming Tones q_{oc} and Power of the Jamming Tones of MTBJ Against FFH/MFSK System for M=2,4,8.

The next section compares all the jamming strategies in order to determine what is the most appropriate jamming strategy against the FFH/MFSK system with a square–law linear combining receiver.

F. SUMMARY

This chapter presented the implementation of the simulation model of the uncoded noncoherent FFH/MFSK communication system with a square–law linear combining receiver. The purpose of the implementation of the simulation model against different jamming strategies was dual. First, to verify that the simulation model is operationally correct by comparing the simulation results with the theoretical results where available. Secondly, to investigate what the best jamming strategy against the FFH/MFSK system is. Both of the above purposes were achieved.

The comparison between the theoretical curves and the simulation curves verified that the system worked as expected. In order to determine what the best jamming strategy was, Figures 46, 47 and 48 were plotted with overlay curves from different jamming strategies for the FFH/BFSK, FFH/4FSK and FFH/8FSK system, respectively.

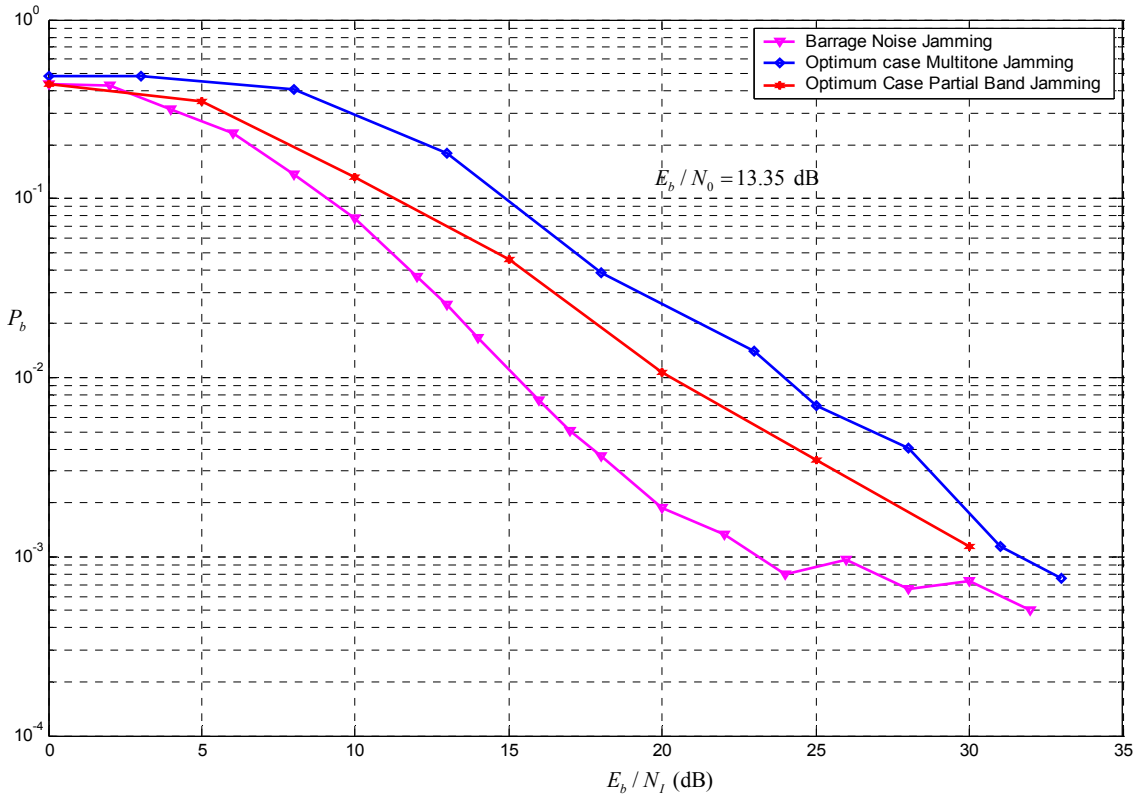

Figure 46. Simulation Results for Barrage Noise Jamming, Optimum Case Partial–Band Jamming and Optimum Case Multitone Band Jamming Against a Noncoherent FFH/BFSK System.

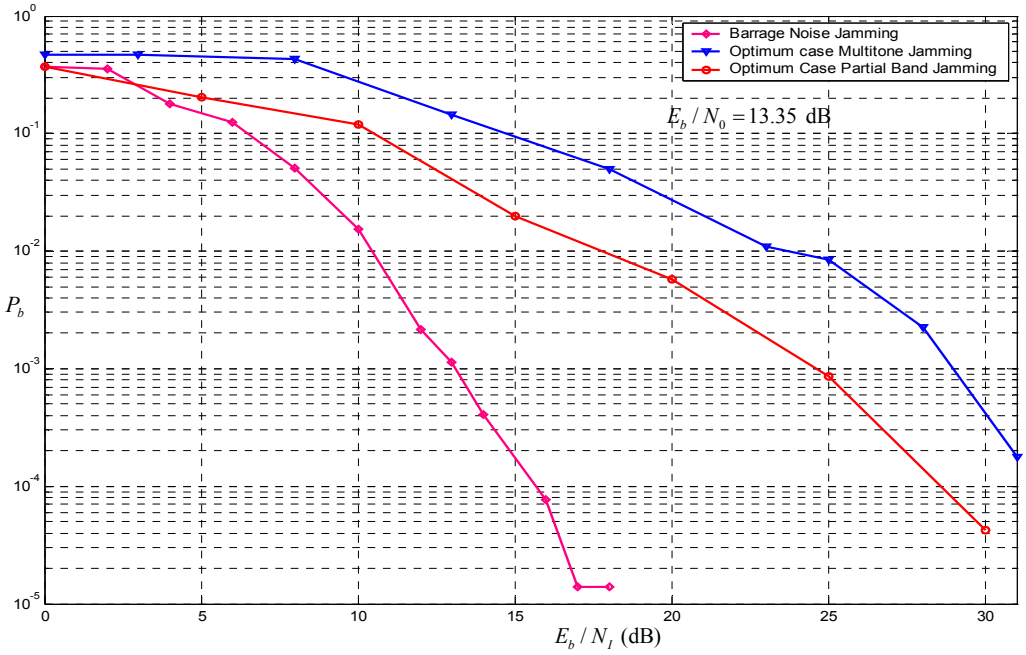

Figure 47. Simulation Results for Barrage Noise Jamming, Optimum Case Partial–Band Jamming and Optimum Case Multitone Band Jamming Against a Noncoherent FFH/4FSK System.

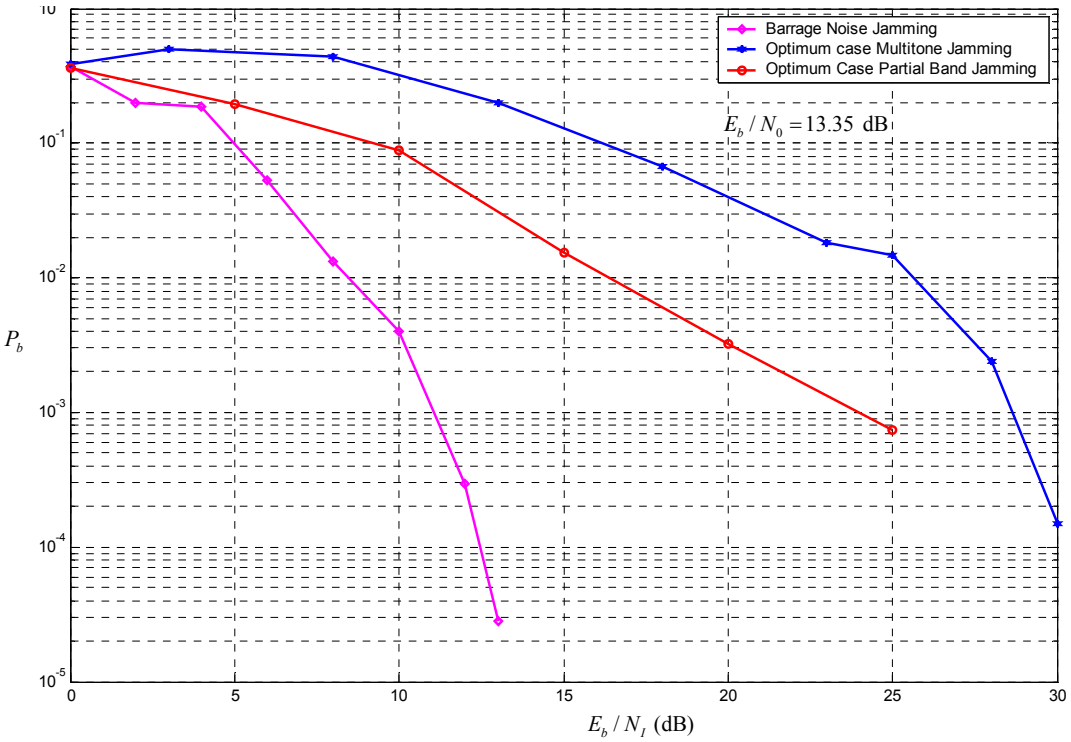

Figure 48. Simulation Results for Barrage Noise Jamming, Optimum Case Partial–Band Jamming and Optimum Case Multitone Band Jamming Against a Noncoherent FFH/8FSK System.

Generally, the multitone band jamming (MTBJ) strategy can be more effective against FFH/MFSK signals than the PBJ strategy because the jamming tone (CW) is the most effective way for a jammer to inject energy into the noncoherent detectors [3]. On the other hand the MTBJ strategy has the disadvantage that the jammer must know the signal's full structure before starting to jam the system. Only then is it capable of selecting jamming frequencies so that no more than one tone coincides with one of the M frequencies in each hop band.

The simulation results proved that the barrage noise jamming strategy, as expected, is the least effective of all jamming strategies against FFH/MFSK systems with a modulation order M=2, 4, 8.

For the case of an uncoded noncoherent FFH/MFSK system with a square–law linear combining receiver, the performance of the MTBJ strategy has the best results compared to the PBJ strategy. Especially as the modulation order M increases from M=2 to M=8, then the partial–band jammer becomes less and less effective.

The next chapter investigates, with the help of the SystemView, the performance of the FFH/MFSK system in a Rayleigh fading channel along with AWGN.

VI. SIMULATION RESULTS OF THE PERFORMANCE OF A NONCOHERENT FFH/MFSK SYSTEM IN A RAYLEIGH FADING CHANNEL

This chapter presents simulation results for the performance of an uncoded noncoherent FFH/MFSK system in a Rayleigh fading channel model for two cases. The first case examines the performance of the system with only AWGN in a Rayleigh channel. The second case examines the performance of a barrage noise jammer against an FFH/MFSK system, also in a Rayleigh channel. The channel is modeled as a frequency–nonselective, slowly fading channel.

A. SIMULATION MODEL OF AN FFH/MFSK SYSTEM IN A RAYLEIGH FADING MODEL

The FFH/MFSK simulation model is the same as the previous chapter. The only difference is the token that simulates the Rayleigh fading channel. The Rayleigh channel can be achieved by adding one of the existing models in the SystemView Communication Library, which is called *rice fading channel* (*Rice Chn*). As mentioned in Chapter IV, the Rayleigh fading channel is a special case of the Ricean fading channel.

The Ricean channel model is used in a line–of–sight case between the transmitter and the receiver, where a portion of the received signal power is due to multipath. In the Rayleigh channel model there is no line–of–sight between the transmitter and the receiver, and the entire received signal's power is due to multipath.

The specific token implements a Ricean amplitude–fading channel [12]. The initial signal $x(t)$ after the influence of the *Rice Chn* becomes

$$y(t) = x(t)z(t), \tag{6.1}$$

where $z(t)$ is the fading amplitude. The fading amplitude is given by:

$$z(t) = \sqrt{x_1(t)^2 + [A + x_2(t)]^2} \tag{6.2}$$

where $x_1(t)$ and $x_2(t)$ are zero mean Gaussian random variables with standard deviation σ_R. The power in the fading channel is normalized to unity by the constraint:

$$2\sigma_R^2 + A^2 = 1 \tag{6.3}$$

where according to the theory $2\sigma_R^2$ indicates the diffuse signal power and A^2 represents the received direct, or line–of–sight, power.

The values of A and σ_R are determined from the Ricean parameter K according to the above relations:

$$A = \sqrt{\frac{K}{K+1}}, \tag{6.4}$$

and

$$\sigma_R = \frac{1}{\sqrt{2(1+K)}}. \tag{6.5}$$

The parameter K is very important and is defined as the ratio of direct–to–diffuse signal power:

$$K = \frac{A^2}{2\sigma_R^2}. \tag{6.6}$$

When $K = 0$, the channel is characterized as Rayleigh fading channel and when $K = \infty$ the channel is not a fading channel. In our case the parameter K of the *Rice Chn* token is chosen to be $K = 0$ in order to simulate the Rayleigh fading channel.

The *Rice Chn* token also has an another parameter. This parameter is the T_{corr} that controls the fade rate of *z(t)*. The basic assumption is that the fade rate is slow compared to the signal–hop rate. In our model this parameter is set as $T_{corr} = 1/R_h$ and is different for every modulation scheme *M*=2, 4, 8. This assures that the signal amplitude can be modeled as a Rayleigh random variable that remains fixed at least for the duration of a single hop. The reason that the parameter was chosen to be exactly $T_{corr} = T_h$ is explained in the next section.

The overall block diagram of the uncoded noncoherent FFH/BFSK in a Rayleigh channel is shown in Figure 49. The Rayleigh channel is implemented with token 73. The diagrams of the FFH/4FSK and FFH/BFSK are similar to the FFH/BFSK and for that reason are not included.

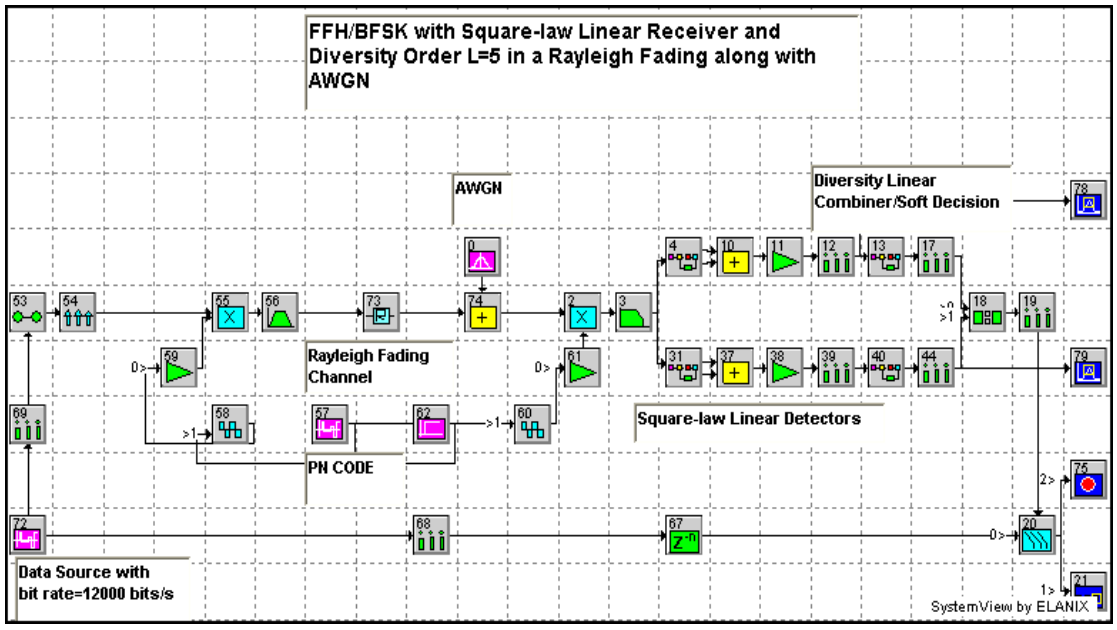

Figure 49. Uncoded Noncoherent FFH/BFSK Model in a Rayleigh Fading Channel.

Figures 50 also presents, with the help of the oscilloscope of the SystemView, the influence of the Rayleigh fading channel on the amplitude of the transmitted hop pulses. The FFH/BFSK system in this case does not include AWGN. The upper plot shows that every transmitted hop pulse has the same amplitude contrary to the lower plot that shows that the amplitude of the transmitted hop pulse is under the influence of the fading channel.

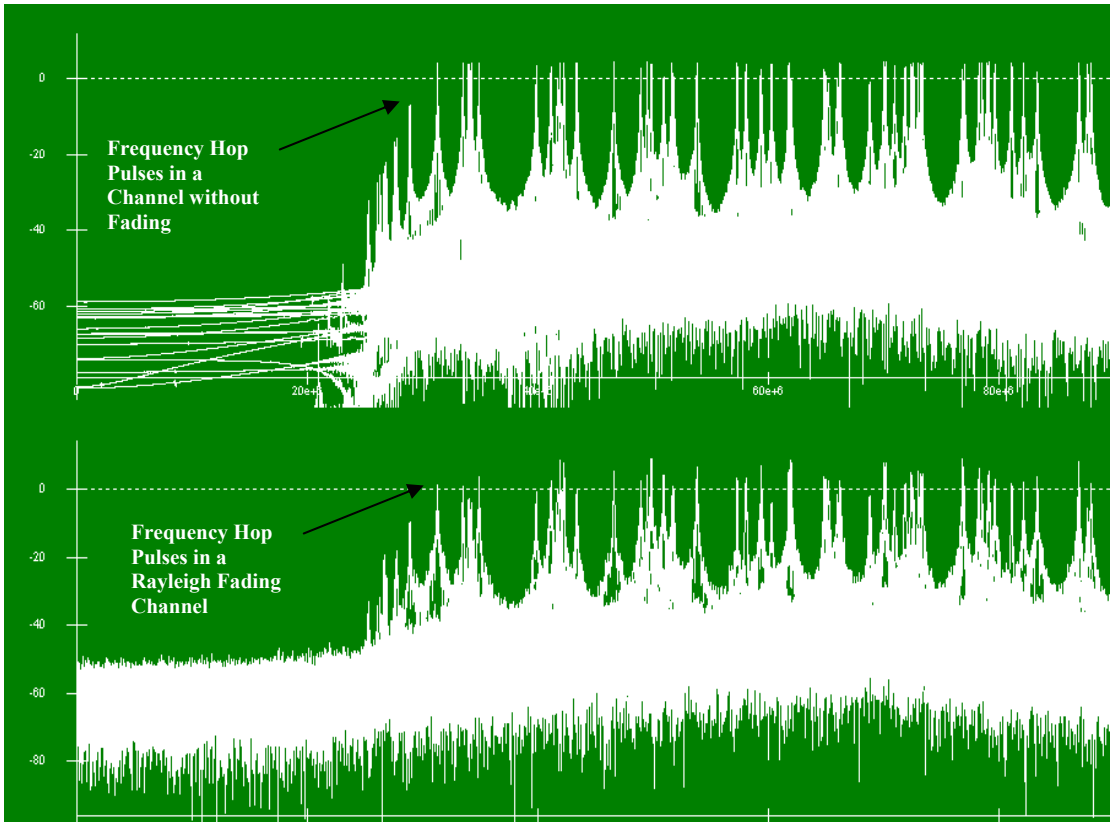

Figure 50. Spread Spectrum of the Uncoded Noncoherent FFH/BFSK System in a Channel without Fading and in a Rayleigh Fading Channel.

The next step examines the performance of the system under the influence of AWGN.

B. UNCODED NONCOHERENT FFH/MFSK SIMULATION MODEL IN A RAYLEIGH FADING MODEL ALONG WITH AWGN

The simulation model of the FFH/BFSK system in a Rayleigh channel along with AWGN is illustrated in Figure 49. Before the simulation was executed, a necessary setting of the parameter T_{corr} had to be made. According to the theory, every value of the fading rate $R_{corr} = 1/T_{corr}$ that satisfies the relation

$$R_{corr} = \frac{1}{T_{corr}} \leq R_h \tag{6.7}$$

is valid for the simulation system. In practice this proved incorrect.

Figure 51 presents the probability of bit error P_b with $E_b / N_0 = 13.35$ dB for different values of T_{corr}.

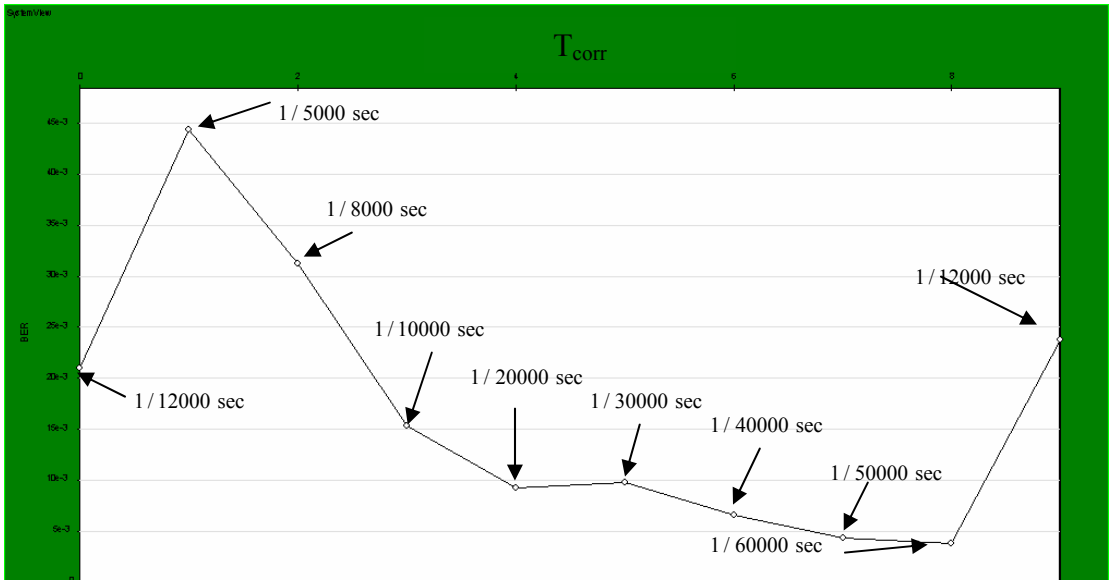

Figure 51. Simulation Results of an Uncoded Noncoherent FFH/BFSK System for Different Values of T_{corr} with $E_b / N_0 = 13.35$ dB.

It is very interesting that the token *Rice Chn* that represents the Rayleigh channel for higher values of T_{corr} is not working very well. It creates higher values of probability of bit error than expected. The simulation system worked fine when the parameter T_{corr} was set exactly as $T_{corr} = 1/R_h$ for every modulation order *M*.

Following this assumption and defining the density of AWGN (token 0) as a variable parameter, the simulation was executed eight times for the FFH/BFSK, seven times for the FFH/4FSK, and six times for the FFH/8FSK system. Every time the simulation made a loop, the value of the power density N_0 decreased. This reduction corresponds to a continuous increase of E_b / N_0.

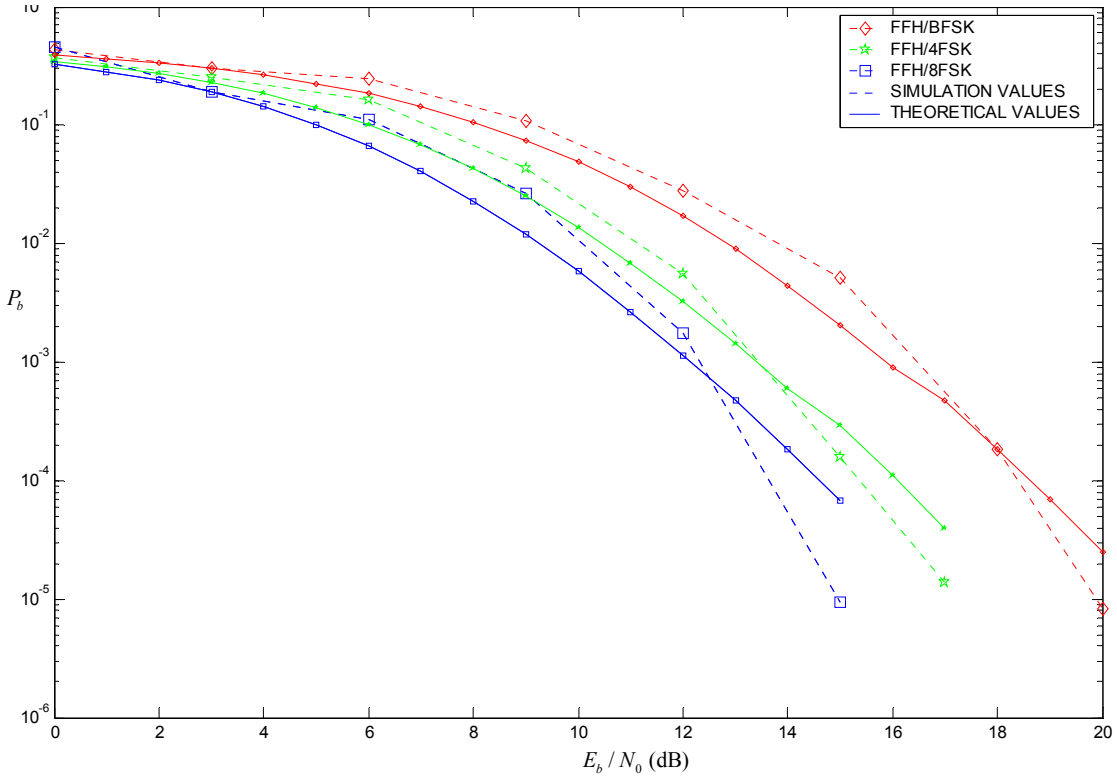

Figure 52. Simulation Results of Uncoded Noncoherent FFH/MFSK System Performance with AWGN in a Rayleigh Fading Channel as Compared to Theoretical Results.

Figure 52 illustrates the probability of bit error for the FFH/MFSK system with M=2,4,8 in a Rayleigh fading channel under the influence of AWGN. The theoretical curves calculated according to Equation (4.17). The results verify that the simulation model behaves in AWGN as the theory predicts with small variations $(\leq 1\,\text{dB})$.

The next step is to construct the simulation model of the BNJ and observe its influence in the performance of uncoded noncoherent FFH/MFSK in a Rayleigh channel.

C. UNCODED NONCOHERENT FFH/MFSK SIMULATION MODEL IN A RAYLEIGH FADING MODEL UNDER THE INFLUENCE OF THE BARRAGE NOISE JAMMING

The noise interference that the barrage noise jammer uses is characterized as AWGN. The power density of the jammer derives from

$$N_I = \frac{P_I}{W_T} \tag{6.8}$$

where P_I is the available power of the jammer.

Figure 53 illustrates the simulation model for a FFH/BFSK system in a Rayleigh channel under the influence of BNJ. The BNJ consists of the token 75 that represents the noise source and the token 77 that limits the jammer's noise power density into the SS operational bandwidth.

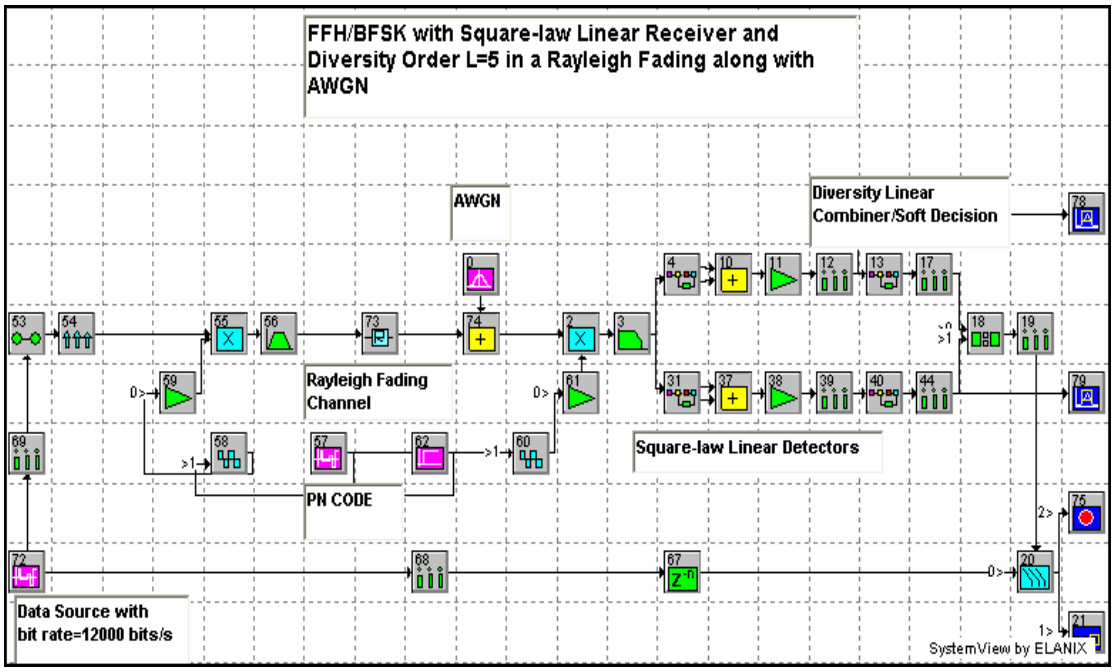

Figure 53. Simulation Model of an Uncoded Noncoherent FFH/BFSK System in a Rayleigh Channel under the Influence of BNJ.

The AWGN of the channel is considered to be constant with $E_b / N_0 = 17$ dB. The variable parameter in this case is the noise density power N_I that is represented by token 75.

The results of the simulation for *M*=2, 4, 8 are illustrated along with the theoretical results in Figure 54.

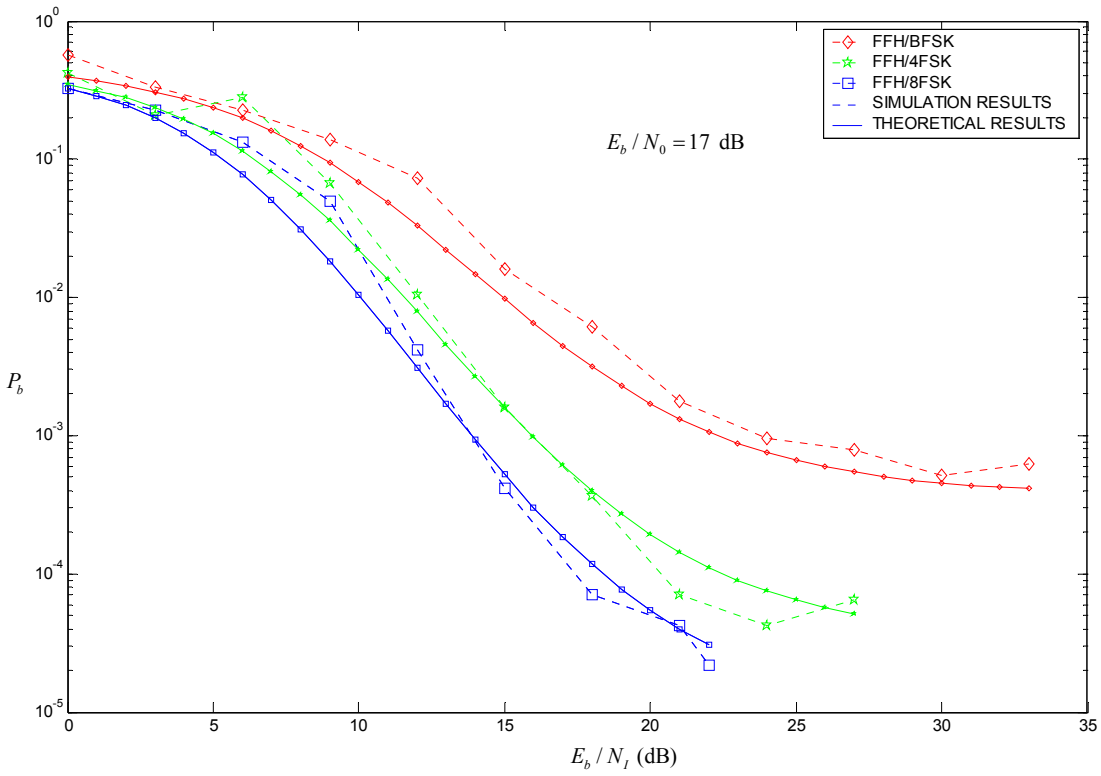

Figure 54. Simulation Results of the Effect of BNJ in an Uncoded Noncoherent FFH/MFSK System in a Rayleigh Channel Along with AWGN.

The results in Figure 54 prove that the simulation model behaves in BNJ as the theory predicts with a small variation in the case of an FFH/BFSK system.

The analysis of this chapter, along with the theoretical analysis of Chapter IV, consist of the initial steps for a further investigation of the FFH/MFSK system with a square–law linear receiver in a fading channel. The results from this chapter also can be used as a benchmark for a future analysis for other jamming strategies against this type of FFH system. The simulation model operates in a Rayleigh channel as the theory predicts, so this simulation model forms a useful tool for a more complicated analysis of an FFH system.

VII. CONCLUSIONS AND FUTURE WORK

The main scope of this thesis was to evaluate the performance of different jamming strategies against an uncoded noncoherent FFH/MFSK communication system with a square–law linear combining receiver. Another goal was to present a preliminary theoretical and simulated analysis for the FFH/MFSK system in a Rayleigh fading channel.

The results of the theoretical analysis and the simulation modeling can be used as guidelines for selecting the most effective jamming strategies, depending on the type of hostile waveform. The same models with the appropriate changes can also be used to evaluate other types of more complicated jammers over various communication channels.

In order to proceed in our analysis the various assumptions made are listed below:

- The hostile communication system uses an uncoded noncoherent FFH/MFSK system with a square–law linear combining receiver. This type of receiver does not have any information for the jammed frequency hop bands (side information).
- The channel environment is characterized as an AWGN channel for the analysis of a non–fading case and is characterized as a Rayleigh channel in the case of the analysis of a fading channel.
- The SS bandwidth for all modulation orders M=2, 4, 8 are considered the same for all simulation models.
- The information bit rate R_b remains fixed for all modulation orders. This results in a non–fixed hop rate as the diversity order L increases.

The main points and conclusions of the investigation are summarized by chapter with suggestions for future work.

A. CONCLUSIONS

Chapter II provides a general description of the FFH/MFSK communication system. This chapter also presents the geometrical restrictions of a follower jammer over a FFH/MFSK communication system. Fast frequency–hopping prevents the follower jammer from having sufficient time to determine the communicator's frequency and to transmit interfering signals. The greater the hopping rate, the more protected the FFH system is against the follower jammer.

Chapter III presents the performance of different jamming techniques against the uncoded noncoherent FFH/MFSK system. The jamming techniques that were analyzed are barrage noise jamming, partial band noise jamming, and multitone band jamming. According to the theoretical analysis of this chapter the optimum case multitone band jamming proved to be–at least for the case of FFH/BFSK–the most effective method and the barrage noise jamming the least effective. It was shown that as the modulation order increases from M=2 to M=8 the jammer influence degrades.

In Chapter IV a preliminary analysis was made for the performance of the FFH/MFSK system in a fading Rayleigh channel. It was proved that as the diversity order L increases, the performance of the FFH/MFSK system improves (as measured by P_b). The influence of the BNJ against a FFH/MFSK system in a Rayleigh channel was also examined. The results confirm that this jamming strategy cannot degrade the system enough. The interesting point was that the system can improve itself using a greater diversity order, a greater number of frequency hop bands, and a greater modulation order.

In Chapter V, simulated models for a FFH/BFSK, FFH/4FSK and FFH/8FSK systems were constructed under the influence of different types of jammers. The implemented simulated jammers were the barrage noise jammer, the partial band jammer and the multitone band jammer. Both the simulated results and the theoretical results confirmed that the most effective jamming strategy against an FFH/MFSK system is the optimum case multinone band jamming strategy for all modulation orders. It was also shown that as the modulation order increases from M=2 to M=8, then the performance of the optimum case multitone jamming remains approximately the same.

Chapter VI presented the simulation FFH/MFSK models from the previous chapter in a fading channel environment. The chosen fading channel was the Rayleigh channel. The simulated results agreed with the theoretical results from Chapter IV. The simulation model operates in a Rayleigh channel as the theory predicts and is a useful tool for a more complicated analysis for an FFH/MFSK system in various fading channels.

In conclusion, the probabilistic comparison of all types of jamming showed that the most effective jamming strategy over an uncoded FFH/MFSK system is the optimum case multitone band jamming.

B. FUTURE WORK

There are three major areas that can be identified for future work. First, completing the analysis for the performance evaluation of partial band and multitone band jamming strategies against the uncoded noncoherent FFH/MFSK system in a Rayleigh channel. Secondly, investigating the performance of a coded noncoherent FFH/MFSK system in a fading channel (Rayleigh or Ricean fading channels) under the influence of different jamming strategies. This would model the operational environment of the system more accurately. Finally, it would be useful to observe how the performance of the coded noncoherent FFH/MFSK system changes under the influence of combinations of jamming strategies by using two or more jamming schemes.

THIS PAGE INTENTIONALLY LEFT BLANK

LIST OF REFERENCES

[1] George T. Katsoulis, "ECCM Potential of a Noncoherent FH/MFSK Communications System Under Worst Case Hostile ECM an Fading Channels," MSEE Thesis, Naval Postgraduate School, Monterey, California, March1997.

[2] John G. Proakis, *Digital Communications*, Fourth Edition, New York: McGraw Hill, 2001.

[3] Marvin K. Simon, Jim K. Omura, Robert A. Scholtz and Barry K. Levitt, *Spread Spectrum Communications Handbook*, New York: McGraw Hill,1994.

[4] Don J. Torrieti, *Principles of Secure Communication Systems*, Artech House, 610 Washington Street, Dedham, Massachusetts, September 1985.

[5] T. Aaron Gulliver and E. Barry Felstead, "Anti–Jam by Fast FH NCFSK – Myths and Realities," in Conf. Record IEEE Milcom'93, pp. 187 – 191, Boston, Massachusetts, October 1993.

[6] Barry E. Fealstead, "Follower Jammer Considerations for Frequency Hopped Spread Spectrum," Communication Research Centre, Upper Ottawa Canada, 1998.

[7] Clark Robertson, Notes for EC4550 (M–ary Digital Communication Systems), Naval Postgraduate School, Monterey, California, 2001 (unpublished).

[8] Clark Robertson, Notes for EC4560 (Spread Spectrum Communications Systems), Naval Postgraduate School, Monterey, California, 2001 (unpublished).

[9] I. S. Gradshteyn and I. M. Ryzhik, *Table of Integrals, Series, and Products, Corrected and Enlarged Ed*., translated and edited by Alan Jeffrey, New York, Academic Press, 1980.

[10] Jhong S. Lee, Robert H. French, and Leonard E. Miller, "Probability of Error Analyses of a BFSK Frequency–Hopping System with Diversity under Partial–Band Jamming Interference–Part I: Performance of Square–Law Linear Combining Soft Decision Receiver," *IEEE Trans. Commun*., vol. COM–32, pp. 645–653, June 1984.

[11] Kah C. Theh, Kwok H. Li, and Alex C. Kot, "Performance Analysis of an FFH/BFSK Linear–Combining Receiver Against Multitone Jamming," *IEEE Commun. Lett.*, vol. 2, pp .205–207, August 1998.

[12] R. Clark Robertson and Kang Yeun Lee, “Performance of Fast Frequency–Hopped MFSK Receivers with Linear Combining in a Rician Fading Channel with Partial–Band Interference,” *IEEE Commun. Lett*., vol. SAC–10, pp .731–741, May 1992.

[13] Elanix, *SystemView Communications Library*, Nov. 2002.

INITIAL DISTRIBUTION LIST

1. Defense Technical Information Center
   Ft. Belvoir, Virginia

2. Dudley Knox Library
   Naval Postgraduate School
   Monterey, California

3. Chairman, Code IS/Bo
   Department of Information Sciences
   Naval Postgraduate School
   Monterey, California

4. Professor Tri T. Ha, Code EC/Ha
   Department of Electrical and Computer Engineering
   Naval Postgraduate School
   Monterey, California

5. Professor David C. Jenn, Code EC/Jn
   Department of Electrical and Computer Engineering
   Naval Postgraduate School
   Monterey, California

6. Embassy of Greece, Defense and Military Attaché Office
   Washington, DC

7. Konstantinos Karkatzounis
   Agias Anastasias 69, Peristeri
   Athens, GREECE
   TK: 12136